Tampere University

Hongfei Liu

STATIC vs. DYNAMIC DISSOLUTION AND CELLULAR COMPATIBILITY TESTS OF BIOACTIVE BOROSILICATE GLASS SCAFFOLDS

Master's Thesis
Faculty of Engineering and Natural Sciences
Examiner: Jonathan Massera
Examiner: Ville Santala
February 2020

ABSTRACT

Hongfei Liu: Static vs dynamic dissolution and cellular compatibility tests of bioactive borosilicate glass scaffolds
Master's Thesis
Tampere University
Bioengineering, MSc
February 2020

The tissue engineering strategy is an optimal solution for the shortage of grafts and other limitations in bone implantation. In this approach, an ideal scaffold made by biomaterial is used to provide mechanical support and improve bone regeneration. Bioactive glass has been found to be suitable to produce scaffolds for bone application. The incorporation of ions, such as B, Mg, and Sr can bring extra benefits, such as higher conversion rate into hydroxyapatite, mechanical strength, chemical durability and the promotion of cell proliferation and differentiation. The scaffold should own the controlled and optimal internal structure as well as enough mechanical properties which are comparable with nature bones. The 3D printing technologies can achieve the mechanical and structural requirements, customized design and high reproducibility of ideal scaffolds.

In this project, borosilicate glass (B12.5) and borosilicate glass containing Mg and Sr (B12.5-Mg5-Sr10) were prepared using the robocasting method and the porogen burn-off technique for comparison. The basic structural properties were measured and compared between different types of scaffolds. The dissolution behaviour of obtained scaffolds was tested in static and dynamic conditions. Finally, the ability of the scaffolds to support cell attachment and proliferation was assessed using MC3T3 pre-osteoblastic cells.

As a result, the 3D printing methods efficiently produced scaffolds with excellent porosities, pore size, and reproducibility, but the resolution of printing and the stability and homogeneity of ink cannot be controlled very well. Comparing with the static dissolution, the pH and ionic concentrations in the dynamic dissolution test were closer to the condition in vivo which can alleviate the risk for toxicity. In the cell viability test, 3D printed scaffolds which contained Mg and Sr exhibited the best performance. And the pre-incubation time was supposed to be 72 hours at least in order to prevent the burst of ions that could lead to cell death. Furthermore, the size of the scaffolds should be adjusted to limit the release of ions.

Keywords: Borosilicate glass, Dynamic dissolution, 3D printing, cellular compatibility

PREFACE

This study was performed in Bioceramics, -glass and composites research group at Tampere University. Part of the experiment was conducted during researcher exchange in Extracellular Matrix-Cell Interactions Laboratory at University of Cergy-Pontoise, France.

First of all, I would like to express my sincere gratitude to my supervisor, Associate Professor Jonathan Massera, who provided this opportunity to study a new field through an interesting and meaningful project. I learned a great deal from his guidance. The detailed revision of my thesis, conducted with plenty of patience, will affect me in the future.

My deep gratitude goes also to other people who were supportive and helpful during my thesis work in Tampere, especially Assistant Professor Ville Santala and Outi Vaisanen.

I am also extremely grateful to Associate Professor Michel Boissiere for his guidance and caring in living during my exchange period in France. Besides, I heartily acknowledge other people who offered me generous help there, e.g. Professor Emmanuel Pauthe, Amel Houaoui, Hassan Rammal, and Rémy Agniel.

Last but not least, I am forever thankful for the support from my family, and the encouragement from my dear friends.

Tampere, February 2020

Hongfei Liu

CONTENTS

LIST OF FIGURES

LIST OF SYMBOLS AND ABBREVIATIONS

AMT	Additive manufacturing techniques
CAM	Computer-aided manufacturing
CSD	Critical size defect
DAPI	4′,6-diamidino-2-phenylindole
ECM	Extracellular matrix
FBS	Fetal bovine serum
FDM	Fused deposition modeling
HA	Hydroxyapatite
ICP-OES	Inductively coupled plasma optical emission spectroscopy DAPI 4′,6-diamidino-2-phenylindole
MAPK	Mitogen-activated protein kinase
mol%	Molecular percentage
SLS	Selective laser sintering
SEM	Scanning electron microscope
SBF	Simulated Body Fluid
SLA	Stereolithography
vol%	Volume percentage
wt%	Weight percentage
XRD	X-Ray Diffraction
ρ	Density (g/cm^3)
W	weight (g)

1. INTRODUCTION

The demand for bone implants is high. Bone can be impaired by various accidents or diseases, and the market will keep growing with the increasing in senior population (B. Gullberg 1997;Fernandez-Yague *et al.* 2015). However, the shortage of grafts, both autologous and allogeneic, along with their limitations are calling for alternative strategies (Polo-Corrales, Latorre-Esteves and Ramirez-Vick 2014;García-Gareta, Coathup and Blunn 2015;Kohli *et al.* 2018). The optimal solution appears to be the tissue engineering strategy which makes use of biomaterials. In this approach, a scaffold is used to provide enough mechanical support but also to recruit cells during the healing. The scaffold should be degraded after the guidance of tissue regeneration (Fernandez-Yague *et al.* 2015). Such a strategy could solve the problems of graft shortage, disease transmission, infection and immunogenicity (Porter, Ruckh and Popat 2009).

Bioactive glass has been found to be promising in such strategy due to i) its close chemical composition to the natural bone, after immersion, ii) its osteoconductivity and sometime osteoinductivity, as well as iii) its controllable rate of degradation and controllable release of ions of therapeutic interests (Jones 2013;Hench, Roki and Fenn 2014;Fernandez-Yague *et al.* 2015;Kargozar, Baino, *et al.* 2018). However, the clinical application of bioactive glass, especially as a scaffold, is limited due to 1) its rapid crystallization rate which leads to partially to fully crystalline scaffolds, post-sintering, with decreased bioactivity and ii) its incomplete degradation (Chen, Thompson and Boccaccini 2006;Bi *et al.* 2013).

In order to overcome the challenges and even bring extra benefits, many ions were incorporated into the network of bioactive glass. The incorporation of B, to produce the borosilicate glass, was associated with improved cell behavior and higher conversion rate into hydroxyapatite (Brink *et al.* 1997;Huang, Day, *et al.* 2006;Gu *et al.* 2013). Mg can enhance the thermal properties of traditional silicate glasses, thus increasing the hot forming domain, allowing to produce the porous scaffold with enhanced mechanical strength and chemical durability (Diba *et al.* 2012;Massera, Hupa and Hupa 2012;Souza *et al.* 2013). Furthermore, Sr in silicate bioactive glasses was reported to promote the proliferation and differentiation of osteoblasts (Hesaraki *et al.* 2010;Hoppe *et al.* 2014;Hupa *et al.* 2016).

An optimum scaffold should have controlled porosity (>50%) with large pores (50 - 500 μm) and high interconnection between the pores. Furthermore, the mechanical

properties should, at minimum be similar to the one of the cancellous bone or, better, similar to the cortical bone, for load-bearing applications (Rahaman *et al.* 2011;Nommeots-Nomm and Massera 2017). The emerging 3D printing technologies enables improving the mechanical properties of the scaffolds through control of the scaffold internal structure and overall design. The scaffold can be customized with patient specificity and produced with high reproducibility (Lee 2015;Lee and Cho 2015). From all the available 3D printing technologies, robocasting is the most widely used for scaffolds made from bioactive glass (Nommeots-Nomm and Massera 2017).

In this project, borosilicate glass (B12.5) and borosilicate glass containing Mg and Sr (B12.5-Mg5-Sr10) were prepared using the robocasting method and the porogen burn-off technique for comparison. The dissolution behavior of the obtained scaffolds was tested in static and dynamic conditions. The bioactivity of the scaffolds was assessed by the presence of hydroxyapatite at the scaffold surface (or within the scaffold structure). And the mechanical properties of the scaffolds were tested in compression during previous work (Pohjola 2017). Successively, the ability of the developed scaffolds to support cell attachment and proliferation was assessed using MC3T3 pre-osteoblastic cells. The aim was to assess the pre-incubation time to prevent burst of ions that could lead to cell death.

This thesis is composed of six chapters, including the Introduction, Background, Materials and Methods, Results, Discussion, and Conclusion. The background aims at reporting the state of the art with regard to bioactive glass scaffolds along with the challenges faced by the scientific community. In the Materials and Methods, the procedures, operations, instruments and materials used during the project are introduced in detail. The fourth and fifth chapters report on the obtained results and their discussion. Finally, the Conclusion aims at evaluating the progress made in the project and consider the future experiment to be performed.

2. THEORETICAL BACKGROUND

2.1 Tissue engineering in bone repairing

The function and structure of bone can be impaired by various situations including trauma, diseases, tumor removal and orthopedic surgery. The high demand for bone graft, in such circumstances, is a challenge (Fernandez-Yague *et al.* 2015). Even though the bone possesses its natural ability for regeneration, when a critical size defects (CSDs) is formed the bone lose its self-regeneration ability (Fernandez-Yague *et al.* 2015;Li *et al.* 2015). Within our aging society, bone fracture is expected to increase by more than 300% for men and 240% for women by 2050, along with osteoporosis and bone cancer (B. Gullberg 1997). Bone, already being the second most transplanted tissue worldwide, the high bone graft demands cause concerns (Lewandrowski *et al.* 2000).

Autologous grafts are considered as the gold standard pertaining to its osteoinductive property, as well as the lack of immune response. However, limitations are the need for additional surgery to harvest the bone, the extra rehabilitation period and the increased risk of infection. Furthermore the amount of bone that can be harvested is limited (García-Gareta, Coathup and Blunn 2015;Kohli *et al.* 2018). Allografts can be considered (bone from a donor) in order to suppress the need for additional surgery and to overcome the limitation in availability. However, the absence of osteo-inductive signals and the immune rejection hinder their utilization. Furthermore, one should keep in mind the risk for disease transfer (Polo-Corrales, Latorre-Esteves and Ramirez-Vick 2014).

Biomaterial could eliminate the risks of disease transmission and immunogenicity, and resolve the shortage of living tissues and organs for transplantation (Porter, Ruckh and Popat 2009). The approach of tissue engineering in the bone application is to combine cells, scaffolds, and specialized biochemical and physical stimuli to achieve the regeneration and formation of bone in vivo (Hutmacher 2006). In addition, the biomaterial scaffolds bring some new chances of therapy, attracting increasing interest. For example, the bioactive glass can be modified to improve the angiogenesis ability which is a critical challenge during the bone implantation (Kargozar, Baino, *et al.* 2018). There are also new functional bioactive ceramic scaffolds which can not only promote bone regeneration but also possess anti-cancer agent. This is of particular interest in bone tumor therapy through fixing the defects from the operation and killing the residual cancer cells (Ma *et al.* 2018).

The optimal bone graft for regenerative bone treatment is a scaffold which 1) offers mechanical support during the healing process, and after the initial cellular adsorption, 2) releases ions of therapeutic interests while promoting new bone formation. Ideally, the tissue will regain its structure and function after the total degradation/dissolution of the scaffold, without need for a secondary surgery to take the implant out (Fernandez-Yague *et al.* 2015). And if the scaffold does not degrade, it becomes a permanent implant and is unlikely to restore the bone (Treiser *et al.* 2013).

There are some general requirements for optimal biomaterial scaffolds used in bone tissue engineering. The aim remains to imitate the structure and biological function of natural bone.

(1) **Biocompatibility** is required to ensure the cells can adhere and proliferate without evoking severe inflammation or immune response (Williams 2008). Of course, no dissolution by-products should be toxic (Kumar *et al.* 2016).

(2) **Bioactivity** induces the formation of chemical bonds between the materials and surrounding tissue (hard and soft tissues) (Kumar *et al.* 2016). As part of the bioactivity, the material should be at least osteoconductive and, in the best scenario, osteoinductive (Nommeots-Nomm and Massera 2017;Zhang *et al.* 2019).

(3) **Degradability or absorbability** in vivo is also critical. The rate of degradation of the scaffold is supposed to match the rate of regeneration of new tissue as closely as possible (Nommeots-Nomm and Massera 2017).

(4) **Mechanical support** should be provided by the scaffold. The scaffolds should have at least similar mechanical properties than the cancellous bone and, eventually, similar to the cortical bone for load bearing applications (Fu *et al.* 2011;Jones 2013).

(5) Open interconnective **porous structure** is required for the transport of nutrients and waste, as well as the migration of cells. The scaffolds overall porosity of should be 50% to 90% and the size of the pores from 100 µm to 500 µm (Karageorgiou and Kaplan 2005;Gerhardt and Boccaccini 2010).

(6) **Reproducibility** and scaling up of the manufacturing should be possible to ensure clinical relevance. Furthermore, new methods can provide customized geometries which matched the defects, i.e. 3D prototyping (Zhang *et al.* 2019).

(7) The **cost** of the implant as well as the ability to **easily and efficiently sterilized** the scaffolds are of, also, of paramount importance (Rahaman *et al.* 2011).

The ideal scaffold is designed to satisfy the structural and functional demands of the natural bone tissue with respects to the chemical compositions and hierarchical construction (Ma *et al.* 2018).

2.2 Scaffolds compositions

The materials used for the scaffolds in tissue engineering can be classified into natural and synthetic materials. Various marine species, like coral, are used to design 3-dimensional porous scaffolds with natural interconnection, various densities, shapes and sizes of pores, but there are also limitations. For example, inadequate mechanical properties and uncontrollable degradation rate are limiting factors when using coral – based scaffolds (Ivankovic *et al.* 2010;Battistella *et al.* 2012;Panda, Pramanik and Sukla 2014). Chitosan is also considered pertaining to its high biocompatibility and other beneficial properties such as osteoconductivity and biodegradability. However, chitosan scaffold do not match the mechanical properties of the bone (Venkatesan and Kim 2010). Natural polymers, including collagen, also exhibit insufficient mechanical support (Haugh *et al.* 2010).

Synthetic materials have been widely investigated for use in bone reconstruction. Their pros and cons are well known and can be briefly summarize: polymers typically have low mechanical strength and have long degradation time; ceramics are brittle and difficult to shape, and metals are, generally, non-degradable and their corrosion can lead to negative results (Witte *et al.* 2005).

Bioactive glass which belongs to bioactive ceramics has been extensively applied in bone tissue engineering. Their high stiffness, hydrophilicity, and similarity with the chemical composition of bone makes it a promising material for bone tissue engineering. Furthermore, bioactive glasses can exhibit osteoconductivity and osteo-inductivity, which are key requirements for bone regeneration. Recently, these materials were also found to improve angiogenesis. Finally glass can be doped with ions of therapeutic interest, which will be released in a control manner (Jones 2013;Hench, Roki and Fenn 2014;Fernandez-Yague *et al.* 2015;Kargozar, Mozafari, *et al.* 2018).

The traditional and classical bioactive glass, for example, 45S5 and S53P4, has already been used clinically as fillers in bone cavity, after tumor resection. The limitation of traditional bioactive glass is the challenge to manufacture the 3D porous scaffolds with adequate mechanical strength through the sintering process, while preventing crystallization, known to reduce the materials' bioactivity (Filho, La Torre and Hench 1996;S. Fagerlund *et al.* 2012). Another limitation is the slow and incomplete conversion

of the glass into Hydroxyapatite (HA), due to the low solubility of silica. In turns, this leads to difficulties in matching the glass dissolution and the rate of new tissue growth (Bi *et al.* 2013). After the surgery, unreacted glass particles were still detected in a mandible of live Macaca fascicularis even 4 years later (Suzuki *et al.* 2011).

In order to overcome the limitations, many approaches have been researched, especially incorporating various metal ions into the original silicate network (Hoppe, Güldal and Boccaccini 2011).

2.2.1 Boron doped bioactive glass

Both controlled degradation rate and enhanced regeneration of bone are able to be potentially achieved through the scaffolds containing both silicate and borate bioactive glass in the optimal proportions (Gu *et al.* 2013).

The degradation rate of bioactive glass can be controlled over a wide range by manipulation of the composition, such as partially or fully replacing the SiO_2 in the original glass with B_2O_3 to produce the borosilicate glass or borate glass (Huang, Day, *et al.* 2006;Yao *et al.* 2007).

Boron doped bioactive glass samples exhibited bioactivity and an increased rate of conversion of the glass into HA, in vitro (R. F. Brown *et al.* 2009). In addition, boron ions improved the angiogenic and osteogenic effects as well as the thermal behavior of bioactive glass (Brink 1997;Brink *et al.* 1997;Haro Durand *et al.* 2015).

However, the cellular tests using the medium with increasing Boron content to culture osteoblasts showed that the proliferation of cells was inhibited and even the amounts of cells decreased over time when the concentration of B was above 1.5 mmol (R. F. Brown *et al.* 2009).When the concentration of B was below it, the proliferation of cells was supported. And in other tests using the boron doped glass, the thresholds of B concentration were 0.65 and 0.5 mmol (Fu *et al.* 2009;Ojansivu *et al.* 2018).

In contrast, there was no toxicity, and even benefit tissue infiltration in the rat test in vivo (Gorustovich *et al.* 2006;Q Fu *et al.* 2010;Jung *et al.* 2013). The inconsistent results from tests in vitro and in vivo suggested the cellular experiments need to be improved, such as the pre-treatment and more dynamic culture system, which can reduce or diminish the toxic effect (R. Brown *et al.* 2009;Rahaman *et al.* 2011).

2.2.2 Magnesium doped bioactive glass

The main purpose for introducing Mg into the bioactive glass is to enhance the mechanical strength of the scaffolds. Indeed Mg is known to decrease the glass viscosity

at lower temperature and thus improve the sintering (Diba *et al.* 2012;Souza *et al.* 2013). In previous work, the Mg substitution of Ca increased the chemical durability and decreased the rate of degradation because of the more compact glass network (Massera, Hupa and Hupa 2012). Mg ion is also considered to affect the regeneration of bone and vascularization in the implantation area, when it was released from the Mg-contained silicate bio-ceramic scaffolds (W. Zhang *et al.* 2017).

2.2.3 Strontium doped bioactive glass

The SrO does not change the general glass structure when it is introduced into the glass, at the expense of CaO (Massera and Hupa 2014). However, the initial dissolution rate will increase with increasing the SrO content in the glass, because of the more open network. The partial replacement of SrO for CaO is able to increase the degradation and promote bone regeneration simultaneously (Hupa *et al.* 2016).

It is noteworthy that SrO was observed to decrease the rate of HA precipitation, however, Sr ion was able to enhance the bone cells activity when it is released from the Sr-doped bioactive glass (Gentleman *et al.* 2010). It was reported that this type of glass improved the proliferation and differentiation of osteoblasts in vitro for different types of cells (Hesaraki *et al.* 2010).

2.3 Scaffolds structure

The structure of scaffolds is also significant for the microenvironment where the new tissue regenerates and the ions diffuse in, and the desired scaffolds work as the template to guide the regeneration process of bone (Hutmacher 2000;Rahaman *et al.* 2011). The macrostructure of scaffolds and related fabrication methods are investigated optimizing the rate of degradation and mechanical properties. In order to mimic the function of natural bone, the understanding of its basic properties is essential.

2.3.1 Natural bone

Bone tissue can be considered as a three-dimensional composite scaffold that consists of nano-HA and type-I collagen, and generally classified as the cortical bone and cancellous bone according to their structure, mechanical characters, and porosity (Fernandez-Yague *et al.* 2015). The hierarchical structure of bone, including the macroscopic structure (upper part), microscopic and nanoscopic structures (lower part) is showed in Figure 1.

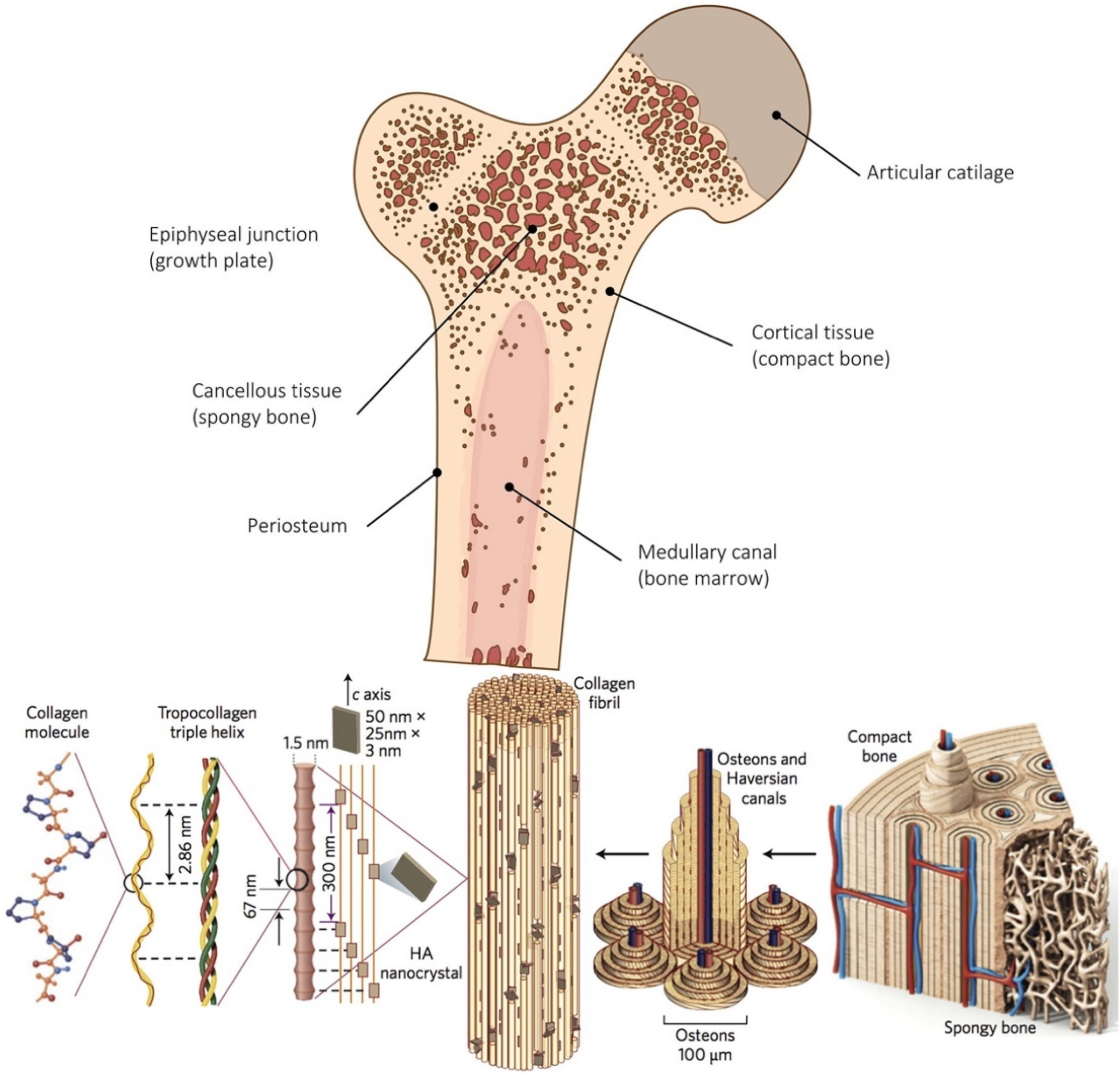

Figure 1. *The hierarchical structure of bone tissue (Ma et al. 2018; Wubneh et al. 2018). Reproduced with permission (order number #4776950748178 and #4776960048387).*

The cortical bone, also referred to as “compact bone”, is fairly dense and consists of osteon packets, and Haversian canals which are channels consisting of blood vessels surrounded by concentric rings of bone matrix. The porosity is generally 5% to 20% (Katsamenis *et al.* 2013;Cambra-Moo *et al.* 2014;Martin *et al.* 2015). The mechanical properties of the cortical bone, because of the oriented microstructure, are highly anisotropic, leading to compressive strength reaching 100 to 190 MPa with an elastic modulus from 5 to 20 GPa (Reilly, Burstein and Frankel 1974;Rho, Hobatho and Ashman 1995;Koester, Ager and Ritchie 2008;Katsamenis *et al.* 2013;Cambra-Moo *et al.* 2014). The trabecular bone, or referred to as “cancellous bone”, is less dense and the trabeculae structure provides a larger surface area which is more effective for the exchange of ions (Beddoe, Darley and Spiers 1976). This bone is more porous with porosity from 50% to 90%, and the mechanical properties are reported to be 2 to 12 MPa with an elastic modulus of 0.1 to 5 GPa (Goldstein 1987).

2.3.2 Strategies to optimize graft structure

In order to allow the adhesion and proliferation of cells, and to offer the space for the vascularization and ingrowth of tissue, the scaffolds used in bone tissue engineering must be 3D porous structures with the interconnection between pores. The high porosity is usually desired, however, the large void volume affects the mechanical properties greatly (Mohamad Yunos, Bretcanu and Boccaccini 2008;Loh and Choong 2013;El-Rashidy *et al.* 2017). By their poor mechanical properties, the application of many biological materials including bioactive glass, is primarily limited to the CSDs (critical size defects) of the non-weight-bearing sites (Daga *et al.* 2018).

Macrostructure, including the porosity, size, geometry of pores, and interconnectivity influence the performance of scaffolds greatly, not only in terms of the mechanical properties but also the degradation and bioactivity (Ma *et al.* 2018). The higher porosity and larger surface area lead to faster degradation and conversion into HA. The pore geometry can affect the invasion of cells and vascularization (Gariboldi and Best 2015;Daly *et al.* 2018;Ma *et al.* 2018). The cellular response is a function of the grafts chemical composition, its topography, porosity, the roughness of the surface, as well as grain size (Hutmacher 2000;Gough, Notingher and Hench 2004;Karageorgiou and Kaplan 2005).

(1) Porosity

The porosity is critical to increasing the available surface area for the interaction with the environment and cells, but also to allow the cells migrating into the scaffold. As a result, scaffolds with high porosity usually show the ability to improve osteogenesis (Roy *et al.* 2003;Cavo and Scaglione 2016). However, the conflict for the high porosity is to maintain the migration and growth of cells whilst adequate mechanical support is acquired (Zhang *et al.* 2019).

Generally, the minimal porosity is considered at 50% which is required for the tissue ingrowth, and the optimal value reported is at 90% (Karageorgiou and Kaplan 2005;Fu *et al.* 2011). Although the high porosity is required, the expense of mechanical strength is not always necessary. The equal effects of proliferation and osteoconductive were exhibited between the 3D PLA scaffolds with quite different porosities, 30% and 50%, that suggested the compromise of the porosity could be made owing to the strength and bone integration (Gregor *et al.* 2017;Zhang *et al.* 2019).

(2) Pore size

In previous studies, the pore size was suggested to be over 100 μm, due to the requirements for penetration, migration, and colonization by cells (Karageorgiou and

Kaplan 2005;Jones *et al.* 2007). But there is still no clear consistent standard for the pore size (Tarafder *et al.* 2015;Cavo and Scaglione 2016;Wang *et al.* 2016). There were no obvious different effects exhibited between three groups of PLA scaffolds with the pore sizes of 50, 200, 250 μm separately, as a result, cells migrated throughout the scaffolds in all samples (Grémare *et al.* 2018). Thus, the minimal and maximal values of the pore size are likely not very strict.

In order to mimic the natural tissue, one strategy is to simulate the feature of sizes in different levels of bone in the same scaffold. For instance, the micropores, smaller than 20 μm, are to help the adhesion and retention of cells. And the macropores, 100 to 400 μm, as well as the interconnective pores are able to enhance the transport, cellular migration, and vascularization (Hutmacher 2000).

(3) Pore geometry

The bio-ceramic including bioglass scaffolds are extensively applied and studied in bone regeneration because of their advantages but usually limited by the poor mechanical properties. Thus, there are some studies on the effects of different macropores geometry in order to improve the mechanical properties of scaffolds. The better fatigue resistance was exhibited in the scaffolds with circular pores, comparing with the group with triangular pores, under cyclic load (Gong *et al.* 2017). 3D printed scaffolds with different porosities, from 50% to 70%, and different shapes of pores including rectangle, curved shape, zigzag and hexagon, were used to investigate the compressive strength. As a result, the scaffolds with hexagonal pores and porosity of 50% exhibited the highest strength which was 180 MPa. The hexagonal pattern possessed the maximum contact area between layers and at intersections, whilst the high porosity could be attained. In addition, the compressive strength decreased with the increased pore size, among the scaffolds with the same geometry of pores (Roohani-Esfahani, Newman and Zreiqat 2016).

Additionally, the geometry of macropore is also able to influence the cell network formation and ingrowth of tissue (Gariboldi and Best 2015). The migration and proliferation of cells and the tissue growth rate are strongly affected by the parameters of geometry of pore or channel, for example, the high local curvature can enhance the tissue growth (Nelson *et al.* 2005;Rumpler *et al.* 2008).

(4) Hierarchical structure

The conflict of the mechanical properties and the mass transport could be resolved by a hierarchical structure (Kureshi *et al.* 2010). For example, the bio-ceramics scaffolds which were designed with a hierarchical structure, including nanostructure,

microstructure, and macrostructure, allow the effective mass transport and migration /ingrowth of cells, while showing lower overall porosity (Bose, Vahabzadeh and Bandyopadhyay 2013). As a result, the scaffolds are not only able to provide the anchoring sites for the adhesion and colonization of cells by the rough surface but also overcome one disadvantage of 3D scaffolds which is the leakage of cells from the big pore (Ma *et al.* 2018).

There are various methods likely to achieve 3D porous scaffolds with a hierarchical structure, for example, nano-stereolithography, freeze drying method, spin coating method, self-assembly method, hydration process, and so on (Ma *et al.* 2018).

2.4 Scaffolds processing

In order to process scaffold with the above-mentioned properties some solutions use existing materials combined with computer-aided manufacturing (CAM) and additive manufacturing techniques (AMT), such as 3D printing. Those techniques can help in developing scaffolds with a complex and precise design, as well as enhanced mechanical properties, to improve the performance of the grafts and, ultimately, bone regeneration, with potential in load-bearing sites (Doiphode *et al.* 2011;Derby 2012;Thavornyutikarn *et al.* 2014;Baino, Verné and Massera 2018).

2.4.1 Conventional methods

Most of the conventional manufacturing techniques utilize the foaming agent or sacrificial phase to form the pores, which is usually not able to match the porous and mechanical requirements of the target tissue (Baino and Vitale-Brovarone 2011;Baino, Verné and Massera 2018). The porogen method is to use a polymer as the space holder or referred to as the porogen, by mixing with the glass powder and loading into a mold. The 3D porous scaffold is produced after the sintering and the porogen is burnt away during this process (Jones 2013;Nommeots-Nomm and Massera 2017). This method is simple and produce scaffolds with high porosity, but the sizes of pores are usually not homogeneous, and the internal structures may not be uniform among the same batch. Furthermore some excessively big pores can make the scaffolds fail at excessively low stress (Fu *et al.* 2011;L. Zhang *et al.* 2017).

Freeze casing can produce scaffolds with high strength but is not usually studied for bone regeneration because of the small pore size and low interconnectivity (Nommeots-Nomm and Massera 2017). The foam replica process can satisfy many requirements such as porosity (85 ± 2%), pore size (100 - 500 μm), interconnectivity, compressive

strength (11 ± 1 Mpa) as well as elastic modulus (3 ± 0.5 Gpa) But the preparation is complex and the remnants of the sacrificial templates raise question over the materials toxicity (Fu *et al.* 2008;Nommeots-Nomm and Massera 2017).

There are more conventional manufacturing methods, for example, salt leaching, fiber bonding, emulsification and so on. However, no control over the architecture and structural properties, such as pore geometry and interconnectivity can be achieved (Butscher *et al.* 2011;Lee 2015). In order to overcome the shortages of these methods, new techniques like CAM are developed to design and manufacture customized scaffold with complex structure and controllable morphology (Bose, Vahabzadeh and Bandyopadhyay 2013;Brunello *et al.* 2016;Guvendiren *et al.* 2016).

2.4.2 Additive manufacturing methods

There are many additive manufacturing methods, called 3D printing techniques. They can be classified into four types, selective laser sintering (SLS), stereolithography (SLA), fused deposition modeling (FDM) and binder-based 3D printing including robocasting (Hwa *et al.* 2017). The schematic diagrams of FDM, SLA and SLS are demonstrated in Figure 2, the binder-based 3D printing which was used in this study will be presented in the section of Materials and Methods.

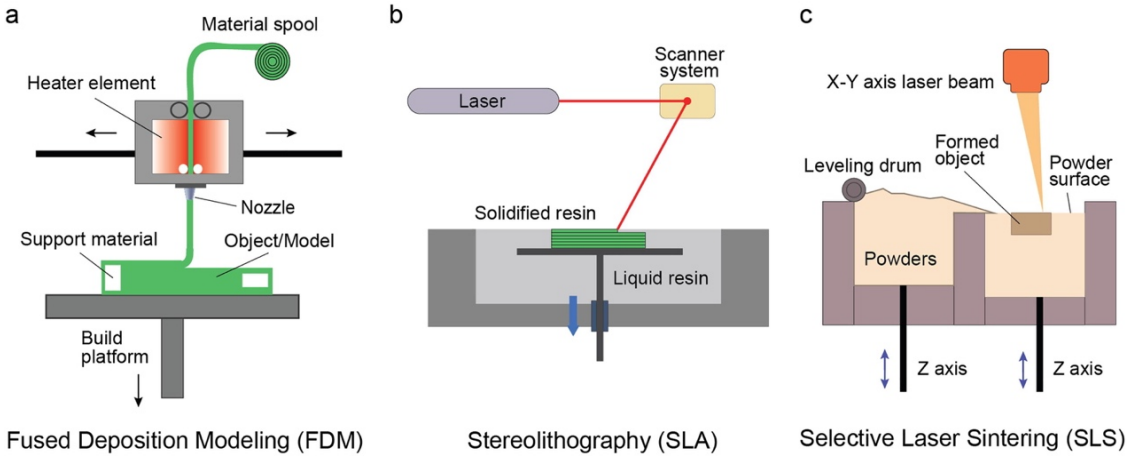

Figure 2. *Schematic diagrams of the methods of FDM, SLA and SLS (Zhang et al. 2019). Reproduced with permission (order number #4776951247264).*

(1) Selective laser sintering (SLS)

Selective laser sintering is a powder-based technique. The metal or ceramic particles are fused into large parts by the heating effect of laser (Williams *et al.* 2005;Kolan *et al.* 2012). Complex geometries could be produced by this method (Kolan *et al.* 2012;Du, Fu and Zhu 2018). Metallic scaffolds used for load-bearing application can be manufacture directly by a layer by layer process (Bae *et al.* 2014;Du, Fu and Zhu 2018).

However, this method is limited by the accuracy of the laser and the cost of the machine (Kolan *et al.* 2012;Du, Fu and Zhu 2018;Ma *et al.* 2018). Additionally, the process is much slower compared to the other options such as the ink writing technique (Nommeots-Nomm and Massera 2017).

(2) Stereolithography (SLA)

Stereolithography is a slurry-based technique, which uses a UV laser to harden the photosensitive polymer liquid and manufacture the complex structure slice by slice (Griffith and Halloran 2005;Nommeots-Nomm and Massera 2017). The SLA can provide the highest resolution and reproducibility for complex construction mimicking biological tissue (Baino, Verné and Massera 2018;Du, Fu and Zhu 2018).

However, the normal photocurable materials are not usually used in bone tissue engineering, because of their inadequate biodegradation, biocompatibility, and mechanical properties (Lee *et al.* 2007;Du, Fu and Zhu 2018). In addition, the slow processing time and expensive equipment also limit the application of the SLA technique (Nommeots-Nomm and Massera 2017;Baino, Verné and Massera 2018).

(3) Fused deposition modeling (FDM)

Fused deposition modeling is a filament-based technique. The filament, a polymer or a polymer/ceramic composite, is melted using heat and extruded through a nozzle, and then deposited and hardened layer by layer to form a solid structure (Pham and Gault 1998;Zein *et al.* 2002;Du, Fu and Zhu 2018). This technique can produce scaffolds with designed 3D structures which exhibited favorable mechanical properties (Zhang *et al.* 2019).

However, FDM is only able to manufacture the limited and regular shapes and structure, because the viscosity of melted filament leads resolution is not too high. In addition, the material used needs to be in filament form that restricts the application of bioactive glass as part of a composite (Chia and Wu 2015).

(4) Robocasting

Robocasting is one of the binder-based 3D printing techniques which is mostly used for the scaffold made by bioactive glass. The process relies on the ink, which is a mixture of the ceramics powder and binder and works as the carriers of ceramic particles and binds them together before sintering. The ink is extruded through a nozzle and deposited on a platform and hardened at room temperature. The green body is then sintered (Nommeots-Nomm and Massera 2017).

An ideal ink should be easily mixed with glass powder in a high load and maintain viscosity applicable for printing. The pseudoplastic properties, adequate storage modulus as well as yield strength are needed to undertake the weight of layers and the spanning distance (Nommeots-Nomm and Massera 2017). Pluronic F-127 is commonly used to prepare the binder because it owns a thermally reversible property, i.e. it is liquid at low temperature and turns to solid at room temperature, and is able to dissolve in water as a stable suspension (Lenaerts *et al.* 1987;Cohn, Sosnik and Garty 2005;Franco *et al.* 2010;Nommeots-Nomm and Massera 2017).

Robocasting possess several advantages, such as the preparation of ink is simple and easy to adjust, the printing process is faster than other competing techniques, the cost of the machine is relatively affordable, and it can be used for bio-fabrication (Nommeots-Nomm and Massera 2017;Baino, Verné and Massera 2018). However, the spatial resolution is relatively low and scaffold may collapse before or during the sintering due to non-optimal particle packing (Baino, Verné and Massera 2018;Du, Fu and Zhu 2018).

There are two main advantages of 3D printing techniques, firstly, the internal and overall structures are controlled and adjusted easily to achieve customized grafts (Lee and Cho 2015). Secondly, the quick manufacture and reproducible product can decrease the experimental period and errors (Lee 2015).

2.5 Biological response and bone regeneration process

The host response to the implant is activated within minutes with the thrombus formation, inflammatory cells and cytokines which as illustrated in Figure 3 (Kohli *et al.* 2018). The hematoma is formed first and the immune system is active when the material is implanted in vivo, and then the new formation of bone takes place approximately four weeks later (Nuss and Rechenberg 2008;Woodruff *et al.* 2012;Chen *et al.* 2016;Matsumoto *et al.* 2016). The angiogenesis is critical for the healing. Vessels invade into the biomaterial before the regeneration of bone. In the next six months or even at longer time, the woven bone will be formed and remodeled to the lamellar bone (Schindeler *et al.* 2008;Matsumoto *et al.* 2016). The inflammation, formation of new bone and remodeling are overlapped with each other during the whole regeneration process of bone (Kohli *et al.* 2018).

The immune system is able to generate the vascularization and regeneration or foreign body reactions depending on the materials, and the result is affected by various factors including the ions released, surface properties of the material, and porosity of the scaffold (Sheikh *et al.* 2015).

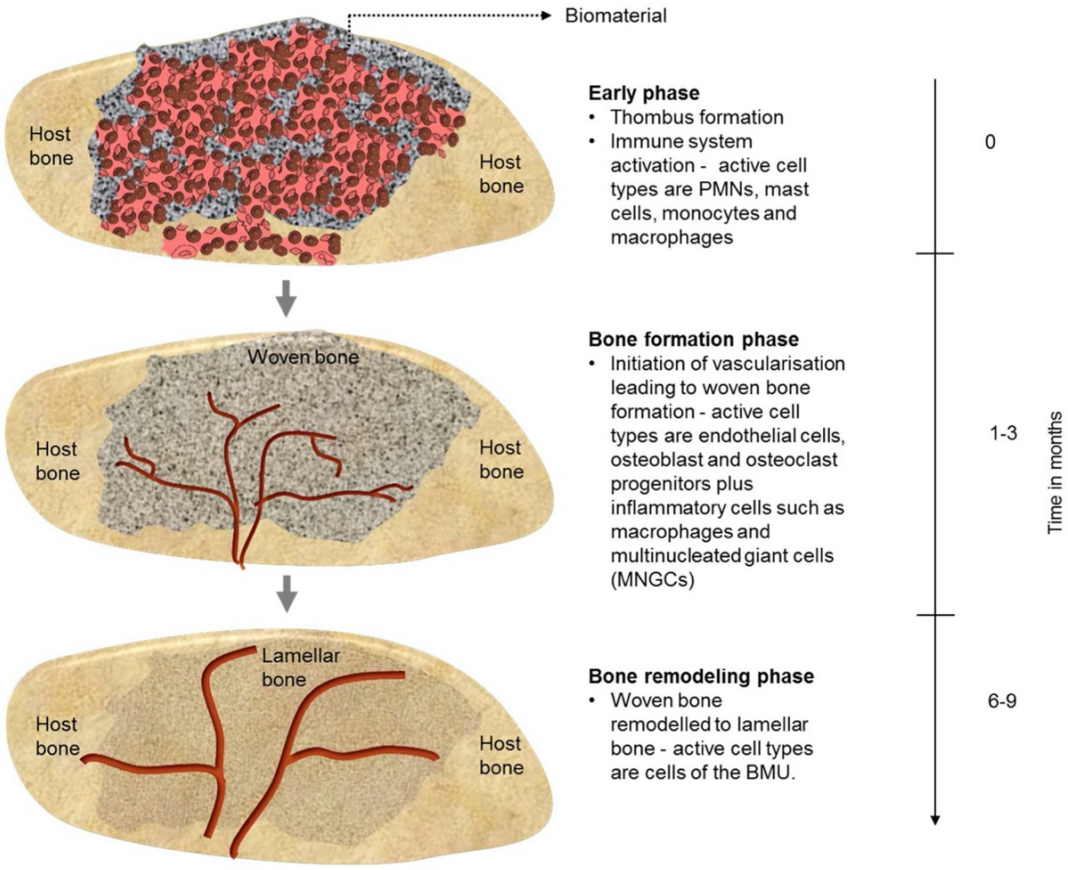

Figure 3. *Host response to implantation (Kohli et al. 2018). Reproduced with permission (order number #4776951061715).*

2.5.1 Biological responses to elements

The key to understanding the behavior of the scaffold is to investigate the ions released from the material, and many studies incorporated different ions into a basic bioactive glass to control the dissolution rate and dissolution by-product, to improve the function of the scaffold. Some ions like Ca and P are the main components of human bone which play an important and essential role obviously in the formation of bone. Moreover, the mechanism of interactions between ions and cells at a specific concentration could be also critical to design and manufacture the scaffold with favorable biological reactions and ionic dissolution (Hoppe, Güldal and Boccaccini 2011). Especially the metal ions usually work as the co-factors with enzymes, that active signaling pathways (Beattie and Avenell 1992;Sun, Wataha and Hanks 1997).

Ca can activate Ca-sensitive receptors in osteoblasts through the regulation of the expression of insulin-like growth factors to increase the proliferation of osteoblast (Valerio *et al.* 2009;Marie 2010). In vitro, the low and medium concentration of Ca, 2 - 4 and 6 - 8 mmol, benefits to the proliferation and differentiation of osteoblasts, and the

mineralization of extracellular matrix (ECM), however, then it becomes toxic when the concentration is over 10 mmol (Maeno *et al.* 2005). P can promote the expression of MGP (matrix Gla protein) of osteoblasts which is a crucial regulator for the osteogenesis, at the concentration of 10 mmol in vitro (Julien *et al.* 2009). $Si(OH)_4$ is able to stimulate the differentiation and the formation of collagen I in the culture of osteoblasts of human in vitro, at the concentration of 10 μmol (Reffitt *et al.* 2003). Si is able to induce the calcification of bone at a high concentration which was detected in the matrix environment at early stages (Carlisle 1970, 1981).

Sr and Mg are from the same main group and have similar chemical properties of Ca, therefore they are used to substitute the Ca in bioactive glass for the improvement of the scaffold. They are also found in the HA layer of bone (Boivin *et al.* 1996;Hoppe, Güldal and Boccaccini 2011). Sr exhibits a positive effect on the osteogenesis in vivo by increasing bone formation and decreasing bone resorption (Marie *et al.* 2001;Verberckmoes, De Broe and D'Haese 2003). Similarly, the SrO containing bioactive glass enhanced the proliferation of pre-osteoblasts and inhibited osteoclasts both in vivo and in vitro(Gentleman *et al.* 2010). It was reported that 3D printing of Sr-doped silicate glass scaffolds markedly promote the gene expressions which were related to the osteogenesis and proliferation in the culture of rBMSCs (rabbit bone marrow-derived mesenchymal stem cells) (Zhu *et al.* 2016). Mg is also elementary in the metabolism of bone and interacts with the integrin which affects the stability and adhesion of osteoblastic cells (Yamasaki *et al.* 2002;Zreiqat *et al.* 2002). Mg is beneficial for the formation of new bone in vivo, and the depletion of it will impair the growth of bone (Rude *et al.* 2003, 2004, 2005).

It has been investigated in vivo, in rats, that dietary B can promote osteogenesis and in turn, a boron-free diet could affect bone remodeling (Gorustovich *et al.* 2008;Uysal *et al.* 2009). In addition, B ions can promote the translation of the mRNAs which encode the growth factors, such as VEGF and TGF-b, to simulate the angiogenesis and wound healing (Dzondo-Gadet *et al.* 2002). B, in the form H_3BO_3, at a low concentration, can also improve the proliferation and growth of cells, by the activation of the MAPK (mitogen-activated protein kinase) pathway (Park *et al.* 2004).

Finally, bioactive glass scaffolds containing boron can improve angiogenesis by increasing the release rate of therapeutic ions, including B itself (Wang *et al.* 2014). However, there are some in vitro tests showing that the boron was toxic at a relatively high concentration (Modglin *et al.* 2013). The cellular test using the medium with increasing Boron content to culture osteoblasts showed that the proliferation of cells was inhibited and even the amounts of cells decreased over time when the concentration of

B was above 1.5 mmol (R. F. Brown *et al.* 2009). When the concentration of B was below it, the proliferation of cells was supported. And in other tests using the boron-doped glass, the thresholds of B concentration were 0.65 and 0.5 mmol (Fu *et al.* 2009;Ojansivu *et al.* 2018). But this toxicity could be alleviated by dynamic culture conditions or using animal testing (Ning *et al.* 2007). There was no toxicity and exhibited beneficial tissue infiltration in the rat test in vivo (Gorustovich *et al.* 2006;Q Fu *et al.* 2010;Jung *et al.* 2013). The inconsistent results about the toxicity of boron among different conditions suggested that there is a threshold value for the B which is significant for the design of scaffolds and improvement of cellular tests, such as the pre-treatment and more dynamic culture system, which are able to reduce or diminish the toxic effect (R. Brown *et al.* 2009;Rahaman *et al.* 2011).

2.5.2 Remodeling process of bone

Bone plays provide attachment sites for tendons and muscles, to protect the soft tissue and organs, and to store the mineral elements and marrow (Robling, Castillo and Turner 2006;Datta *et al.* 2008). It is a vascular mineralized connective tissue containing four types of cells, osteoblasts, osteocytes, osteoclasts as well as bone lining cells, and it is very dynamic which is critical for the homeostasis of Ca (Buckwalter *et al.* 1995;Downey and Siegel 2006;Dallas, Prideaux and Bonewald 2013). Bone remodeling is a continuous process of resorption and formation of bone, that is necessary for the regeneration and healing (Florencio-Silva *et al.* 2015).

Bone remodeling is a series of events, which involved the activation, resorption as well as formation of the bone and interactions between different types of cells (Dimitriou *et al.* 2011;Mello *et al.* 2016;Katsimbri 2017). In the bone marrow, the mesenchymal stem cells are able to differentiate to osteoblasts and the hemopoietic precursors can turn to osteoclasts (Sims and Martin 2014). The cycle of remodeling can be simplified using three phases. Firstly, osteoclasts initiate the resorption of bone. Secondly, it is the transition from the resorption to the formation of new bone, which is also called the reversal period. Thirdly, the osteoblasts form the new bone (A. Sims and H. Gooi 2008;Matsuo and Irie 2008).

The structure of bone is essential for its function and behavior like the remodeling, and the interactions between the material and those types of cells need to be considered (Kohli *et al.* 2018). Therefore, it is significant to understand the process of remodeling of bone for the development of biomaterial scaffolds used in bone tissue engineering.

2.6 Evaluations in vitro

The test performed in vitro aims at evaluating 1) the release rate of ions, 2) the ability of the material to precipitate HA and 3) the cell/material interactions. There is no inflammation, immune response, clot formation, wound healing and vascularization (Ratner *et al.* 2004). Therefore, the results from materials evaluation in vitro are questionable in the clinical context. However, those tests are necessary to predict the in-vivo outcome. Furthermore, 3D culture using scaffolds is becoming more popular because the traditional 2D studies are not able to mimic the 3D environment in vivo (El-Rashidy *et al.* 2017).

2.6.1 Methods for the evaluation of dissolution

The bioactivity and biodegradability are the requirements for the ideal biomaterial scaffold used in bone repair, and critical for the interactions between the tissue and material. Therefore, the study of the detailed degradation is necessary to design an ideal scaffold, and the dissolution rate is controlled by the composition of the material, which can be tailored in a broad range (Susanne Fagerlund *et al.* 2012). The effect of the ions released by the bioactive glass on the physiological responses related to bone generation was studied and reviewed, as the results, some ions are able to simulate the osteogenesis and angiogenesis, as well as antibacterial effect. However, ions could be beneficial or toxic depending on the concentration, thus understanding and controlling the dissolution of those glasses is required (Hoppe, Güldal and Boccaccini 2011;Fagerlund, Hupa and Hupa 2013).

The dissolution behavior and the conversion of HA of the bioactive glass are typically evaluated through immersing the samples in TRIS buffer solution or simulated body fluid (SBF) at 37 ^{o}C (Huang, Day, *et al.* 2006;Huang, N. Rahaman, *et al.* 2006;Yao *et al.* 2007;Qiang Fu *et al.* 2010). The bioactivity for the bioactive glass is generally exhibited when the material is exposed to the SBF or other buffers and then HA layer is formed on the material surface (Susanne Fagerlund *et al.* 2012).

The evaluation of the dissolution is usually performed via the static method in vitro, but there is also another type of method, which is the dynamic flow test, providing relative constant pH and ionic concentration in the solution (Fagerlund, Hupa and Hupa 2013). With the SBF flow throughout, the situation is closer to the dynamic condition in vivo, and the toxicity by the high level of ions could be reduced for the application in cell culture (Fagerlund *et al.*, 2012).

2.6.2 Cellular evaluation in vitro

(1) The selection of available cell models

There are various osteoblastic cell models used in vitro to investigate the biocompatibility, osteogenesis of biomaterials, and also the mechanism and regulation of bone regeneration. The various cell models include, but are not limited to, induced pluripotent stem cells, primary cells from humans or animals and immortalized cell lines. They all exhibit advantages and drawbacks. Therefore, the selection of the cell model for the subsequent research needs to be considered (Richards *et al.* 2016).

For the application of human primary cells, the principal advantage is the clinical applicability and without the difference of interspecies. However, human cells tend to exhibit different phenotypes because of the isolation from different sites of the body. Additionally, another disadvantage is the limited accessibility of human cells (Kasperk *et al.* 1995;Martínez *et al.* 1999). To overcome these limitations, cells isolated from animals are developed for research models (Pearce *et al.* 2007). In particular, the rat osteoblasts are attractive as a model because of its availability and well known genome sequence (Aronow *et al.* 1990;Abe *et al.* 2000). Although the cells can be harvested easily from rats, controlled age, and gender, the interspecies difference is the main disadvantage. In addition, the different weight and sizes of animals affect the composition, structure and mechanical properties of bone, and the healing process and signal pathways could also be affected (Pearce *et al.* 2007).

The application of commercial cell lines possesses many advantages including the infinite amounts of cells without isolation from donors, simple maintenance and stable phenotype. The main disadvantage is that the cells do not reflect the impact features of phenotypes as the normal osteoblasts, and the proliferation is non-physiological (Grigoriadis *et al.* 1985;Leis *et al.* 1997;Wang *et al.* 1999;Richards *et al.* 2016). Nevertheless, the cell lines are prevalently used in the studies, including the MC3T3- E1, hFOB, MG- 63, SaOs-2 and U2OS (Richards *et al.* 2016). The MC3T3- E1 is one of the most used osteoblastic cell lines which is from the calvaria of the mouse, with a typical pre-osteoblastic phenotype (Wang *et al.* 1999). it is reported that the MC3T3 cells presented inconsistent cell cycling at high passages and this senility of replication was similar to the cells from humans, which makes them more attractive for the studies of bone regeneration (Grigoriadis *et al.* 1985;Richards *et al.* 2016).

The primary cells from the mouse are usually utilized for the study of mutation of specific genes which are related to the osteogenesis or development of bone (Bouvard *et al.* 2001;Malaval *et al.* 2009;Monfoulet *et al.* 2010;Watabe *et al.* 2011). MC3T3-E1 actually

is always used to study the properties of biomaterial and interactions with cells, because of the similar growth rate compared to the osteoblasts of human (Richards *et al.* 2016).

The appropriate selection of the cell line is critical to design the experiment in vitro, which enables a better understanding of the physiological responses and regeneration process. MC3T3-E1 enables the study of some phenotypic phases of osteoblasts and provides a homogenous population for standardized studies, which is effective for the cytocompatibility and toxicity evaluation at the early stage. It seems like a suitable alternative for human primary cells. However, the cell line does not present all the cell behaviors and interspecies differences. Meanwhile, the other elements, including the culture medium, operation of cell seeding, culture system and the geometry of scaffolds, can also affect the behavior of cells in vitro and finally lead various results (Richards *et al.* 2016).

(2) Cell culturing system

The extracts of glass are used to test the effects of ions released from the material, which influence the cellular behaviors without the concerns about the surface features, pore size and other structural properties of the scaffolds (Schneider *et al.* 2006;Mitrossilis *et al.* 2009). But the monolayer culture is quite different from the physiological condition of bone regeneration, and the continuous dissolution of materials, as well as the changes (conversion to HA), are also ignored by this method. Therefore, the 3D model is becoming more and more popular which is ought to more closely simulate the natural condition (Richards *et al.* 2016).

The culture systems for the study of bone formation usually have some features in common. There has to be enough number of cells and the media for the cell growth, and also allows the mineralization if required. Additionally, a substrate where the cells grow on is needed. Finally, the media need to keep at the physiological pH, or a little bit more alkaline (Boskey and Roy 2008). Most of the cultures are implemented in the incubators with 5% CO_2, in order to simulate the hypoxic environment of osteocytes (Hirao *et al.* 2007).

For the 3D culture, a high density of cells in a low volume of media is seeded to the scaffold a few hours before the media added, which is to promote the attachment of cells to the scaffold (Malladi *et al.* 2006;Soung *et al.* 2007). The bovine or fetal calf serum is normally contained in the culture medium (1% to 20%). The serum is added to enhance the growth and differentiation of cells by exposing more cells to the growth factors and cytokines. And the antibiotics, mostly penicillin and streptomycin, are added to the culture media to prevent bacteria (Boskey and Roy 2008). Additionally, the glutamine or glucose

are also added in the media to maximize the metabolism (Bettger and McKeehan 1986). To be noticed, those additives above generally don't change the concentrations of mineral ions in the culture medium (Boskey and Roy 2008).

The cellular experiments in vitro are able to significantly reduce the sacrifice of animals and the period of testing, examine the specific exogenous factor, as well as provide better reproducibility (Boskey and Roy 2008). However, dead cells usually are not removed automatically, and the interactions between different cell types are absent (Boskey and Roy 2008). In the last few years, some models to mimic the interactions between immune cells, osteoblasts, and osteoclasts using a co-culture system has been developed. Its application is mainly to understand the mechanism of the regeneration process rather than the evaluation of the materials (Wu *et al.* 2010;Bongio *et al.* 2016;Chen *et al.* 2016;Kohli *et al.* 2018).

However, it is difficult to design a feasible and comprehensive model in vitro to research the whole regeneration of bone (Kohli *et al.* 2018). Because the remodeling process depends on the dynamic balance of resorption and formation of bone (Seeman 2009;Florencio-Silva *et al.* 2015). Tests in vitro are normally related to bone formation, but the bio-resorbability cannot be accurately simulated (Kohli *et al.* 2018).

Another challenge in vitro is to test the ability of the implant to maintain enough mechanical support until the scaffold is replaced by the degradation of material and tissue ingrowth (Hutmacher 2000). The advantages of using animal models are to evaluate the biomaterials scaffolds in different types of tissues, under different loading environments for a long period (Li *et al.* 2015).

3. MATERIALS AND METHODS

This study aims to evaluate the dissolution behavior (static vs. dynamic) and the cell compatibility of 3D printing bioactive borosilicate glass scaffolds. Scaffolds were manufactured via two routes: 1) porogen burn-off and 2) 3D prototyping. The glasses were thoroughly studied in (Tainio 2016;Pohjola 2017).

3.1 Preparation of scaffolds

The borosilicate glasses used were labeled B12.5 and Mix. The B12.5 glass is based on the commercial bioactive silicate glass S53P4 (BonAlive Biomaterials Ltd, Turku, Finland) where 12.5 mol% of SiO_2 is substituted by B_2O_3. The Mix glass is based on the B12.5 and with the substitution of CaO with 5 mol% MgO and 10 mol% SrO. The process of the preparation of glass powder was described in detail in the Master thesis of Jenna Tainio, including the process of mixing, melting and grinding (Tainio 2016). The diameter of the particles is less than 38 μm to meet the requirement for 3D printing and porogen burn-off processes.

3.1.1 Scaffolds made by Porogen burn-off

In this process, a porogen is introduced into the scaffolds, before sintering. The porogen is assumed to fully decompose and volatilize during the heating cycle used for the firing of the scaffolds, leaving pores behind. The porogen should not be toxic. The ammonium bicarbonate, NH_4HCO_3 (Sigma-Aldrich, 99.5%, CAS No. 1066-33-7), was used as the porogen and mixed with glass powder in the ratio of 30 vol% (glass powder): 70 vol% (porogen). The appropriate mass of each constituent was calculated knowing the densities of B12.5, Mix, and porogen, which were 2.64, 2.80, 1.586 g/cm^3 respectively. The mixture of porogen and glass powder was made and stored in plastic bottles separately for each batch.

A similar mass of the mixture was loaded into a cylindrical mold with a diameter of 15 mm. Then a hydraulic pressure around 25 MPa was applied to compress the mixture. The compacted pellets were taken out and collected on a ceramic plate for the following sintering.

3.1.2 Scaffolds made by 3D printing

The ink was manufactured for each type of glass powder with the size under 38 μm and 25 wt% Pluronic 127 solution which acted as the binder. The 25 wt% Pluronic solution was made by mixing the Pluronic 127 (Sigma-Aldrich, CAS No. 9003-11-6) and distilled water with a magnetic stirrer in a beaker in an ice bath overnight, until the solution turned clear. The solution was then stored at 4 ^{o}C. This glass-containing ink consisted of 30 wt% glass powder and 70 wt% Pluronic in weight was mixed in a plastic bottle. Then this bottle was vibrated on the Vibrofix VF1 electrical shaker (IKA®-Labortechnic, Staufen, Germany) at 2500 rpm for 30 seconds and then cooled for another 30 seconds in the ice bath. The mixing-cooling cycles usually were repeated 5 times at least until the ink was homogenous. The formation of bubbles is unavoidable, but the bubbles are expected to be invisible. The homogenous ink was loaded into a 10 ml syringe and then was transferred into Optimum® 3cc special printing syringe barrels (Nordson EFD, Bedfordshire, England), which was blocked by a plastic plug. The parafilm was used to seal the tip of the syringe to prevent the ink flowing out. There was always an interval between the ink preparation and the printing process which was from 10 min to 30 min depending on the variation in room temperature, to ensure the proper viscosity of the ink. The ink was prepared fresh prior to any printing.

The 3D printing process was conducted using a 3Dn-Tabletop (nScrypt Inc., Orlando, Florida, USA) layer by layer, and controlled via the Machine Tool 3.0 system software. The ink was loaded in the machine and extruded through the SmoothFlow Tapered Tips with inner diameter of 0.41 mm (Nordson EFD Optimum® SmoothFlow™, Westlake, Ohio, USA) and then onto the acrylic Color Laser Printer & Copier OHP Film sheets (Folex AG, Seewen, Switzerland). The material feed was set to 18.0–22.0 psi pressure, to maintain a continuous flow during movement of the tip. The diagram of this robocasting process is shown in Figure 4. The script designed for the layer pattern was described in detail elsewhere, in order to obtain cylindrical scaffolds with controlled interior structure (Pohjola 2017). Printed scaffolds needed to be dried at room temperature for 24 h to reduce the risk of collapse, and then the redundant parts are removed by the scalpel. Finally, these green bodies were ready for sintering.

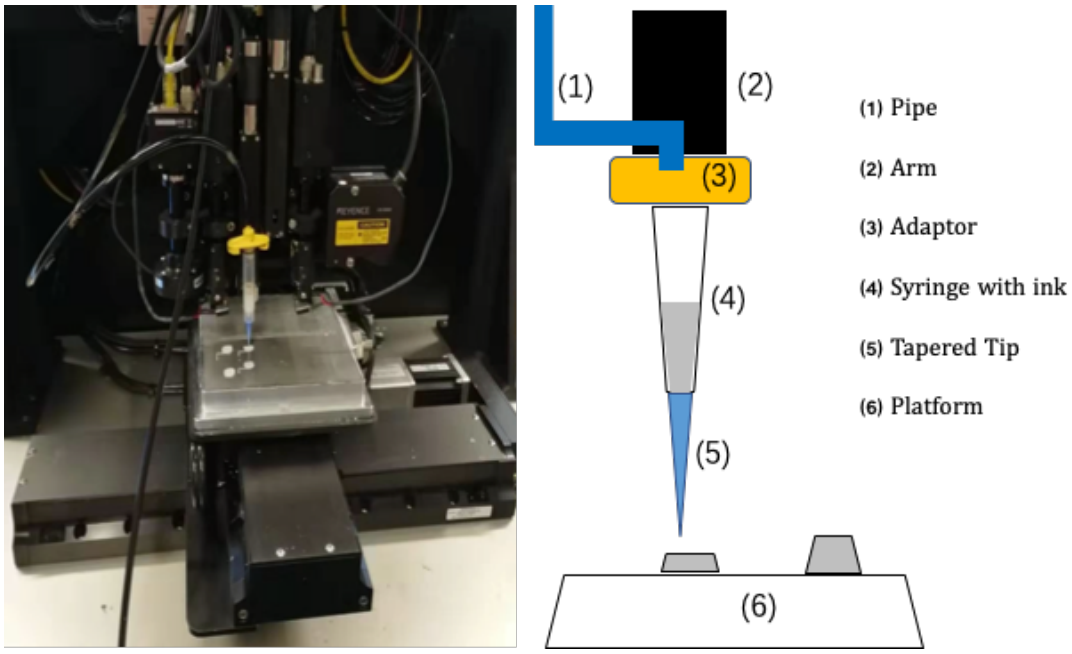

Figure 4. *The diagram of robocasting. The left part is the photo of the 3D printer during scaffolds printing, and the right part is the diagram based on the real machine, where the pipe is to provide the air pressure from the machine, the arm is to fix the syringe on it, the adaptor is to connect the pipe and syringe, and the platform can move along x and y axis according to the script.*

3.1.3 Sintering

The sintering temperatures for B12.5 and Mix were 545 and 542 ℃ as determined in the Master thesis of Juuso Pohjola using XRD and DTA (Pohjola 2017). The green bodies were collected onto a ceramic plate in the furnace (Nabertherm LT 9/11/SKM electric muffle furnace) in an air atmosphere. The sintering process had 3 phases: 1) from room temperature to 300 °C at 1 °C/min, 2) then the temperature was increased from 300 °C to the sintering temperature at 5 °C/min and 3) the sintering temperature was maintained for 1 hour. The furnace was then let to cool down to room temperature. Sintered scaffolds were taken out and stored in a desiccator for the subsequent tests. Both Porogen and 3D printing scaffolds were sintered following the exact same protocol. The slow, multistep, heat treatment was not only to sinter glass particles but also to slowly remove the porogen and binder from scaffolds, as well as to avoid sudden shrinkage which might cause cracking of the scaffolds.

3.1.4 Physical and Structural properties

The estimation of the scaffolds' porosity was performed according to previously reported method (Chen, Thompson and Boccaccini 2006). Briefly, the calculations of the volumes of the scaffolds made by Porogen burn-off and 3D printing were according to the cylinder-shaped and truncated cone-shaped volume formula, separately. The mass was

measured using a scale, heights and diameters were measured using a caliber to estimate the volumes and therefore the apparent density of the scaffolds was estimated using the volume divided by mass. The porosity was estimated using the following equation:

$$Porosity = (1 - \rho/\rho 0) \times 100\%$$

where the ρ0 was the bulk density, and ρ was the apparent density (mass divided volume) of each scaffold. The porosity for each type of scaffolds was obtained from all scaffolds prepared, which was around 50 scaffolds per glass composition and scaffold processing and expressed as mean ± standard deviation.

The shrinking rate of the porogen burn-off scaffolds was not done due to difficulties in analyzing the sample mass and size before sintering. This was due to the crumbly nature of the green body. The shrinking rate of 3D printing scaffolds was calculated looking at the pores area and strips width, before and after sintering. Measurement were made by optical microscopy

3.2 Dissolution tests

The dissolution tests were performed in static and dynamic conditions in Simulated Body Fluid (SBF). The dissolution/reaction of the scaffold in SBF was studied by measuring the mass loss, pH and ionic concentrations at various time interval. SBF solution was prepared according to the protocol developed by Kokubo (Kokubo & Takadama 2006). Solution preparation is described in detail in Appendix A.

3.2.1 Static dissolution test

Scaffolds were enclosed in a 50 ml polypropylene (PP) centrifuge tube (Sarstedt AG & amp; amp; Co, Nümbrecht, Germany) and immersed in SBF or TRIS solution. The SBF groups aimed to test the bioactivity of scaffolds in immersion which can be reflected from the formation of HA and the change in ionic concentration. The parallel TRIS groups were used to test the ions leaching while the risk of ionic supersaturation was limited (Fagerlund, Hupa and Hupa 2013). The volume of SBF or TRIS in each tube was calculated to maintain a mass/V ratio constant at 20 mg/ml. There were three parallel samples for each type of scaffold and two parallel blank samples for each time point (6, 24, 28, 72, 168, and 336 h). Those tubes were placed into a shaking incubator (Multitron AJ 188g, Infors, Bottmingen, Switzerland) at 37 °C under 100 RPM. The tubes were taken out from the incubator after the corresponding intervals and the pH of the solutions measured using a S47-K SevenMultiTM pH-meter (Mettler-Toledo LLC, Ohio,

USA) at 37.0 ± 0.1 °C. And then the scaffolds were extracted from tubes and rinsed with ethanol in order to stop the reaction. The rinsed scaffolds were dried in 24-well plates at 37 °C for 48 h before measuring the dry mass. And 1 mL of the solution was taken and diluted with 9 mL 1M high purity nitric acid for ion concentration analysis.

3.2.2 Dynamic dissolution test

The dynamic dissolution was evaluated with a flow-through system which is illustrated in Figure 5. One scaffold was loaded in a home-made reactor, which was connected to the bottle of SBF solution on one end (inlet) and the outlet to tubes to collect the fluid. There was a detachable Teflon ring to adjust the cross-section of the reactor to match the size of the different type of scaffolds. The outflow was collected in 20 ml centrifuge tubes which were changed once per hour and a 500 ml beaker was used to collect the fluid during the night. The experiment for each sample was performed with SBF at 37.8 °C and 0.4 ml/min flow rate for 74 hours. The whole set-up is exhibited in Figure 5.

Finally, the scaffolds were extracted from the reactor and rinsed with ethanol in order to stop the glass dissolution, and then were stored in the desiccator. The pH of the outflow solutions was measured, and 1 mL of the solution was collected and diluted with 9mL of nitric acid to quantify the extent of the ionic release. The values from the original SBF solution were considered as the start points for the pH and ionic concentration.

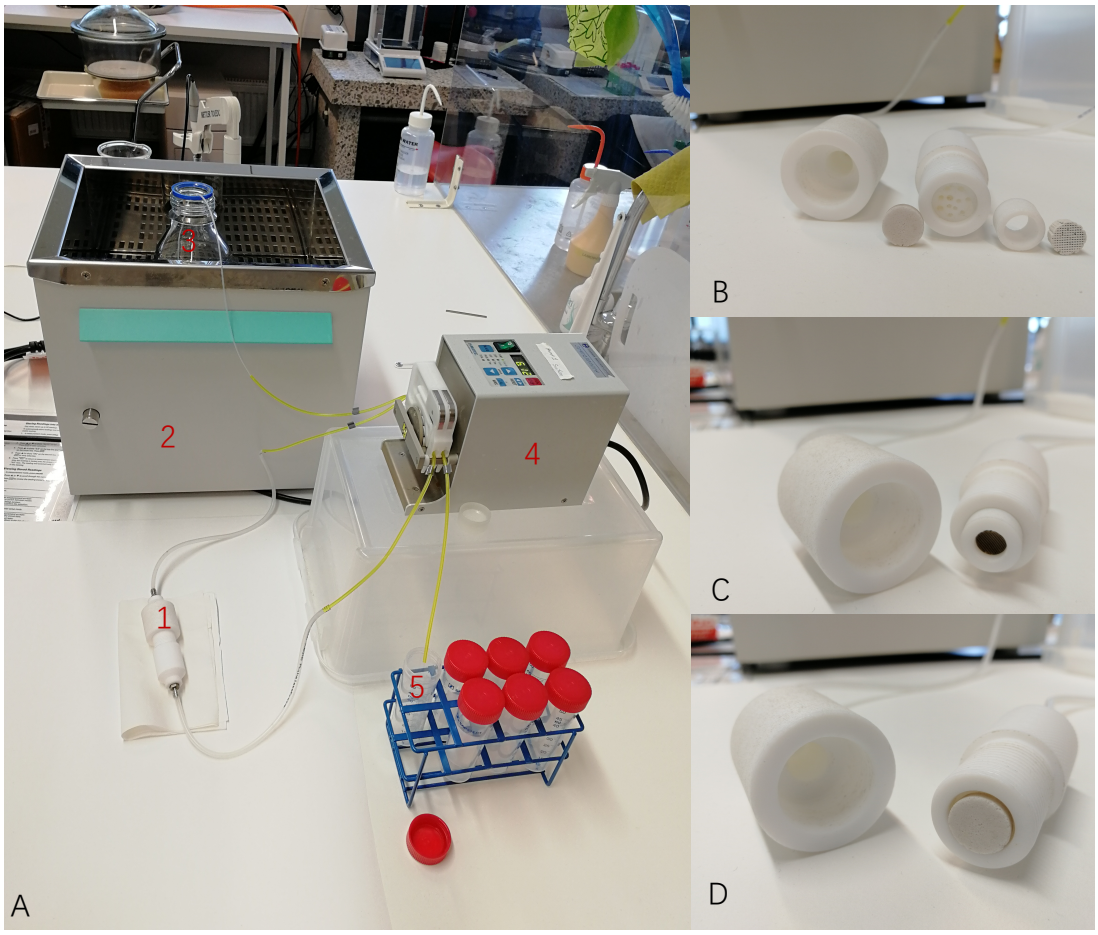

Figure 5. *Picture of the flow-through system. A is the intact system, 1 is reactor, 2 is water bath, 3 is bottle of SBF, 4 is pump, 5 is outflow; B is inner structure of reactor; C is a 3D printed scaffold adjusted by a Teflon ring; D is a porogen scaffold loaded into the chamber.*

3.2.3 Mass loss

Upon static dissolution in TRIS and SBF the mass loss of the scaffolds was quantified. The mass of the samples post-sintering corresponds to the original weight. The scaffolds which experienced the dissolution tests were dried in the incubator for 48 hours and their mass measured again. The mass loss ratio was calculated following the equation:

$$Mass\ loss\ =\ (W0\ -\ Wt)\ /\ W0\ *\ 100\%$$

Where the W_0 is the original mass after the manufacturing, and W_t is the dry mass after post-immersion for a time t.

3.2.4 Ionic concentration

1 ml solution from each sample was diluted 10 times by 9 ml 1M HNO_3. The concentrations of B, Si, P, Ca, Mg, and Sr were measured with the ICP-OES (inductively coupled plasma optical emission spectroscopy) 5110 (Agilent Technologies, California,

USA). The wavelengths used for the analysis of each ion are shown in Table 1. The concentration of Na was not analyzed in the groups with the SBF, because the initial Na content was too high.

Table 1. *Wavelengths used in the ionic concentration analysis.*

Element	B	Ca	Mg	P	Si	Sr	Na
Wavelength (nm)	249.678	422.673	279.553	213.618	250.690	216.596	588.995

3.3 Cellular tests

Cell test was performed on disks (pressed powder into pellets), on the 3D printed scaffolds, and on the porogen burn-off scaffolds, for samples B12.5 and Mix. Live and dead assay was performed to visually compare the density of live cells on the scaffolds qualitatively. WST-1 assay was used to test influence of different materials to the attachment ability and proliferation of cells.

3.3.1 Culture of cell line

The established pre-osteoblastic cell line was MC3T3-E1 syncline 4 (ATCC® CRL-2593™). The Medium for the cell culture was α-MEM (Gibco™, no glutamine, 11430030) which was supplemented with 1% antibiotics (100 U/mL penicillin and 0.1 mg/mL streptomycin), 10% fetal bovine serum (FBS) and 1% L-glutamine (ThermoFisher). The MC3T3 cells were cultured at 37 ℃ in a humidified atmosphere of 5% CO_2 balanced 95% air and were passaged around 3 days to reach over 80% confluence.

3.3.2 Preparation of glass disks

Due to the toxicity of the borosilicate glass by the rapid ions being released, thin glass disks (pressed powder into pellets) were used as reference as they possess lower dissolution rate than the samples with higher surface area. The disks were made from 315 ± 5 mg of glass powder, which was compacted under 6.5 tons for 5 mins, and then the sintering process was according to the previous scaffolds processing. The disks were stored in the Petri dishes and sealed with aluminum foil to prevent the contamination.

3.3.3 Conditioning scaffolds and Seeding on scaffolds

As the fast-initial ion release, bioactive glasses must be pre-conditioned. Similarly, the scaffolds are believed to lead to rapid initial ion released and the pre-conditioning time should be optimized (R. F. Brown *et al.* 2009;Liu *et al.* 2013). Pre-conditioning was conducted in the laminar flow bench. According to the different sizes of scaffolds, the

scaffolds made by porogen burn-off and 3D printing were placed in 24-well plates and 48-well plates, with 2ml and 1ml medium, separately. The well of 24-well plates was too big for the 3D printing scaffolds that many cells would attach on the wall of well rather than on the scaffolds. The plates for pre-treatment were placed in the incubator for 24, 48, 72 h in different batch. After the selected intervals, the medium was sucked off and were stored in tubes for the further ionic concentration analysis. And then the scaffolds and disks were rinsed by PBS 3 times and prepared for seeding. The amounts of cells seeded on the scaffolds were according to the volumes of different type of scaffolds according to a ratio of 1×10^3 cells per mm^3, even the cells were not able to migrate all over the inner space of scaffolds during the limited time. In addition, the total amount of cells that possible to be harvested each batch was limited by the capacity of flasks and incubator, the amounts of cells needed for each well were adjusted.

The concentrated cell suspensions were used to seed cells on the surface of scaffolds, from 50 to 150 ul depending on the amounts of cells required for each well. The scaffolds seeded cells were placed in the incubator for 0.5 to 1.5 h as the pre-culture period which permitted cells to migrate through and adhere on the strips of scaffolds, rather than be flushed away by medium before the adhesion. After pre-culture, the scaffolds with attached cells were placed in the incubator for 24 h with 2 ml or 1 ml medium according to the size of wells. The disks were placed in the 24-well plates and seeded with fewer amounts of cells than the scaffold. The protocol of the seeding process is illustrated in Table 2. There were two parallel samples for each type of scaffolds. The Material control groups were scaffolds without seeding cells which were used to assess the level of autofluorescence from the material. The positive and negative control group were that cells were seeded on the normal glass slides without scaffolds, which is to examine the situation of cells and stains.

Table 2. *The diagram of cell seeding protocol with amounts of cells and volume of medium.*

24-well plate	Sample 1	Sample 2	Disk 1	Disk 2	Material control	Material control
B12.5 P	3×10^5, 2ml	3×10^5, 2ml	5×10^4, 2ml	5×10^4, 2ml	2 ml	2 ml
Mix P	3×10^5, 2ml	3×10^5, 2ml	5×10^4, 2ml	5×10^4, 2ml	2 ml	2ml

48-well plate	Sample 1	Sample 2	Material control	Material control
B12.5 3D	2×10^5, 1ml	2×10^5, 1ml	1 ml	1 ml
Mix 3D	2×10^5, 1ml	2×10^5, 1ml	1 ml	1 ml
Positive control	2.5×10^4, 1ml	2.5×10^4, 1ml		
Negative control	2.5×10^4, 1ml	2.5×10^4, 1ml		

3.3.4 Live & Dead assay

The Live and Dead assay was used to assess the cell viability on different materials. After cells cultured with scaffolds for 24 h, the medium was discarded from each well. According to the Live & Dead Kit (Live/Dead Cell Double Staining Kit, SIGMA-ALDRICH, 04511), the cells were stained for 40 mins in the incubator. The samples were observed under the fluorescence microscope (Olympus) with a Leica DFC450 camera after rinsing with PBS.

3.3.5 WST-1 assay

WST-1 cell proliferation assay (Roche Diagnostics, Indianapolis, Indiana) was performed according to the manufacturer protocol. The first assay was performed to analyze the effect of materials conditioned for 48 h on the cellular viability. 5×10^4 and 2.5×10^4 cells were seeded in 24-well and 48-well plates, respectively for porogen and 3D printing

scaffolds, until cells spread all over the bottom. Materials which were already conditioned for 48 h were moved to the corresponding wells where cells grew well with the new medium. After 24 h culturing in the incubator, the materials and medium were removed from the wells, and fresh medium containing 10% WST-1 was added into those wells and incubated at 37 °C for about 1 h until the color of the medium changed to yellow. An optical microscope was used to image the cells and a Spectrofluorometer Xenius XM (SAFAS) was used to measure the absorbance at 440 nm against a background control as blank. The absorbance indicated the mitochondrial activity was used to compare the cell viability.

The second assay was to analyze the cellular viability using the extract from the 72 h conditioned medium, which diluted to different concentrations. The four types of materials were conditioned in a 12-well plate with 4 ml medium for each well in the incubator. After 72 h, the left medium around 2.5 ml in each well was diluted to different concentrations of 50%, 25%, 10%, 5%, 1%, 0.5%, and 0.1% with the culture medium. There were two 48-well plates, which represented 24 h and 48 h culture period, seeded with 1×10^4 cells in each well. Until cells spread all over the bottom, the medium was discarded, and the different concentrations and types of 72 h conditioned medium were added into the corresponding wells and cultured in the incubator. After the desired culture time, the conditioned medium was discarded and the 10 % WST-1 was added for the absorbance measurements. The photos of the situation of cells were taken from one plate two times after 24 and 48 h.

3.3.6 Ionic concentration of medium

The conditioned medium collected from the pre-treatment for 72 and 24 h were withdrawn and diluted 10-fold with 1M HNO_3, and then the ionic concentration was measured using the ICP-OES, following similar protocol for the dissolution study.

4. RESULTS

This section presents the results from experiments, including the structural properties of scaffolds manufactured using two methods (porogen burn-off and 3D prototyping), the dissolution rate of the scaffolds in both static and dynamic conditions and a preliminary cell culture test.

4.1 Structural properties

The porosity and pore size are the two main properties to be compared when manufacturing scaffolds using various techniques. The overall porosity, scaffolds volume and size of the scaffolds were average values (with standard deviations) from 50 (porogen burn-off) and 90 (3D printed) samples manufactured using the B12.5 and Mix composition. Those parameters are reported in Table 3. The samples produced via porogen burn-off are labeled as B12.5 P and Mix P while the 3D printed scaffolds are labeled B12.5 3D and Mix 3D. Besides, the sizes of pores of the scaffolds made via 3D printing were measured from 12 sides (tops and bottoms of 6 scaffolds) of those scaffolds and 6 pores on each side, which were shown in Table 4.

Table 3. *Porosities, volumes and size of 4 types of scaffolds.*

Type of scaffolds	Porosity (%)	Volume (mm3)	Bottom diameter (mm)	Height (mm)
B12.5 P	72.5±1.4	698±49	14.4±0.2	4.3±0.3
B12.5 3D	69.7±3.2	311±10	9.8±0.2	4.5±0.1
Mix P	60.4±2.8	499±60	12.6±0.3	4.0±0.4
Mix 3D	51.8±5.8	193±13	8.4±0.3	3.8±0.1

Table 4. *Properties of pores of 3D printing scaffolds.*

Type of scaffolds	Area of pore (μm^2)	Width (μm)	Length (μm)
B12.5 3D	84000±35000	280±70	290±60
Mix 3D	41000±17000	192±46	208±57

Regardless of the technique used, the porosities of scaffolds made of B12.5 were higher than the porosities of scaffolds made with Mix. The porogen burn-off method produced

scaffolds with higher porosity compared to those produced by the 3D printing method. This is especially true for the Mix group. The samples of Mix 3D possessed the lowest porosity and the highest standard deviation. For the other three groups, the deviations were relatively lower which represented better reproducibility. The sizes of scaffolds were maintained, as much as possible, in a similar range for all four groups of scaffolds.

The pore sizes of scaffolds produced by porogen burn-off were quite inhomogeneous, ranging from micropores to pores of few millimeters. Therefore, the pore sizes were not measured and discussed here as seen in (Pohjola, 2017). Furthermore, it is noteworthy that the pores of scaffolds made of B12.5 were much bigger, even more than two times than in the Mix group. And the size of pores of B12.5 3D ranged from 210 to 350 μm, and 146 to 265 μm for the Mix 3D group as seen in Table 4. The geometry of pores in the 3D printed scaffolds is exhibited in Figure 6, most of the pores were roughly squares and some of them were rectangles. There were also some pores with irregular shapes because of the bending and deformation of filaments.

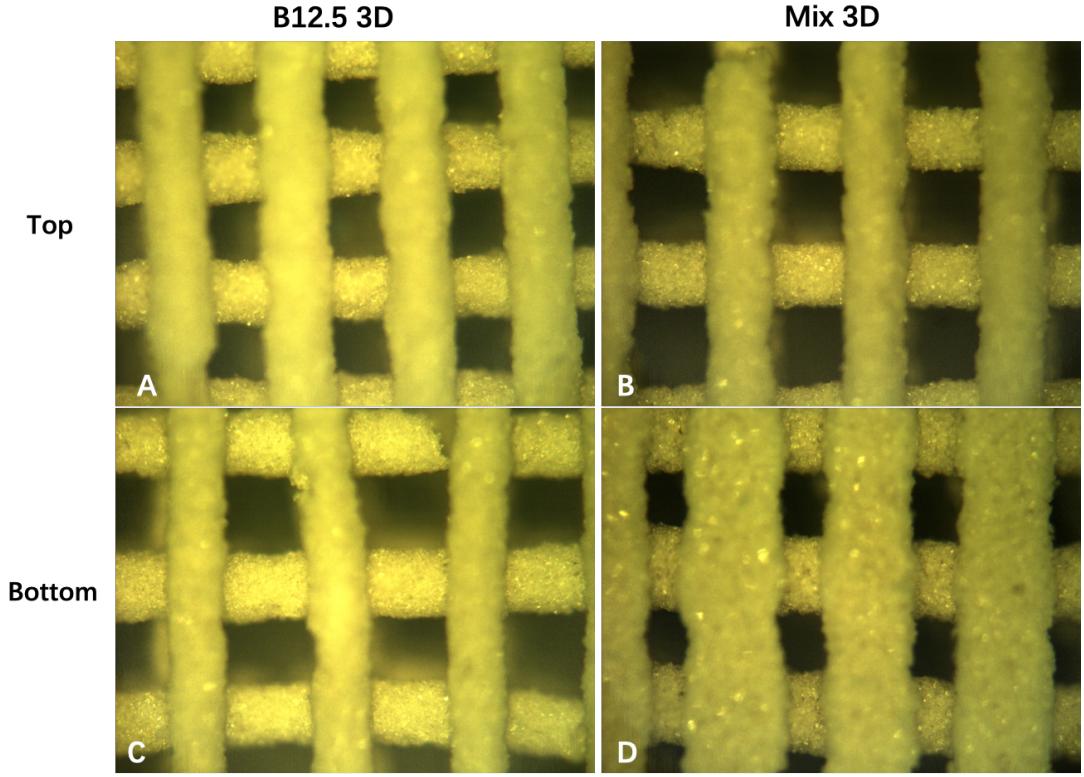

Figure 6. *the geometry of pores in 3D printed scaffolds under optical microscope.*

4.2 Dissolution behavior in static tests

In vitro dissolution was performed in the static condition, i.e. in a shaking incubator, but the solutions (TRIS or SBF) were not refreshed. The study aimed to assess 1) the ions

released from the glass to the solution (TRIS buffer solution) and 2) the ability of the released ions to saturate the solution, thus leading to the precipitation of hydroxyapatite in a solution mimicking the inorganic part of the blood plasma (SBF).

4.2.1 pH and mass loss

The change in pH is presented in Figure 7. As expected from when bioactive glasses were immersed in aqueous solutions, the pH rises with increasing immersion time in SBF (similar results were obtained in TRIS) (Pohjola 2017). In general, the pH raised more in solutions containing the B12.5 glasses than for the Mix glasses, regardless of the scaffold manufacturing technique. The rise in pH was also more important for 3D printed scaffolds than for the corresponding porogen burn-off scaffolds. In all cases at 168 h, the increase in pH seemed to slow down and remained almost constant for increasing immersion time.

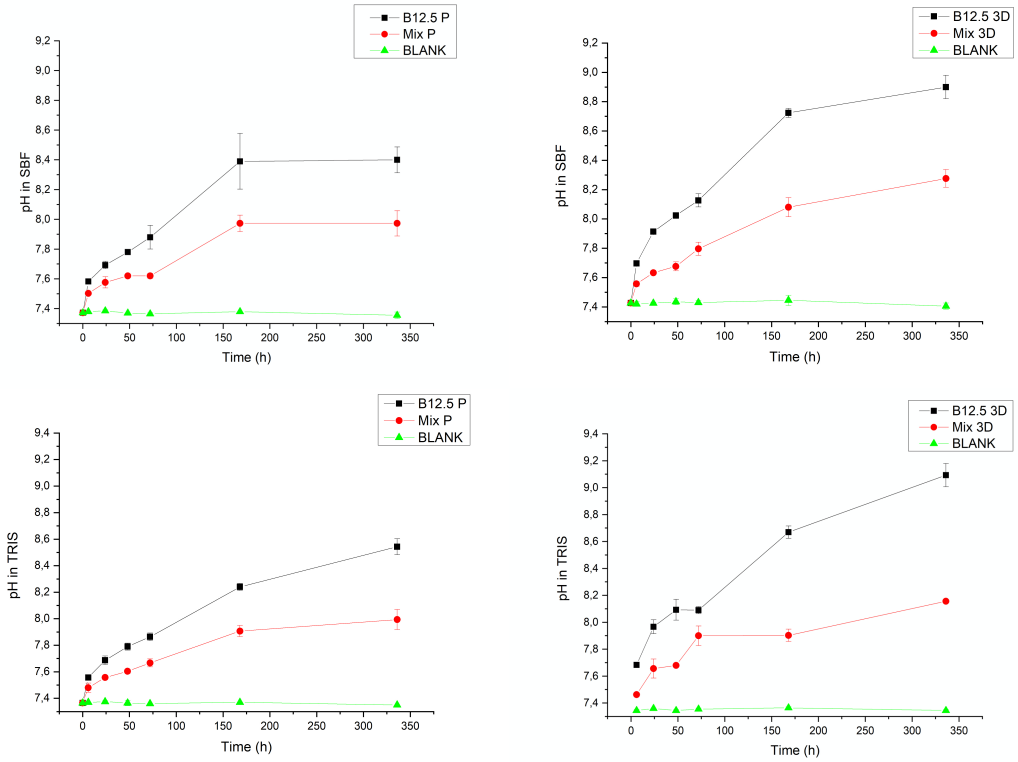

Figure 7. *pH in SBF and TRIS as a function of scaffolds immersion time. The results are related to scaffolds produced by porogen burn-off (P) and by 3D printing (3D).*

Figure 8 presents the mass loss as a function of immersion time, in SBF and TRIS, for each scaffold type and composition.

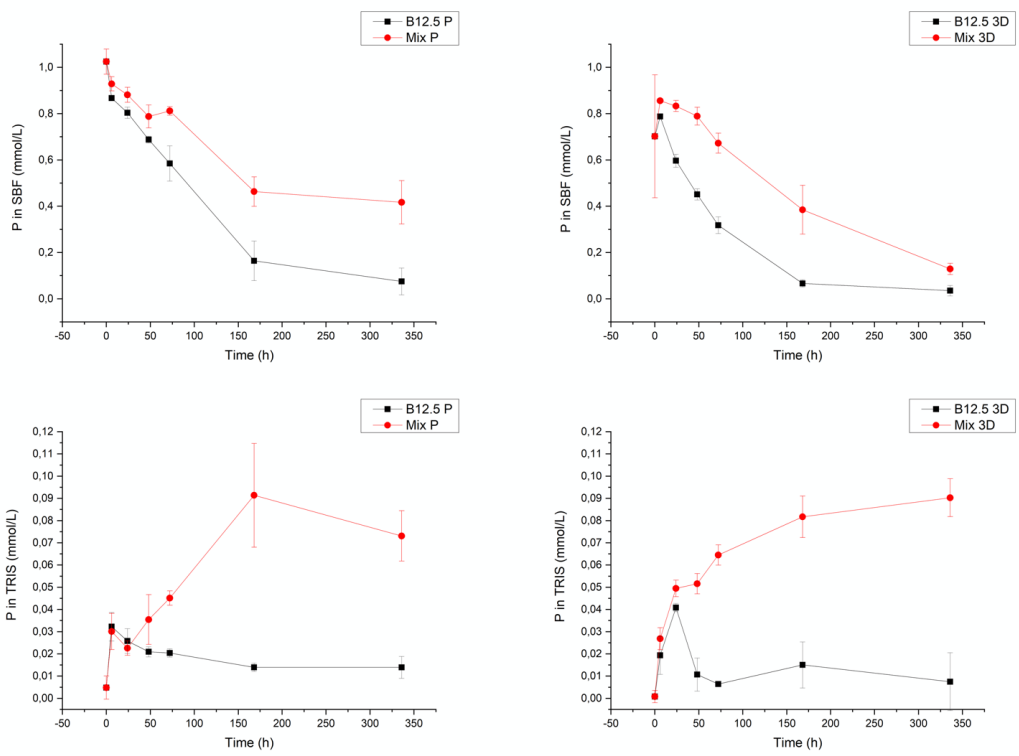

Figure 8. *Mass loss of scaffolds in SBF and TRIS as a function of scaffolds immersion time. The results are related to scaffolds produced by porogen burn-off (P) and by 3D printing (3D).*

All scaffolds lost weight during the immersion in both solutions. For the scaffolds immersed in SBF solution, the mass loss was significantly higher for B12.5 groups than in Mix groups, which is in agreement with the pH change. Furthermore, in agreement with the pH change the mass loss was, generally, more sustained and higher for in the case of scaffolds produced by the 3D printing method than for the porogen burn-off scaffolds. The mass loss values in SBF of porogen groups for B12.5 and Mix at 336 h were 4.28 ± 0.23 % and 2.45 ± 0.42 %, respectively, and 5.91 ± 0.68 % and 4.16 ± 0.31 % in 3D printed groups. The deviations in the B12.5 groups were much higher than Mix groups for the 3D printed scaffolds.

4.2.2 Ionic concentrations in static tests

The ionic concentrations in the SBF and TRIS solutions as a function of immersion time, are presented in Figure 9, for B and Si which are the glass formers.

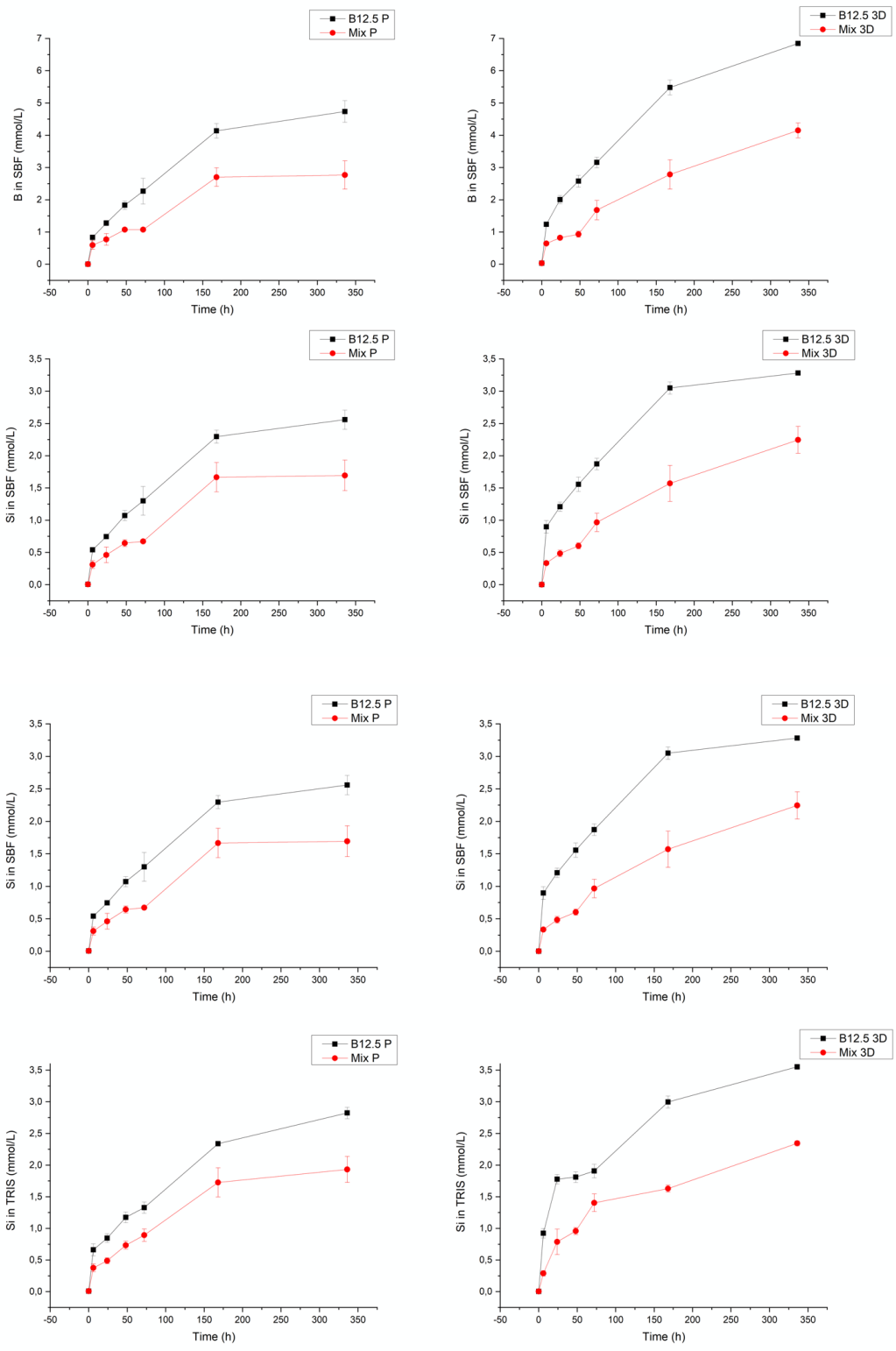

Figure 9. *The concentrations of B and Si in SBF and TRIS as a function of scaffolds immersion time. The results are related to scaffolds produced by porogen burn-off (P) and by 3D printing (3D).*

The release patterns for these two elements were quite identical in both SBF and TRIS solutions. First, there was a fast release of Si and B for immersion up to 168 h and then a plateau for longer immersion time. The ion concentrations in the solution containing the B12.5 glass compositions exhibit a higher ion concentration than in solution containing the Mix glass composition. Finally, the ion concentration was higher in the solution containing the 3D printed scaffolds compared to the porogen burn-off scaffolds.

The Ca ion concentrations in both SBF and TRIS solutions are exhibited in Figure 10.

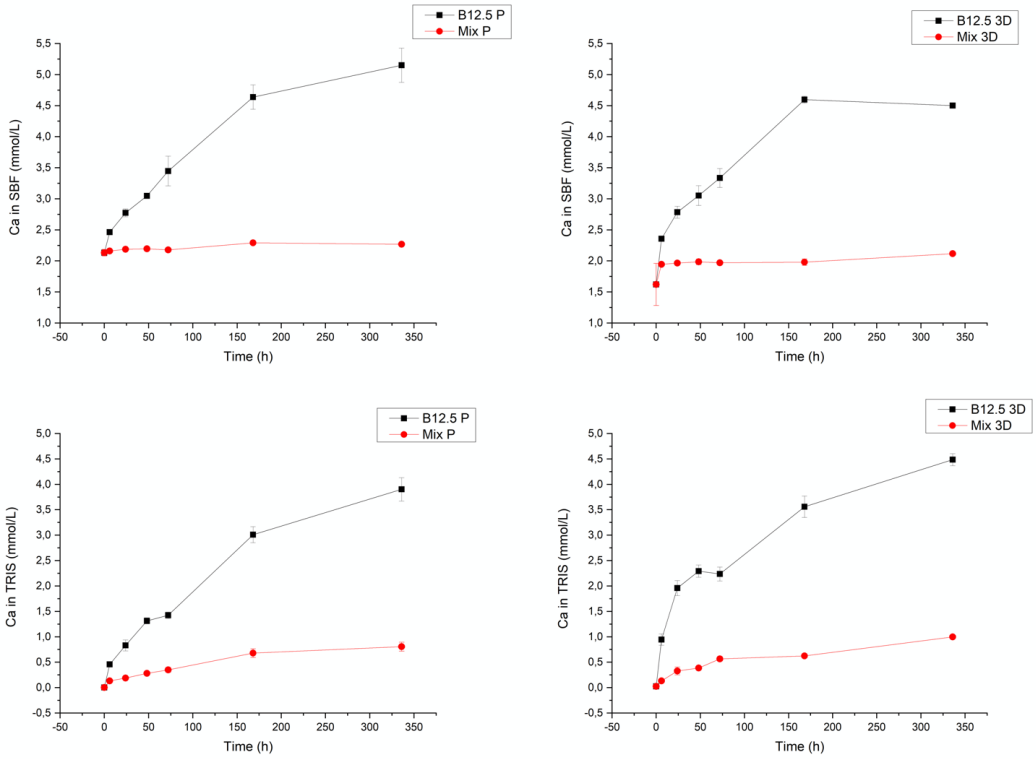

Figure 10. *The concentration of Ca in SBF and TRIS as a function of scaffolds immersion time. The results are related to scaffolds produced by porogen burn-off (P) and by 3D printing (3D).*

The Ca concentrations in B12.5 groups were all much higher and increased faster than in Mix groups. However, here, no significant differences in ion concentration, as a function of immersion time, could be pointed out between 3D printed and porogen burn-off scaffolds immersed in the same solutions. For the Mix groups, the values remained almost constant in SBF but increased slowly in TRIS solution.

The P concentrations in SBF and TRIS, as the function of immersion time, are shown in Figure 11.

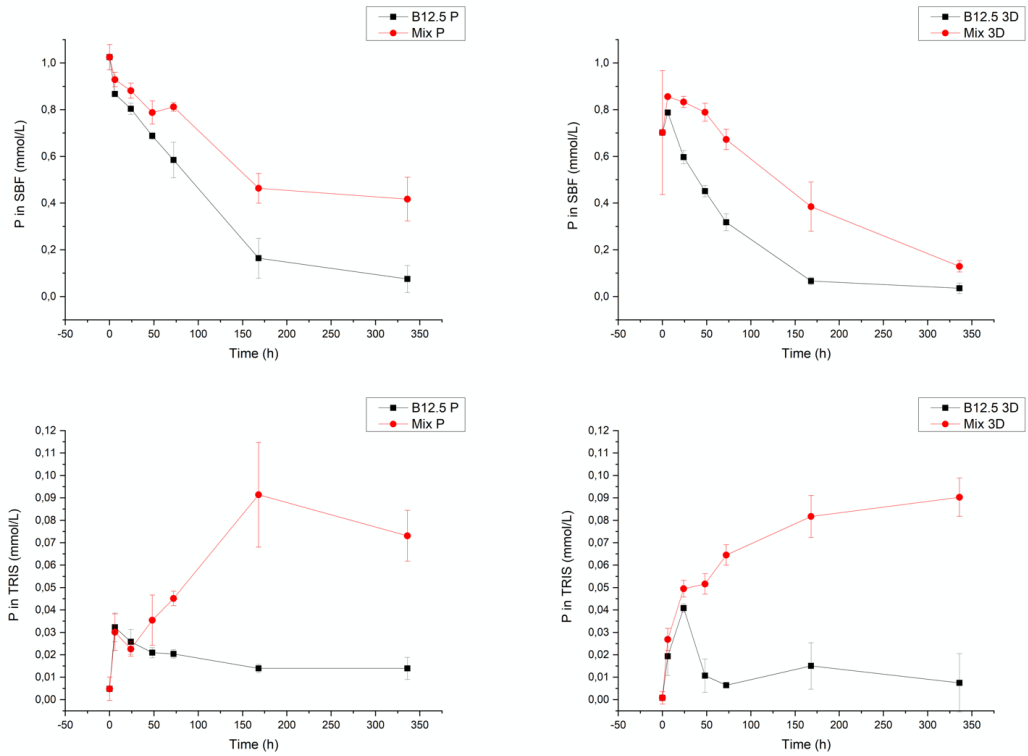

Figure 11. *The concentration of P in SBF and TRIS as a function of scaffolds immersion time. The results are related to scaffolds produced by porogen burn-off (P) and by 3D printing (3D).*

In SBF, regardless of the scaffold processing technique, the P concentration was found to decrease with increasing immersion time, to reach almost 0 between 168 and 336 h of immersion. The P consumption, from the SBF, appeared to be faster for the scaffolds made from the B12.5 composition and for the scaffolds produced by 3D printing. In TRIS, the P concentration maintained at a low level for the B12.5 groups. But it increased with increasing immersion time for the Mix groups. There was no significant difference between the scaffolds produced by different techniques in TRIS solution.

The Mg and Sr ionic concentrations in SBF and TRIS solutions, as a function of immersion time, are shown in Figure 12.

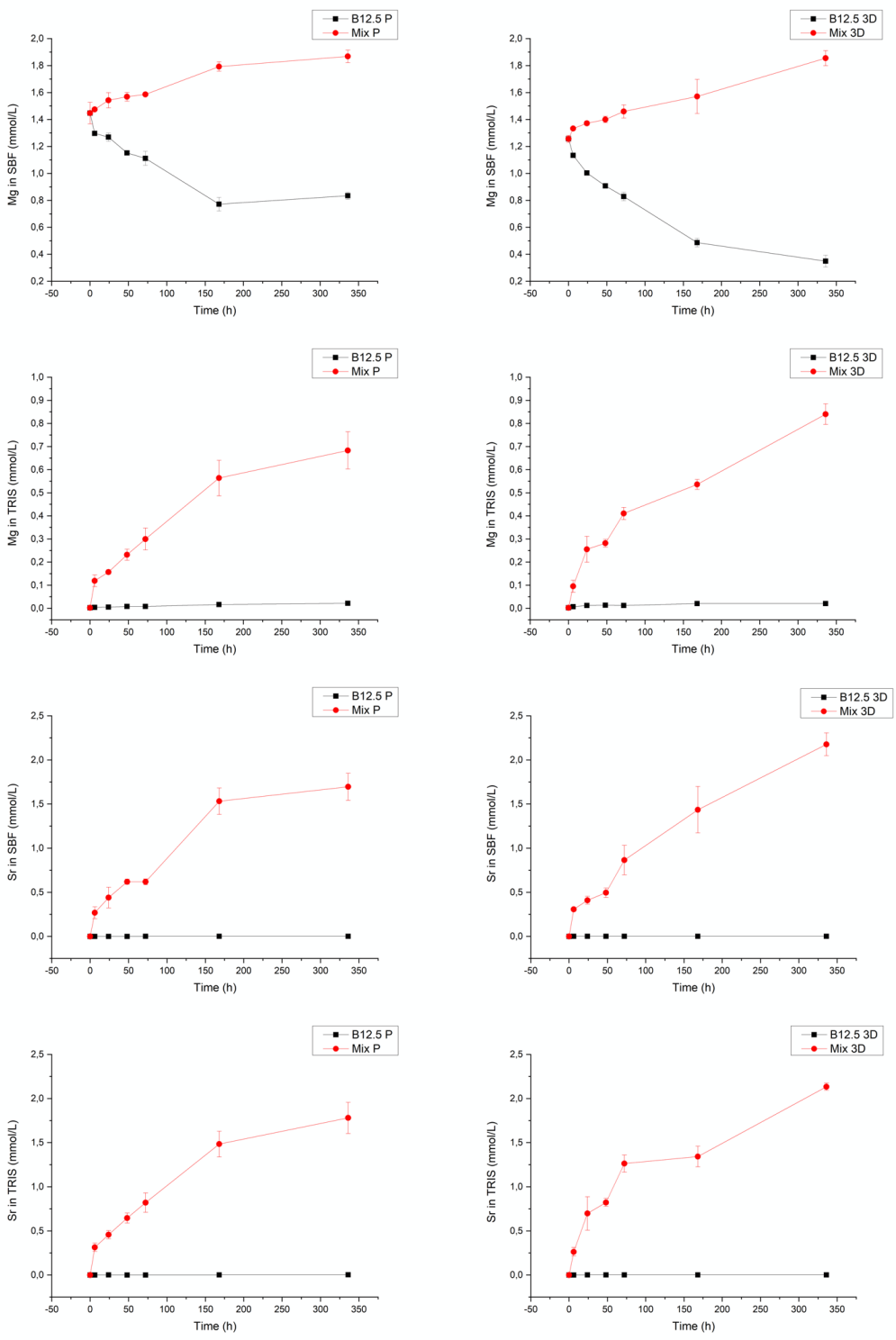

Figure 12. *The concentrations of Mg and Sr in SBF and TRIS as a function of scaffolds immersion time. The results are related to scaffolds produced by porogen burn-off (P) and by 3D printing (3D).*

It is interesting to point out that, the Mg concentration, in the solution containing the B12.5 glass scaffolds also decreased significantly over the course of the immersion in SBF.

However, in the case of the Mix glass composition, the Mg concentration in the SBF slightly increased.

Finally, as expected from the glass composition, the Sr concentration remained null in the solution containing the B12.5 glass whereas it increased with increasing immersion time for the scaffolds made from the Mix glass composition.

4.3 Dissolution behavior in Dynamic tests

The Dynamic tests for each type of scaffolds only were run one time with the flow-through system, if the results were consistent with the expectation. And all tests only used SBF as the solution which flowed through the scaffolds. The aim of this study was to mimic more closely the physiological conditions to which the graft might be exposed.

4.3.1 pH in dynamic tests

The changes in pH, in dynamic condition, are presented in Figure 13. There was a drastic increase in pH after the first hour in all cases (glass composition and scaffolds types) and then the pH went rapidly down to the original pH of the SBF. The increase in pH was more pronounced for the B12.5 glass composition. However, while the pH rise was more pronounced in the case of the B12.5 glass scaffold produced by the porogen burn-off compared to the 3D printed one, no significant difference could be seen between the Mix glass produced by both techniques.

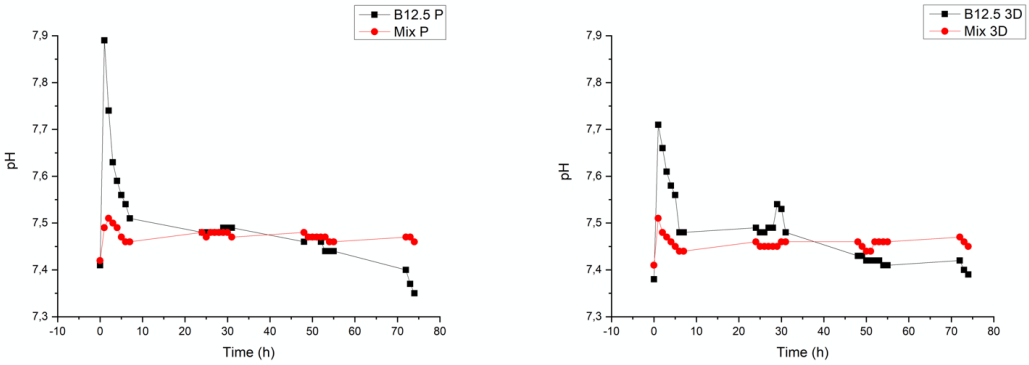

Figure 13. *pH in SBF as a function of scaffolds immersion time in the dynamic condition. The results are related to scaffolds produced by porogen burn-off (P) and by 3D printing (3D).*

4.3.2 Ionic concentrations in dynamic tests

Figure 14 presents the B ion concentration in the SBF as a function of immersion time. The B ionic concentrations raised rapidly in the first hour, then decreased gradually and remained stable after 7 h. No significant difference between the 3D printing and porogen

groups of Mix glass could be noticed. However, it is noteworthy that the B concentration was higher for the porogen burn-off scaffolds compared to the 3D printed one for the groups of B12.5 glass. This is in agreement with the pH change but reflects the opposite behavior compared to the static dissolution test.

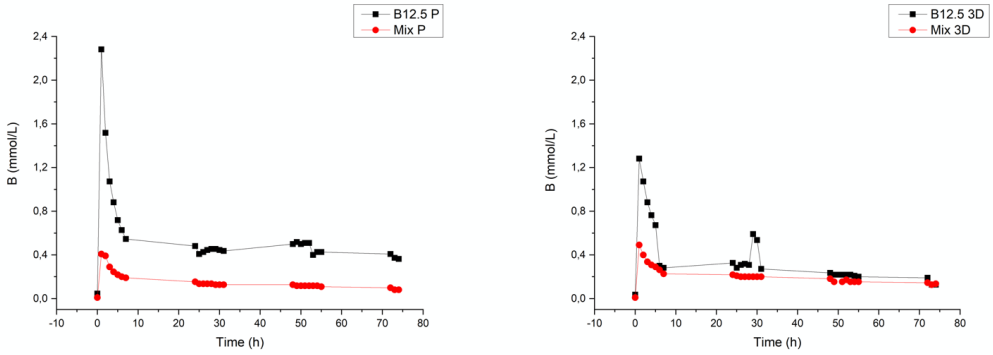

Figure 14. *Concentration of B in SBF as a function of scaffolds immersion time in the dynamic condition. The results are related to scaffolds produced by porogen burn-off (P) and by 3D printing (3D).*

Figure 15 presents the concentration of all ions, Si, B, Ca, P, Mg, and Sr as a function of immersion time.

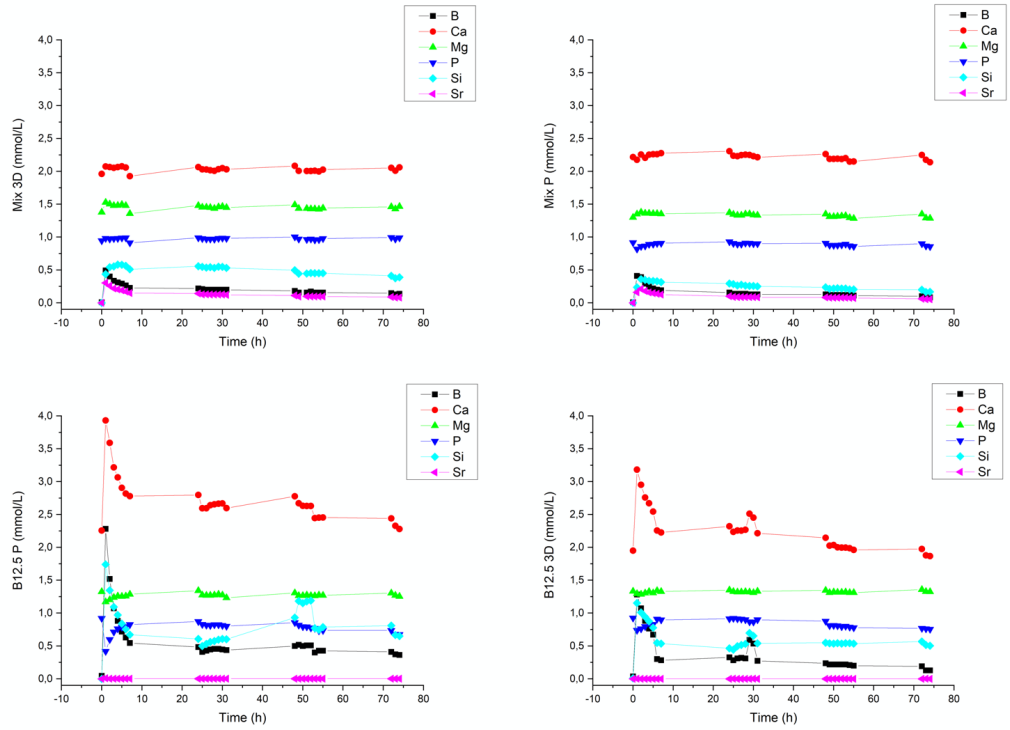

Figure 15. *The summary of all types of scaffolds with different ionic concentrations in SBF as functions with scaffolds immersion time in dynamic conditions. The results are related to scaffolds produced by porogen burn-off (P) and by 3D printing (3D).*

The patterns of other elements including Si, Ca, P, Mg, and Sr exhibited a similar trend than B, which started with a burst of ion release and then a progressive decrease to concentration typical in SBF solutions. Generally speaking, the ionic concentrations of all elements were stable after the initial burst, and the values were lower than the corresponding values in static tests after 6 h for B, Sr, and Si, which was shown in Figure 16.

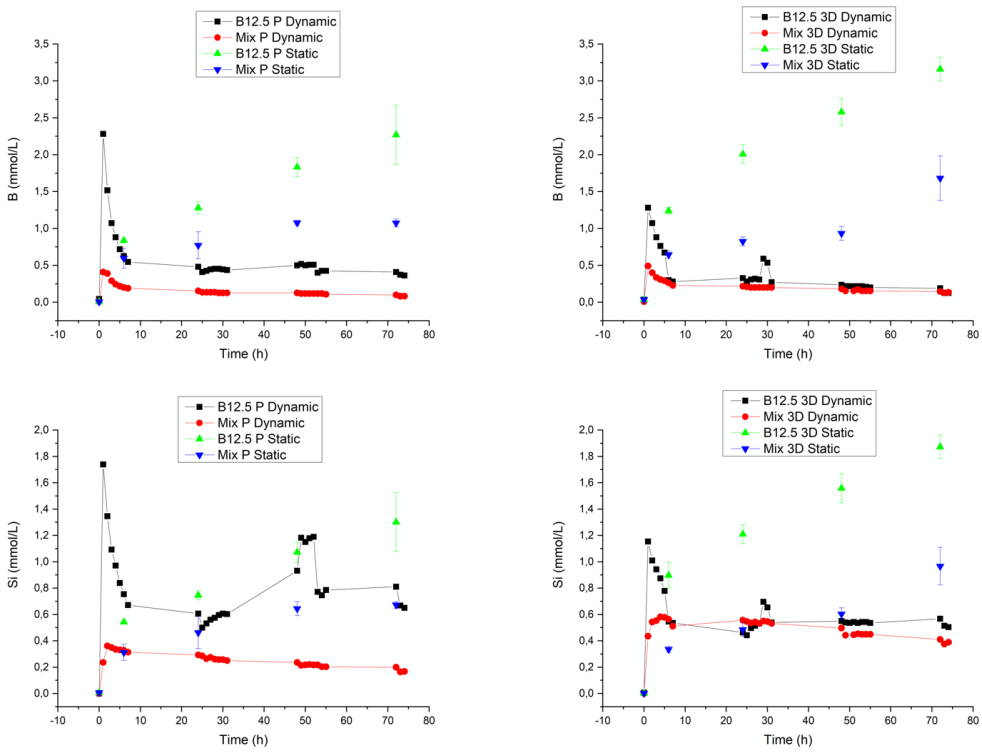

Figure 16. *Comparisons of the ionic concentrations of B, Si in SBF as functions with scaffolds immersion time between the static and dynamic tests. The results are related to scaffolds produced by porogen burn-off (P) and by 3D printing (3D).*

Figure 16 presents the B and Si release in dynamic and static conditions, for comparison. While in the dynamic condition a burst of ions occurred within 6 hours at longer immersion time the Si and B release was fairly low. In contrast in static, the ion concentration kept rising almost steadily for up to 72 hours. It is interesting to note that, often time, 72 hours corresponds to the first time the culture medium was changed during in-vitro cell culture.

Figure 17 presents a similar comparison between the static and dynamic test for the Ca, Mg, and Sr ions concentrations.

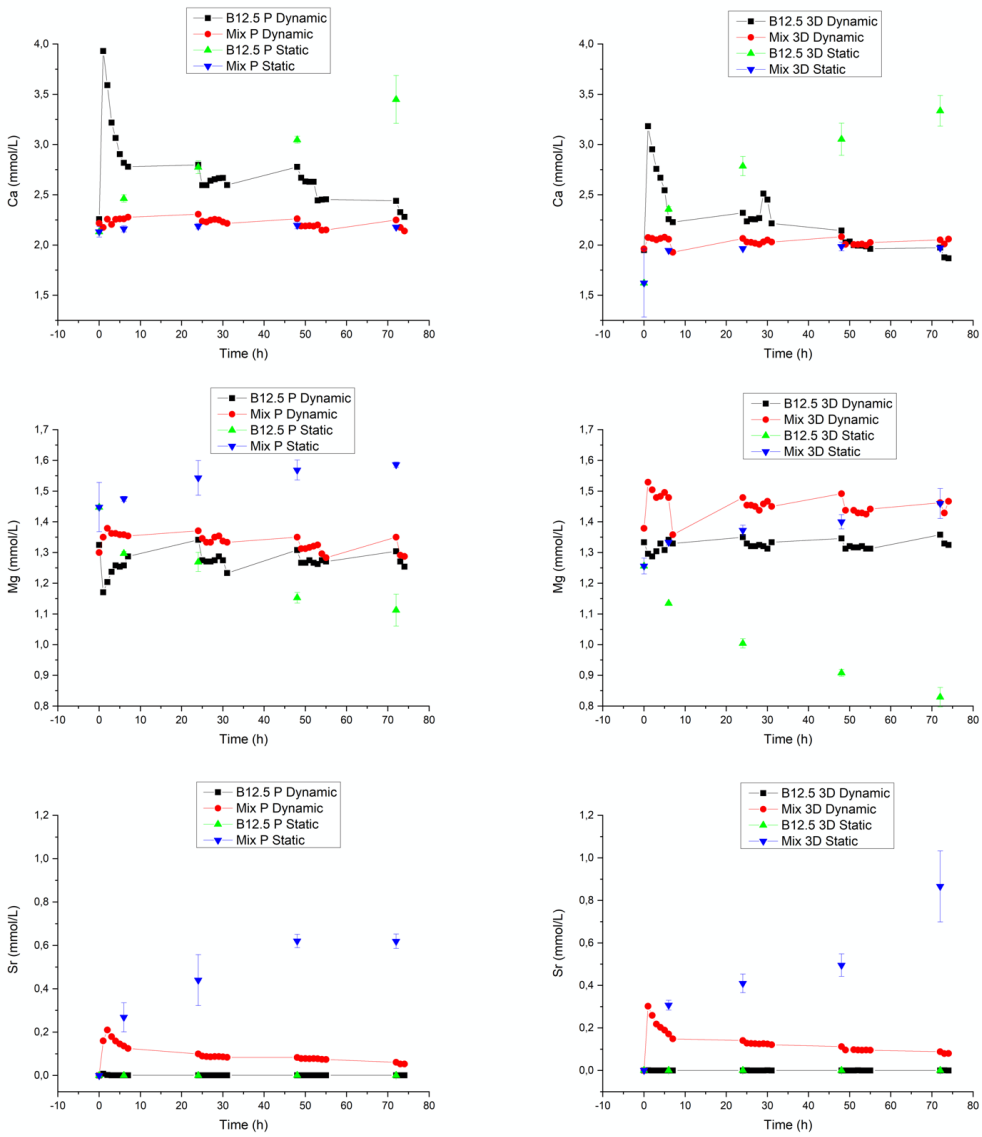

Figure 17. *Comparisons of the ionic concentrations of Ca, Mg, and Sr in SBF as functions with scaffolds immersion time between the static and dynamic tests. The results are related to scaffolds produced by porogen burn-off (P) and by 3D printing (3D).*

Again, while Ca remained at the physiological concentration in the Mix composition and increased steadily for 72 hours for the B12.5 composition in static condition, the Ca concentration rapidly raised and then decreased to typical SBF concentration within the 72 hours of testing in dynamic condition.

The Sr concentration remained slightly higher than the physiological concentration after the initial burst of ions, in the dynamic test for the Mix glass. B12.5 did not contain Sr and therefore the Sr concentration remained 0 in all conditions.

Finally, while the Mg was found to decrease for the B12.5 scaffolds, immersed in SBF in static condition and increased upon immersion of the Mix glass scaffolds. In dynamic

condition, regardless of the scaffold types and/or composition the Mg concentration remained constant.

4.4 The cellular tests

4.4.1 Viability of cells / live and dead assay

The viability of the pre-osteoblastic cells (MC3T3) seeded for 24 h on different types of scaffolds and on sintered disks, pre-incubated for 24, 48 and 72 h, was qualitatively analyzed through the live and dead staining imagines. There were two parallel samples for each type of scaffolds, and several photos were captured from different areas of each scaffold, and finally, the most representative photos in each group were selected and exhibited in Figure 19, 20, and 21. The live cells and dead cells were stained and exhibited green and red fluorescence respectively. Controls were also used to assess dead cells (negative control) and live cells (positive control) shown in Figure 18.

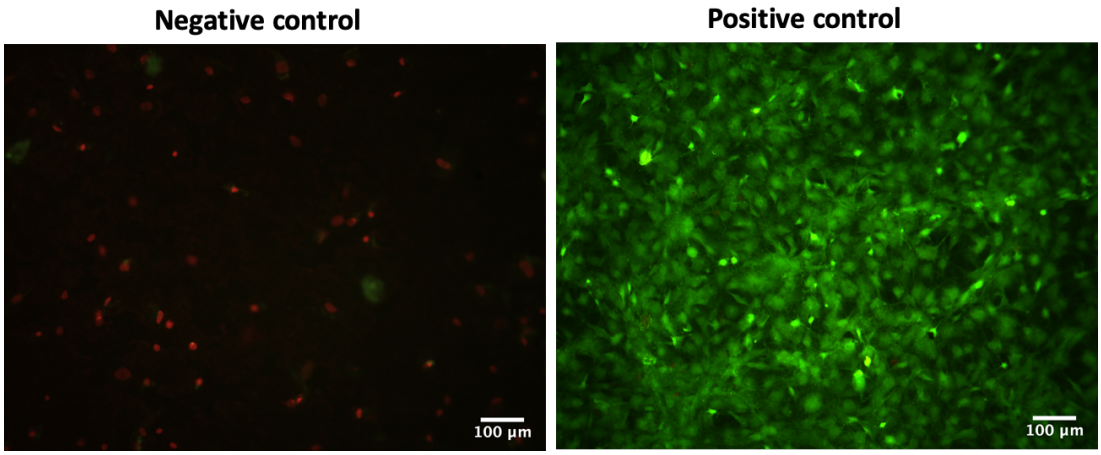

Figure 18. *Example of negative and the positive control in cell viability assay. The red dots are dead cells.*

Figure 18 exhibits the live/dead staining of the negative and positive control. As expected, the negative control killed all the cells during culturing as evidenced by the presence of solely red-stained cells. On the contrary, the positive control exhibited confluent green cells and demonstrated the appropriate proliferation and viability of cells.

Figure 19 exhibits the live/dead staining of cells cultured on top of disks sintered form glass powder.

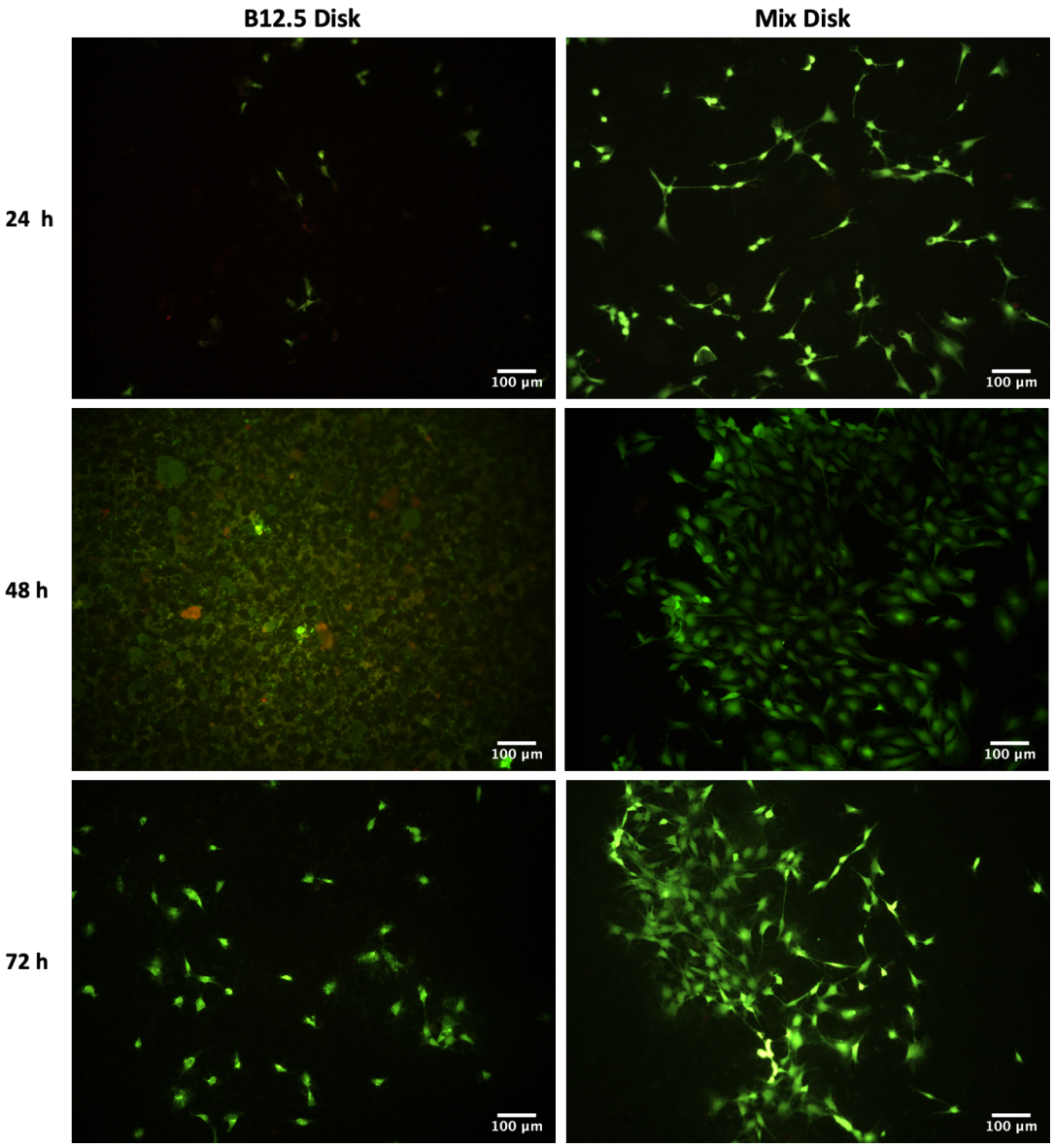

Figure 19. *Cell viability in response to disks made of composition of Mix and B12.5. 24, 48, 72 h are the period for pre-incubation.*

For the glass B12.5, no or few cells could be seen at the surface of the disks pre-incubated for 24 and 48 h, while a significant number of live cells (green staining) could be seen at the surface of the disks pre-incubated for 72 h. For the Mix glass, cells could already be seen with only 24 hours of pre-incubation and the amounts of live cells increased with increasing the pre-incubation time to 72 h. It is noteworthy that, after a pre-incubation of 72 h more cells were seen at the surface of the Mix glass compared to the B12.5 glass and the cells tend to spread more, showing the proper cell attachment and proliferation of these cells on top of the mix glass disks.

Figure 20 presents the live/dead staining of cells plated on top of scaffolds produced by the porogen burn-off technique from the Mix glass only.

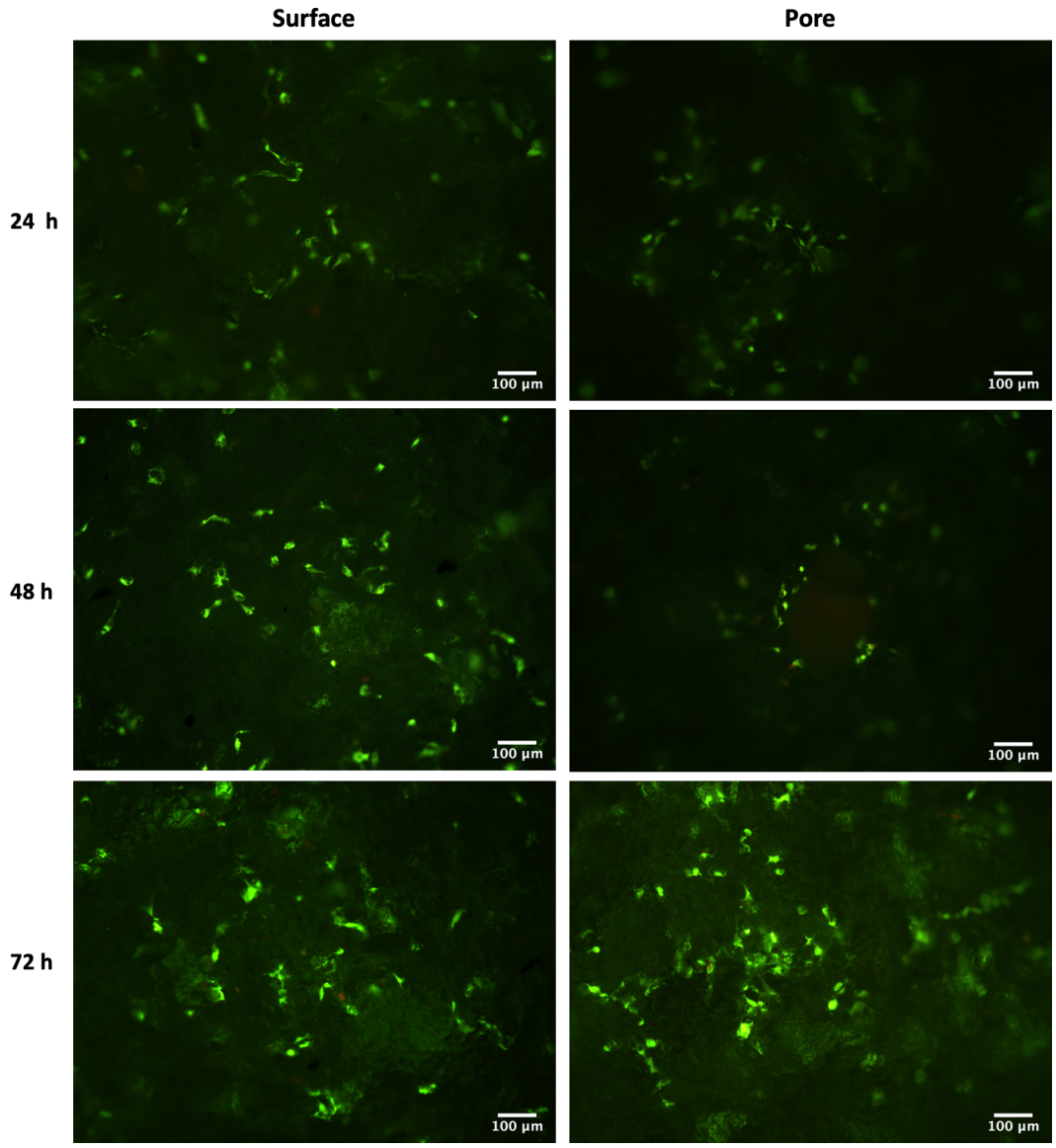

Figure 20. *Cell viability in response to scaffolds made of Mix composition produced via porogen burn-off. 24, 48, 72 h are the period for pre-incubation and the surface and pore indicated the camera focused on the surface on scaffolds or within pores.*

Images were taken from the surface of the materials and within pores. As for the disks, an increase in the pre-incubation period led to an increase in cell viability. For samples pre-incubated for 72 hours, significant number of cells were imaged within the pores of the scaffolds.

Figure 21 presents the live/dead staining of cells plated on top of scaffolds produced by the 3D printing technique from the Mix glass only.

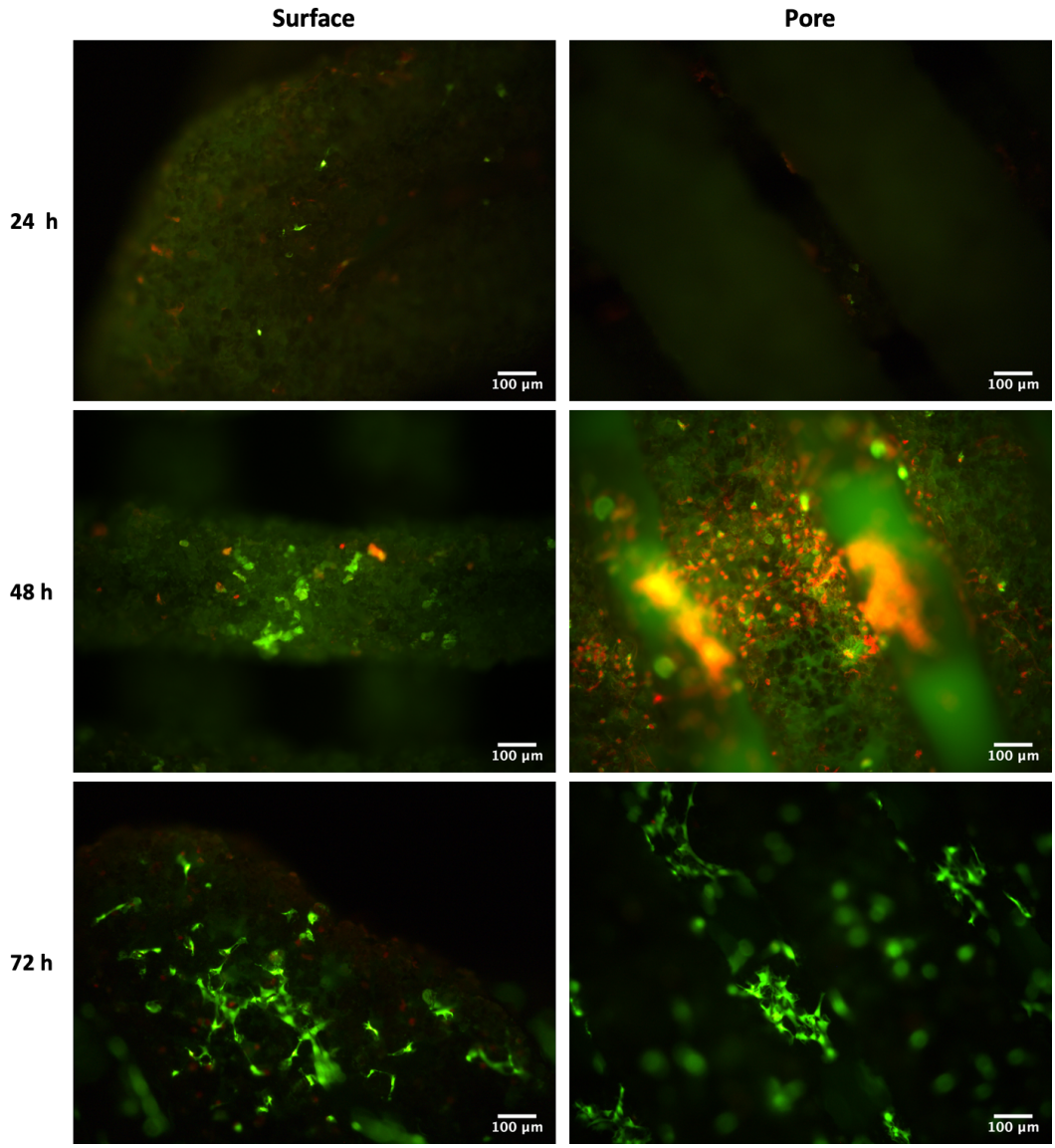

Figure 21. *Cell viability in response to scaffolds made of Mix composition produced via 3D printing. 24, 48, 72 h are the period for pre-incubation, and the surface and pore indicated the camera focused on the surface (1st layer) on scaffolds or within pores (2nd layer).*

For scaffolds pre-immersed for 24 h, no cells could be imaged. For scaffolds pre-incubated for 48h few live cells and a large number of dead cells were imaged. However, for a pre-incubation of 72 h, a significant number of live cells were imaged at the surface of the scaffolds' filaments. The cells were found to migrate within the pores of the scaffolds.

It is important to mention that regardless of the pre-incubation time, no live cells could be imaged on scaffolds produced from the B12.5 glass.

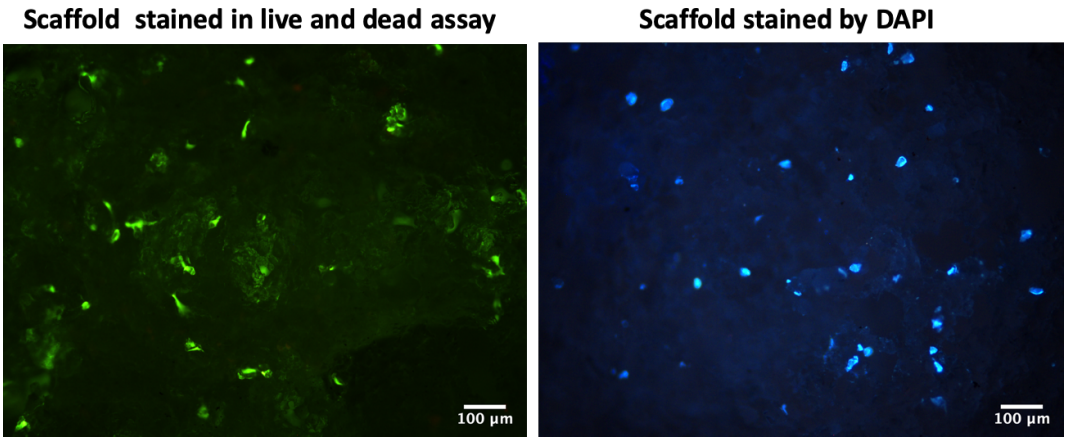

Figure 22. *Examples of autofluorescence from scaffolds stained by two kinds of dyes, the scaffolds weren't seeded with cells.*

Autofluorescence was observed from many samples which can disturb the analysis of the existence of live cells. The typical fluorescence was observed from scaffolds that were stained by the dyes from live and dead assay and DAPI (4′,6-diamidino-2-phenylindole) but without the process of cell culture, which is exhibited in Figure 22. This type of fluorescence originated from the material self, including Mix and B12.5. However, it is still possible to distinguish the fluorescence by live cells and/or materials, even if there are some overlaps, according to the morphology of the cells and the distribution of fluorescence. The living cells tend to assemble together and contact with each other, especially when they grow well. Whereas, the autofluorescence is usually sporadic and homogeneously distributed.

The results of the cells viability in response to different materials and periods of pre-treatment are summarized in Table 5.

Table 5. *Summary of the qualitative results of cellular viability in response to different materials for different pre-treatment periods. The cases which exhibited potential cytocompatibility were marked in red.*

Type of materials	Pre-treatment for 24 h	Pre-treatment for 48 h	Pre-treatment for 72 h
B12.5 P	No cells observed	No cells observed	No cells observed
B12.5 3D	No cells observed	No cells observed	No cells observed
B12.5 Disk	Sporadic cells	No cells observed	Live cells in a low density
Mix P	No cells observed, autofluorescence	Sporadic cells and autofluorescence	Sporadic cells and autofluorescence
Mix P (Pore)	A few Live cells	A few Live cells	Some live cells and autofluorescence
Mix 3D	No cells observed	No cells observed, autofluorescence	Obvious live cells and some dead cells
Mix 3D (Pore)	No cells observed	Cell adherend, and many dead cells	Obvious live cells assembled on stripes
Mix Disk	Live cells in a low density	Live cells in a middle density	Live cells in a middle density

Overall, while the B12.5 glass system seems to not be promising for medical application due to high toxicity, the Mix glass composition can be fabricated into scaffolds and following an appropriate pre-treatment protocol can demonstrate to be a good substrate for pre-osteoblastic cells.

4.4.2 The proliferation test by WST-1

Scaffolds pre-incubated for 48h were used to culture cells which were already confluent. After 24 h of culture, the scaffolds and medium were removed, then the WST-1 assay was performed with cells and the densities of live cells were measured by absorbance as shown in Figure 23.

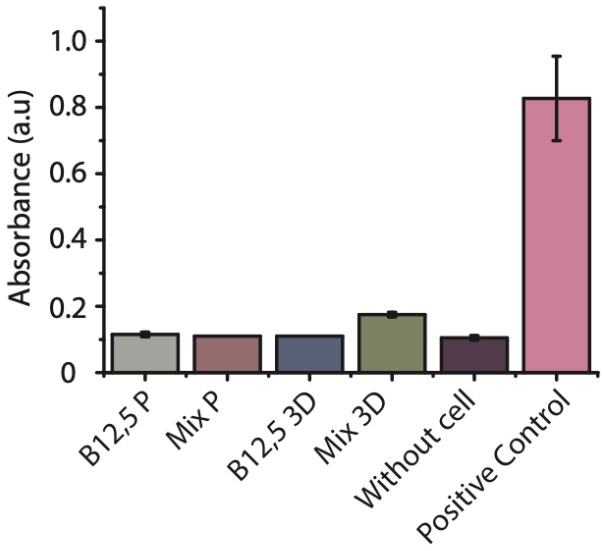

Figure 23. *Proliferation of cells in response to the scaffolds after pre-treatment for 48 h. The Absorbance expresses the density of live cells. The results are related to scaffolds produced by porogen burn-off (P) and by 3D printing (3D).*

It was consistent with results of 48 h pre-treatment from the live and dead assay, that there were no cells alive in groups of all types of scaffolds, comparing with the absorbance from the group without cell after 24 h culture. Additionally, the absorbance in Mix 3D group was a little higher than in the group without cell, because the speed of cellular death was slower than in other groups and there were still some cells adherent on scaffolds, but they were dying. Therefore, the pre-treatment for 48 h was not able to make the scaffolds suitable for cell growth.

From the earlier tests, the toxicity or ionic concentrations of all types of scaffolds after 48 h pre-incubation were still too high for the cell culture.

Conditioned medium from 72 h pre-incubation were diluted 50%, 25%, 10%, 5%, 1%, 0.5%, and 0.1%, and used to culture the confluent osteoblasts for 24 and 48 h and then the proliferation of cell was measured by WST-1 assay, in order to understand the impact of ionic concentrations on cell death. The results of the proliferation from 24 h to 48 h of all types of extracts from scaffolds are exhibited in Figure 24.

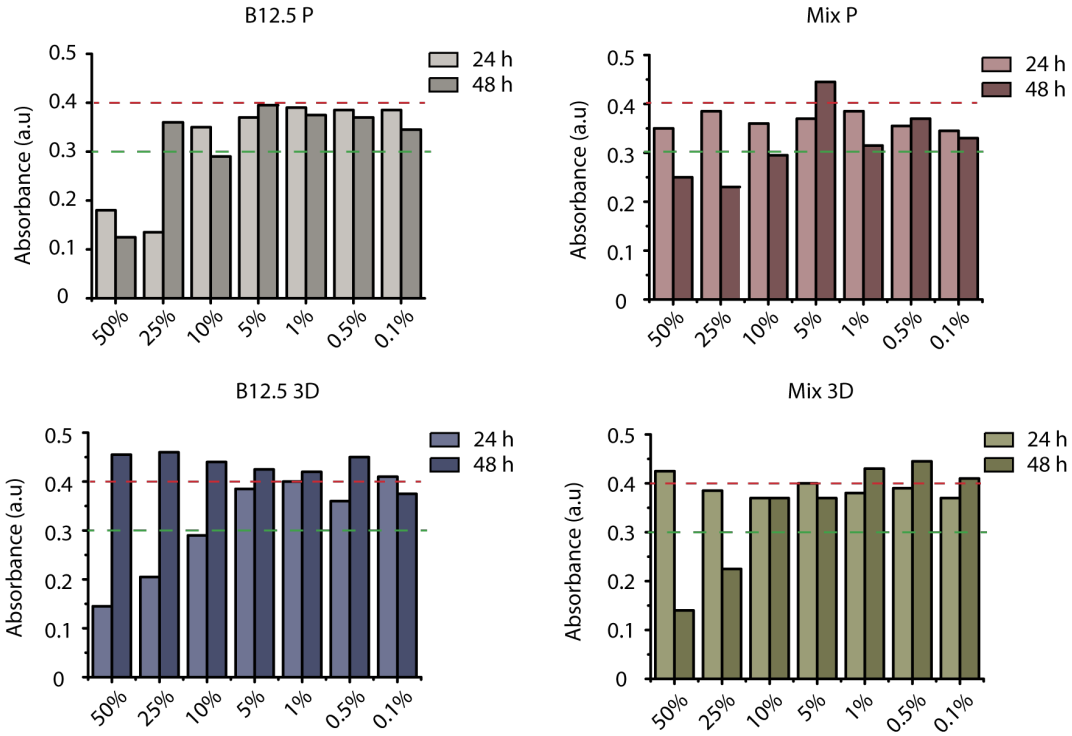

Figure 24. *Proliferation of cells in response to concentration gradients of conditioned medium from 72 h pre-treatment of all types of scaffolds. Dashed green is for positive control of 24h, and dashed red is for positive control of 48h.The Absorbance expresses the density of live cells. The results are related to scaffolds produced by porogen burn-off (P) and by 3D printing (3D).*

The overall pattern was not very clear, because the test was only performed for one time and was not statistically significant. Comparing with the positive control, the density of cells in the B12.5 group didn't show the proliferation improved but inhibited after 48 h. The medium killed many cells in the first 24 h at 50% and 25% of concentration gradients, meaning that the extracts were toxic to cells. The cell densities were higher than the positive control in the first 24 h but became lower than the control after 48 h when the concentrations were at and lower than 10% of the original conditioned medium, which meant the proliferations were improved first and then inhibited during a longer time. For the Mix group, the situation in the first 24 h was better than in the B12.5 group but the medium can improve the proliferation only when the concentration is 5% of the original extract.

The pattern of the groups of scaffolds produced via 3D printing was more regular compared to the pattern of porogen groups. For the B12.5 3D group, the growth of cells was enhanced or not inhibited at least after both 24 h and 48 h at 10%, 5%, 1% and 0.5%. Even the densities of cells increased obviously after 48 h for 50% and 25% of concentration gradients. For the Mix 3D group, the proliferation in all concentration gradients was all improved remarkably during the first 24 h, however, the toxic effects

were still seen at 50% and 25% and the suppression of proliferation showed at 10% and 5% after 48 h. As result, the proper concentrations of ions for the cell culture could be found from the comparison of the values between 10% and 5% of the B12.5 3D group, as well as the values between the 5% and 1% of Mix 3D group.

4.4.3 Ionic concentrations of conditioned medium

After the pre-treatment for 24 h and 72 h, the residual conditioned medium was stored and then diluted 10 times for the measurement of the ionic concentrations by ICP-OES. The ionic concentrations of the elements including B, Si, P, Ca, Mg, and Sr were measured and the representative results from B and Ca were selected and exhibited in Figure 25 and 26.

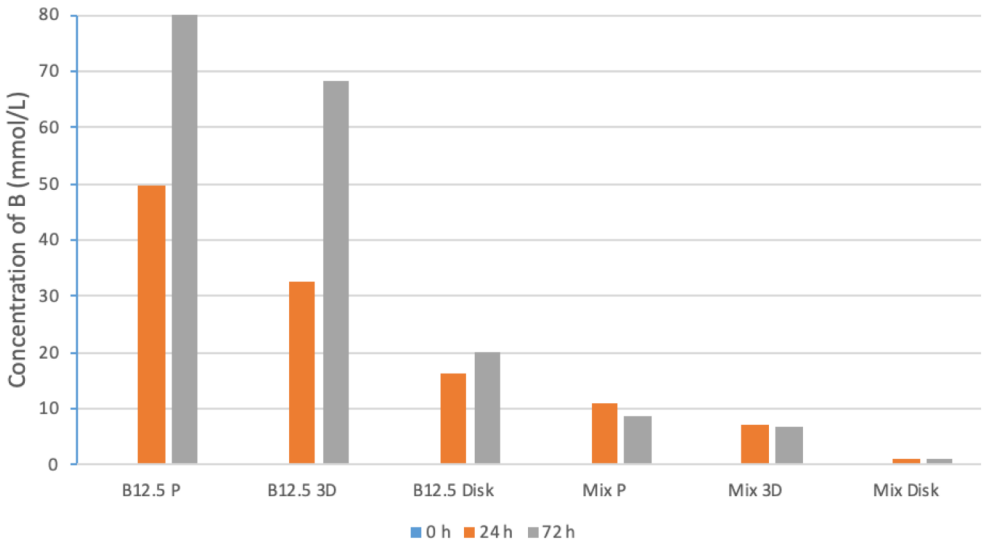

Figure 25. *Concentrations of B in conditioned medium from pre-treatment for 24 and 72 h. The 0 h expresses the original medium. The results are related to scaffolds produced by porogen burn-off (P) and by 3D printing (3D).*

As seen from Figure 25, the concentrations in B12.5 groups were significantly higher than the concentrations in Mix groups, and the ions continued to be released after 24 h. For the Mix groups, the concentrations at 72 h were slightly lower than at 24 h, which can be a non-sustain ion release over 72 h and/or variability in sample mass and morphology. The dissolution rate of B ions was higher for the scaffolds produced via porogen burn-off than scaffolds produced via 3D printing. And the concentration of B for the Mix Disk group was 1-1.1 mmol/L, that might be the reason why live cells were observed during the live and dead assay with the Mix disks even without pre-treatment.

The concentrations of Ca ions in the conditioned medium are shown in Figure 26.

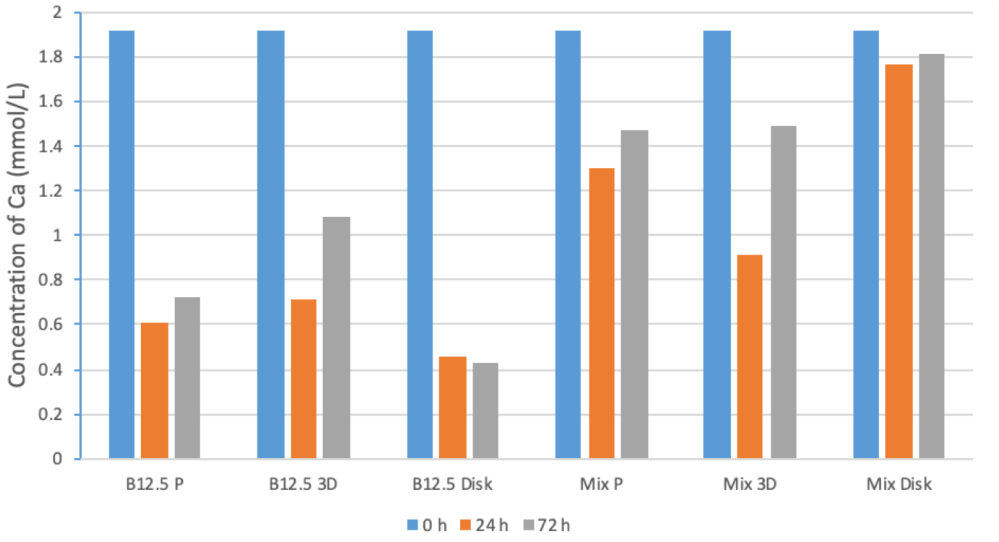

Figure 26. *Concentrations of Ca in conditioned medium from pre-treatment for 24 and 72 h. 0 h expresses the original medium. The results are related to scaffolds produced by porogen burn-off (P) and by 3D printing (3D).*

The Ca decreased compared to the concentration in the original medium which indicated that the Ca ions were consumed during the pre-incubation, especially at the 24h time points. Ca ions were released continuously from 24 h to 72 h for all types of scaffolds but disks. The trends of P concentration in the medium were different between the groups of scaffolds produced by different materials and are exhibited in Figure 27.

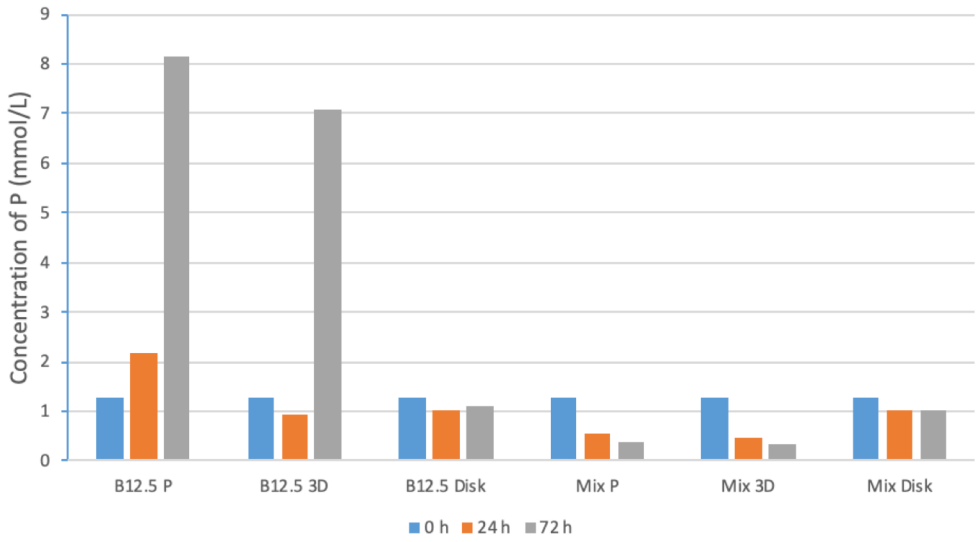

Figure 27. *Concentrations of P in conditioned medium from pre-treatment for 24 and 72 h. 0 h expresses the original medium. The results are related to scaffolds produced by porogen burn-off (P) and by 3D printing (3D).*

The concentrations in the medium immersed with Mix scaffolds went down over time, which were similar to the trends of the dissolution experiment in SBF, but the concentrations for the B12.5 scaffolds increased remarkably after 72 h. For the other ions including Mg and Sr, the patterns were consistent with their dissolution behaviors in SBF, and the concentrations were all in a relatively low range from 0 to 2 mmol/L, as shown in Figure 28.

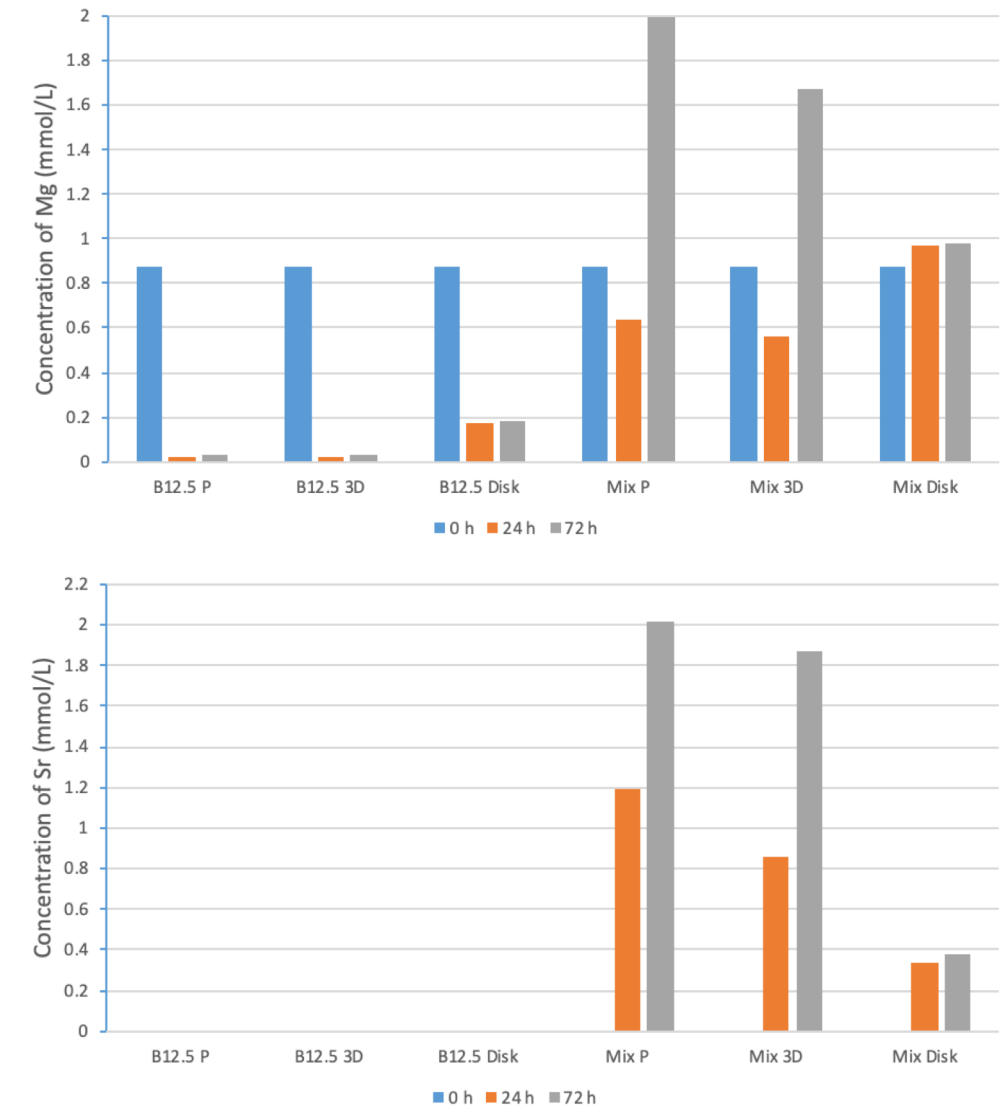

Figure 28. *Concentrations of Mg, Sr in conditioned medium from pre-treatment for 24 and 72 h. 0 h expresses the original medium. The results are related to scaffolds produced by porogen burn-off (P) and by 3D printing (3D).*

According to the proliferation test with conditioned medium from pre-treatment 72 h, the beneficial concentrations of ions might be speculated from the ionic concentrations of groups which exhibited continuous improvement of proliferation which were exhibited in Table 6. It is difficult to conclude which concentration will be beneficial or not harmful for

the cellular proliferation, since the obvious difference of the levels of concentrations between the groups of B12.5 and Mix. Additionally, it is not easy to conclude which ions were beneficial or harmful in one solution when multiple ions existed in the same solution. But because the concentration of B used to be much higher than other ions, thus it should be considered primarily as the threshold value.

Table 6. *Potential beneficial ionic concentrations form the conditioned medium according to the proliferation tests.*

Group of conditioned medium	**B (mmol/L)**	**Si (mmol/L)**	**P (mmol/L)**	**Ca (mmol/L)**	**Mg (mmol/L)**	**Sr (mmol/L)**
B12.5 3D 10%	6.833	0.323	0.709	0.109	0.003	0
B12.5 3D 5%	3.416	0.161	0.355	0.054	0.002	0
Mix 3D 5%	0.344	0.115	0.016	0.075	0.083	0.093
Mix 3D 1%	0.069	0.023	0.003	0.015	0.017	0.019

5. DISCUSSION

This chapter discusses the results obtained and presented in the previous section. All data are discussed based on the material's foreseen application.

The choice of the compositions of investigation in this thesis, B12.5-Mg5-Sr10 (47.12SiO_2-6.73B_2O_3-6.77CaO-22.66Na_2O-1.72P_2O_5-5MgO-10SrO, in mol%) which assigned as Mix and B12.5 (47.1SiO_2-6.7B_2O_3-22.7Na_2O-21.8CaO-1.7P_2O_5, in mol%), was based on previous data obtained by a former MSc student (Tainio 2016). The bioactivity of materials was proved by the conversion of HA on the surface after the immersion in SBF for 2 weeks. The Sr can slow the degradation and ionic releasing of scaffolds when incorporated into scaffolds, and improve the cell proliferation when introduced in the medium (Massera *et al.* 2015;Tainio 2016). The incorporation of Mg can widen the thermal forming domain which allows better sintering (Tainio 2016).

5.1 Structural properties

The overall porosity and pores size are critical properties for scaffolds when planned to be used for bone engineering. The suggested optimum overall porosity is 50% - 90% and optimum pore size ranges between 100 - 500 μm (Karageorgiou and Kaplan 2005;Gerhardt and Boccaccini 2010). From Table 3, all the scaffolds produced in this work had porosity over 50% which is in line with the recommendation for efficient nutrient, mass and cell migration. As expected, the 3D printed scaffolds yield the lower porosity. However, the more organized porosity, as opposed to the porogen burn-off technique, is believed to allow for more efficient fluid penetration. Also, it is noteworthy, that the scaffolds produced using the Mix glass yield lower porosity than the one produced from the B12.5 glass. This can be explained by the increased glass viscosity at the sintering temperature as was reported in (Tainio 2016). The sizes of pores in the 3D printing groups were all above 100 μm required for the migration of MC3T3--E1 cells which have sizes between 20 - 50 μm (Sudo *et al.* 1983).

The standard derivations of 3D printing scaffolds related to the porosity, diameter, and height were low, but they were much higher for the area and length of sides of pores, which indicated that maintaining the shape of the scaffolds post-sintering is more difficult to control. However, the general appearance and internal structure of scaffolds still exhibited a good reproducibility, especially for the relatively simple operation and setup, and the short producing period which was up to 16 scaffolds per day. The reproducibility

of the 3D printed scaffolds was found to be mainly function of the ink homogeneity and change in temperature, known to affect the drying of the scaffolds (Nommeots-Nomm, Lee and Jones 2018). Control of the shrinkage must be considered to decrease the risk of crack formation.

The Mix 3D scaffolds met the requirements of the structural properties and reproducibility, but there might be some modifications that could be attempted in the future experiment. The geometry of pores could be designed as hexagonal to enhance the strength and porosity (Roohani-Esfahani, Newman and Zreiqat 2016). The other way to increase the porosity is to reduce the thickness of filaments during the printing by adjusting the ink formula, and the height of the scaffolds should be decreased as well to decrease the weight applied on each strand and the risk of strand sagging.

5.2 Static Dissolution in different solutions

The pH of the solution in all groups of scaffolds can increase to or even exceed 8 after 168 h. This indicates that the scaffold dissolution is rapid and may lead to harmful ion concentration for the osteoblasts. After 168 h, there were plateaus in the pH change, for the porogen burn-off groups, and the rise in pH slowed down for the 3D printing groups. This can be attributed to the solution becoming saturated with ions and subsequent formation of the HA layer. The difference between the porogen and 3D printing groups may be due to the better interconnectivity which can resist the blocking by the formation of HA layers in small pores, and also increases the interactions between the solution and the surface of scaffolds.

The mass loss was measured from all groups of scaffolds, which indicated that degradation occurred in each type of scaffolds. The scaffolds made with B12.5 degraded faster than the Mix groups. This is in agreement with in-vitro dissolution test performed by Tainio, showing that the presence of Mg and Sr reduced the dissolution rate (Tainio 2016). This implies that the impact of composition is dominant over the scaffold preparation techniques. The mass change also confirms the faster dissolution of the 3D printed scaffold compared to the porogen burn-off one. The smaller standard derivations were measured from the Mix groups of scaffolds, which indicated that might be beneficial for the implant application because the degradation was more controllable, and the scaffolds were less easy to be degraded during immersion.

The dissolution behaviors of the scaffolds related, as evidence by the B, Si, Ca, P, Sr, and Mg ions concentration as a function of immersion time. The ions release profile is in agreement with the previous test done by Pohjola (Pohjola 2017). The Si and B releases

follow similar trends, in both the processing methods used (3D printing vs porogen burn-off). As expected from the faster dissolution rate of the 3D scaffold, the release of the glass-forming element was higher in these types of scaffolds. The release of Ca was measured in all samples. The B12.5 glass compositions released more Ca than the Mix glass composition. This is simply due to the higher Ca concentration in this glass composition. In the case of the scaffolds made from the Mix composition, the Ca concentration remained almost constant. The P was found to decrease over time, in SBF. This indicates the consumption of P ions. In bioactive glasses, this is likely to occur during the precipitation of the HA-like layer. The decrease in P was observed for all scaffolds regardless of the processing techniques. One major difference lies in the speed of P consumption in scaffolds made of the Mix and B12.5 glass composition. Indeed, regardless of the processing technique, the HA precipitation seemed to be faster for the B12.5 than for the Mix glass. This is in agreement with the previous study (Tainio 2016;Pohjola 2017). Indeed, Sr and Mg are known to reduce the speed of HA precipitation. The dissolution behavior of ions might not be exactly identical in the SBF and in culture medium (used for cell culture). However, it was reported that, for borosilicate glasses, the dissolution behavior was fairly similar between the immersion up to 21 days in SBF and conditioned medium (Ojansivu *et al.* 2018).

5.3 Dynamic dissolution

The pH values in the dynamic flow-through testing all generally remained stable in the range of 7.4 to 7.5 for the four types of scaffolds. Only a burst of ions could be seen within the first 6 h. These pH values are appropriate for the culture of osteoblasts. Bursts of ions were also observed as shown in Figure 14 and 15 showing the B, Ca, Si ion releases. This is particularly true for scaffolds made with the B12.5 composition. Scaffolds made with Mix composition exhibit a smaller burst of ions. All concentrations remained within physiological concentration over time. The concentration of Ca did not increase irrespective of the scaffolds type or composition, but eventually slightly decreased. This associated with a slight decrease in the P concentration, especially seen for the scaffolds produced from B12.5 indicate, as seen in the static condition, that the reaction between the Ca and P takes place, most likely to form the HA layer. This still needs to be verified through XRD (X-Ray Diffraction) and SEM (scanning electron microscope).

Generally, the concentrations of ions including B, Si, and Sr in the static tests became higher than the corresponding concentrations in the dynamic tests after 6 h and then got much higher, but the concentration of Ca for the Mix groups kept in the close levels over

time, which indicated the ionic concentrations in the dynamic condition will not be harmful to the growth of cell.

And the steady and friendly condition of the flow-through experiments depended on the flow rate, which was 0.4 ml/min in this experiment. This parameter was according to the lowest rate of peristaltic pump in our lab, but the flow rate of the interstitial fluid was supposed to be slower and difficult to simulated in vitro. Therefore, the problem of accumulation of ions might still exist at a lower rate, and more parameters in different flow rates need to be tested. Also, unlike the static test which can be performed simultaneously on a large number of parallel samples, in dynamic only one sample can be tested at a time. Besides, the process was manual, and the collection of tubes had to be manually performed. Such issues were already pointed out in the previous study where tests were performed for few hours (Susanne Fagerlund *et al.* 2012;Fagerlund, Hupa and Hupa 2013).

5.4 Test of Cellular viability

The test of cell viability was performed to evaluate the cytocompatibility of the scaffolds. Tests were first performed on sintered disks pre-incubated for 24, 48 and 72 h. From Figure 19 - 21, it can be seen that the pre-incubation item drastically affects the cells' ability to attach and proliferate at the material surface. Indeed, especially visible in the case of disks produce from the Mix composition, cells density clearly increases with increasing pre-incubation time. In the case of disks made of B12.5 glass composition, only the disks pre-immersed for 72 h exhibited viable cells at their surface. For shorter pre-incubation, no cells survived. This is a correlation with the static ICP results discussed earlier. Indeed, the release of ions from the B12.5 glass is faster than in the case of the Mix and such fast ion release leads to ions concentration leading to high pH and toxicity. As a result, all scaffolds produced with B12.5 composition were not suitable for the cell culture after the pre-treatments of 24, 48, and 72 h. This is attributed to the fact that when producing scaffolds, the surface area is greater than in the case of disks. Therefore, the ion release is expected to be even greater and to lead to higher toxicity. The scaffolds produced from the Mix glass composition had a higher potential for the attachment and growth of osteoblasts, and the pre-treatment was supposed to be at least 72 h. The Mix 3D group exhibited the best performance. Live cells can be observed in a relatively high density and with a morphology that tends to indicate that the cells are healthy and are not going toward apoptosis. But if comparing to the positive control in Figure 18, the cell densities from the Mix disk samples in Figure 19 were evidently lower. This can be assigned to mild toxicity and/or to difficulties of cells to proliferate on the 3D

structure. The dead cells could be observed in Figure 21 for the 3D Mix scaffold after 72 h pre-treatment, thus even the 3D Mix scaffold was considered as the promising candidate, the test for a longer period of cell culture will be needed.

In order to better understand the change in ionic concentration in the medium as a function of immersion time, ICP-OES was also performed with the culture medium. Figure 29 - 31 present the B, Si and Ca concentration post-immersion for 72 h in culture medium, SBF and TRIS buffer solution.

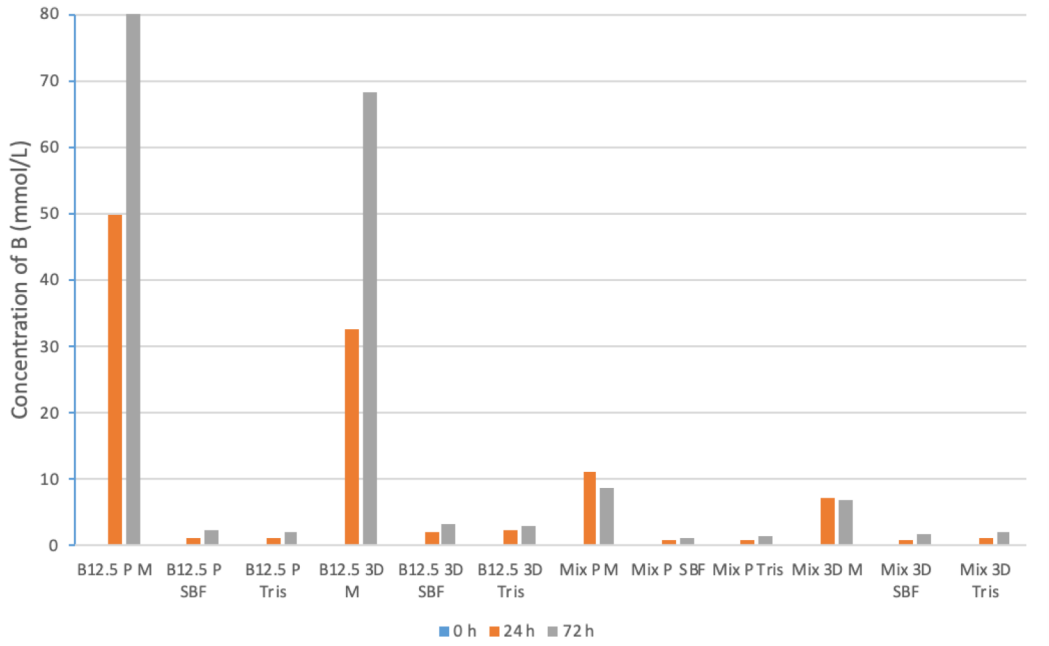

Figure 29. *The concentrations of B in the different solutions for immersion of 24 and 72 h. 0 h expresses the original medium and blank solution. The M, SBF, and TRIS express the scaffolds immersed in the culture medium, SBF and TRIS solution separately. The results are related to scaffolds produced by porogen burn-off (P) and by 3D printing (3D).*

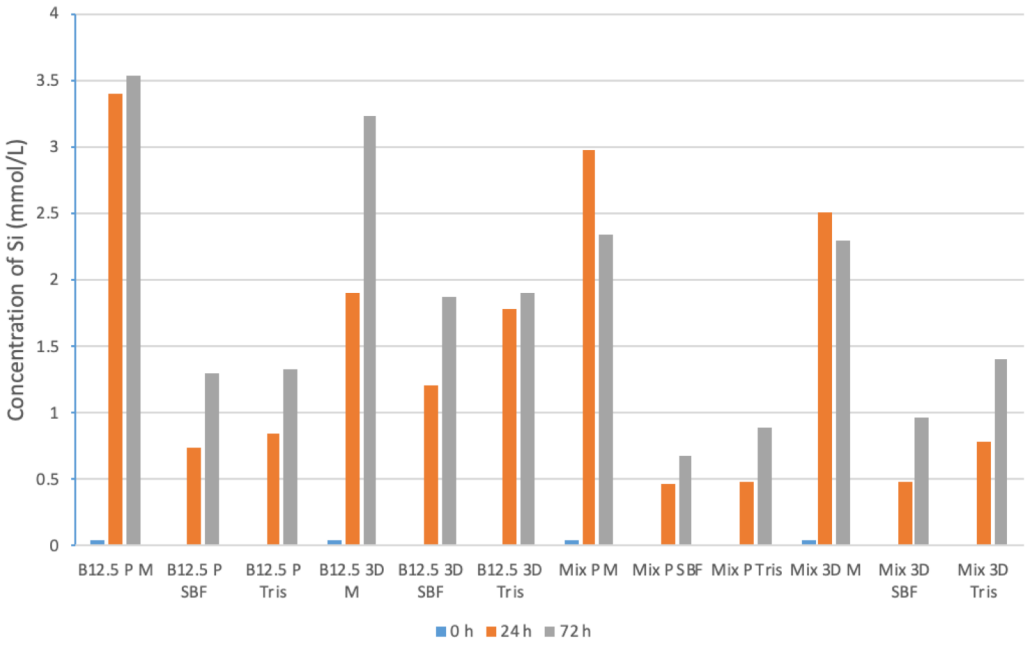

Figure 30. *The concentrations of Si in the different solutions for immersion of 24 and 72 h. 0 h expresses the original medium and blank solution. The M, SBF, and TRIS express the scaffolds immersed in the culture medium, SBF and TRIS solution separately. The results are related to scaffolds produced by porogen burn-off (P) and by 3D printing (3D).*

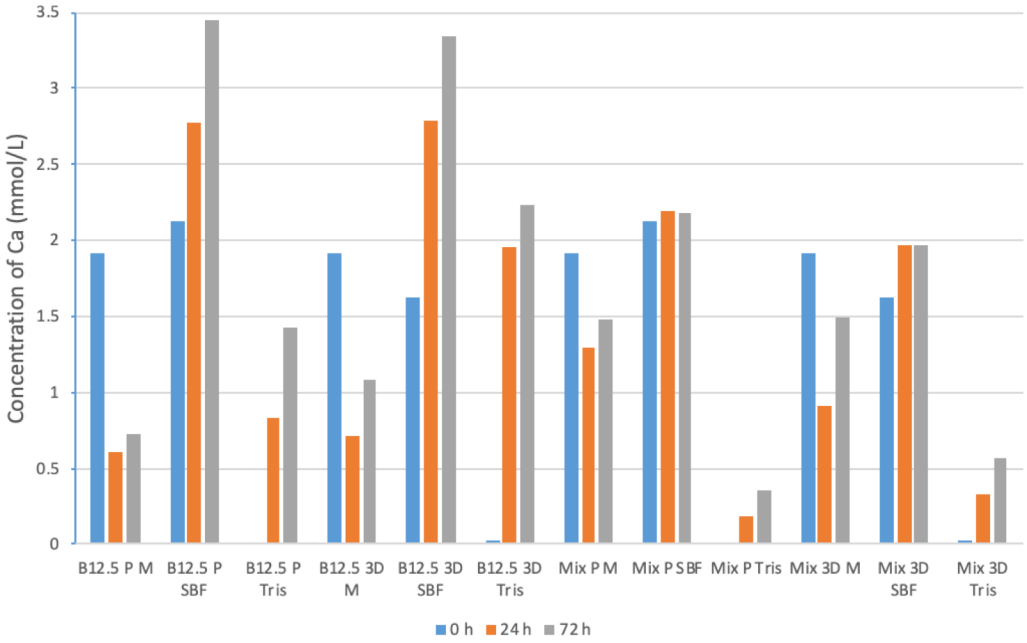

Figure 31. *The concentrations of Ca in the different solutions for immersion of 72 h. 0 h expresses the original medium and blank solution. The M, SBF, and TRIS express the scaffolds immersed in the culture medium, SBF and TRIS solution separately. The results are related to scaffolds produced by porogen burn-off (P) and by 3D printing (3D).*

As expected, the B and Si release was greater for the glass B12.5 than the Mix composition, due to the faster dissolution rate of this glass as discussed earlier. The increase in Si and B in the culture medium was significantly higher in culture medium due to the small volume used in culture tests. Indeed, when the surface area to volume of solution ratio increases the dissolution rate is expected to increase. Finally, the scaffolds prepared by the porogen burn-off technique release ions at a faster rate in agreement with the static test performed. Overall the B ion concentration in the culture medium is very high. At such a concentration, toxicity can be expected (Qiang Fu *et al.* 2010;Ojansivu *et al.* 2018).

As seen in the culture medium, static and dynamic tests, the pre-incubation of the samples, prior to cell test is crucial to avoid the burst of ions which will potentially be toxic to the cells.

In order to improve the cell behavior in contact with such scaffolds, pre-incubation can be extended and/or the size of the samples can be decreased. Another aspect that needed to be considered is related to the observation, even the autofluorescence was not the primary challenge, the problem was to observe the cell within the scaffolds. Now only the first and second layers of scaffolds produced by 3D printing and the surface of scaffolds produced by the porogen burn-off method could be observed and imaged, the growth and distribution of cells inside the scaffolds are yet unknown, and therefore no conclusion can be made on the ability of the cells to migrate within the construct.

5.5 Cellular Proliferation

The results from the first test exhibited the toxicity of scaffolds after pre-treatment for 48 h. The proliferation of osteoblasts could not be improved but killed all the live cells, in agreement with the Live and dead assay performed post-incubation for 48 h. Then the extract from the pre-treatment of 72 h was used to find the optimum concentration for the proliferation of osteoblasts. However, it appeared that the cells could proliferate for 24 h and died by 48 h. Such results could not be explained and can be assigned to the contamination and/or impaired cell lines. For the B12.5 3D group, the cells were stimulated by the medium containing more ions which were the 50% and 25% groups and then some response which can reduce the density of cells, for example, the apoptosis, could be activated. But those levels of ions were not truly harmful and even beneficial and then the proliferation was improved at longer culture time. For the Mix 3D group, the ions at all the levels can improve the proliferation in the first 24 h, but again the cells started to die at 48 h which could not be explained. These results need to be repeated and confirmed with more parallel samples and new cells. Additionally, the

concentrations of ions with good performance in Table 6 were quite different from each other. And the concentrations of B from the B12.5 groups were higher than the threshold values mentioned earlier which were 0.65 and 0.5 mmol/L. As a result, there should be some concentrations of ions that can improve the proliferation of cells continuously, but still, further experiments to establish such concentration levels are required.

For the preferable evaluation of the performance of scaffolds, especially for the Mix 3D group, the osteoblasts should be seeded and cultured with scaffolds for a longer period of 14 days to test the proliferation of cells. The osteogenic differentiation of MC3T3 cells by the scaffolds could be analyzed through the ALP activity and the expression of marker genes, and other additional tests could also be used such as the immunocytochemical staining of osteocalcin and collagen-I. Also, the morphology of cells in response to the scaffolds could be evaluated by the staining methods or SEM which can also analyze the situation of migration of cells. But there is another way is to design and attempt the dynamic culture system before these evaluations of cellular viability, proliferation, and differentiation. It might be a better standard to determine if the performance of scaffolds can be good enough to continue the experiments in vivo.

6. CONCLUSION

Borosilicate glass scaffolds, prepared from the B12.5 and Mix composition, produced using the robocasting or porogen burn-off technique were efficiently manufactured. Of both processes, the 3D printing exhibited excellent porosities, pore size, and reproducibility. This method allows reproducible scaffold manufacturing. The drawbacks of the technique lie in the resolution of the printing, the stability of the ink (time and temperature) and the homogeneity of the ink.

In static dissolution, the consumption of P and Ca ions was indicative of the formation of a HA-like layer in all produced scaffolds. High ion releases were measured which could be assumed to be harmful to cells.

Dynamic tests were performed to more closely mimic the in-vivo conditions. The pH values and ionic concentrations remained at physiological values, after an initial burst release within the first 6 hours. This explains the better in-vitro and in-vivo outcomes of bioactive borosilicate glasses reported in the literature. Indeed, in-vivo the flow of fluids reduces the risk of localized ion concentration rise, above the toxic values.

In the cellular viability tests, the scaffolds of the 3D Mix group exhibited the best performance and the period of pretreatment was supposed to be 72 h at least. Indeed, it was found that due to the lower volume of medium compared to the static test, the ion concentration increased drastically in the medium, leading to a high toxicity level. Furthermore, as in the static test, long immersion in the culture medium led to precipitation of HA, thus decreasing drastically the P and Ca concentration in the culture medium. The pore sizes of scaffolds produced by robocasting were large enough for the colonization and migration of cells. However, the significant density of dead cells could be visualized. This is most probably due to high ion concentration within the core of the scaffolds. This could be alleviated by a dynamic cell culture test which will ensure that the medium is constantly refreshed.

In vitro dissolution and preliminary cell tests confirm that the scaffolds should be pre-incubated before testing to avoid the burst of ions that can harm the cells. Furthermore, the size of the scaffolds used should be adjusted to limit the release of ions.

As expected from the composition of the glass, the Mix composition released ions at a lower rate than the B12.5 glass, leading to better results in in-vitro cell testing. These encouraging results pave the road to evaluate the borosilicate glass scaffolds for application in bone tissue engineering. The cell viability and proliferation test must be

performed for a longer time and complemented with a differentiation test, where markers of early and late osteogenesis would be tracked.

REFERENCES

A. Sims, N. and H. Gooi, J. (2008). Bone remodeling: Multiple cellular interactions required for coupling of bone formation and resorption, Seminars in Cell and Developmental Biology. doi: 10.1016/j.semcdb.2008.07.016.

Abe, Y. *et al.* (2000). Development of mineralized nodules in fetal rat mandibular osteogenic precursor cells: requirement for dexamethasone but not for beta-glycerophosphate, Calcified tissue international, vol.66(1), pp. 66–9. Available at: http://www.ncbi.nlm.nih.gov/pubmed/10602848 (Accessed: 13 July 2019).

Aronow, M. A. *et al.* (1990). Factors that promote progressive development of the osteoblast phenotype in cultured fetal rat calvaria cells., Journal of cellular physiology, vol.143(2), pp. 213–21. doi: 10.1002/jcp.1041430203.

B. Gullberg, O. J. and J. A. K. (1997). Projections for Hip Fracture B, Osteoporos Int. doi: https://doi.org/10.1007/PL00004148.

Bae, E.-J. *et al.* (2014). Bond and fracture strength of metal-ceramic restorations formed by selective laser sintering, The Journal of Advanced Prosthodontics. doi: 10.4047/jap.2014.6.4.266.

Baino, F., Verné, E. and Massera, J. (2018). Additive manufacturing of bioactive glasses, Journal of 3D Printing in Medicine, vol.2(2), pp. 47–49. doi: 10.2217/3dp-2018-0001.

Baino, F. and Vitale-Brovarone, C. (2011). Three-dimensional glass-derived scaffolds for bone tissue engineering: current trends and forecasts for the future, Journal of biomedical materials research. Part A, vol.97(4), pp. 514–35. doi: 10.1002/jbm.a.33072.

Battistella, E. *et al.* (2012). Cuttlefish bone scaffold for tissue engineering: a novel hydrothermal transformation, chemical-physical, and biological characterization, Journal of applied biomaterials & functional materials, vol.10(2), pp. 99–106. doi: 10.5301/JABFM.2012.9257.

Beattie, J. H. and Avenell, A. (1992). Trace element nutrition and bone metabolism, Nutrition research reviews, vol.5(1), pp. 167–88. doi: 10.1079/NRR19920013.

Beddoe, A. H., Darley, P. J. and Spiers, F. W. (1976). Measurements of trabecular bone structure in man, Physics in medicine and biology, vol.21(4), pp. 589–607. Available at: http://www.ncbi.nlm.nih.gov/pubmed/972924 (Accessed: 11 July 2019).

Bettger, W. J. and McKeehan, W. L. (1986). Mechanisms of cellular nutrition, Physiological reviews, vol.66(1), pp. 1–35. doi: 10.1152/physrev.1986.66.1.1.

Bi, L. *et al.* (2013). Effect of bioactive borate glass microstructure on bone regeneration, angiogenesis, and hydroxyapatite conversion in a rat calvarial defect model, Acta Biomaterialia. doi: 10.1016/j.actbio.2013.04.043.

Boivin, G. *et al.* (1996). Strontium distribution and interactions with bone mineral in monkey iliac bone after strontium salt (S 12911) administration, Journal of bone and mineral research : the official journal of the American Society for Bone and Mineral Research, vol.11(9), pp. 1302–11. doi: 10.1002/jbmr.5650110915.

Bongio, M. *et al.* (2016). A 3D vascularized bone remodeling model combining osteoblasts and osteoclasts in a CaP nanoparticle-enriched matrix, Nanomedicine. doi: 10.2217/nnm-2015-0021.

Bose, S., Vahabzadeh, S. and Bandyopadhyay, A. (2013). Bone tissue engineering using 3D printing, Materials Today, pp. 496–504. doi: 10.1016/j.mattod.2013.11.017.

Boskey, A. L. and Roy, R. (2008). Cell Culture Systems for Studies of Bone and Tooth Mineralization, Chemical Reviews, vol.108(11), pp. 4716–4733. doi: 10.1021/cr0782473.

Bouvard, D. *et al.* (2001). Functional consequences of integrin gene mutations in mice, Circulation research, vol.89(3), pp. 211–23. doi: 10.1161/hh1501.094874.

Brink, M. *et al.* (1997). Compositional dependence of bioactivity of glasses in the system Na2O- K2O-MgO-Cao-B2O3-P2O5-SiO2, Journal of Biomedical Materials Research. doi: 10.1002/(SICI)1097-4636(199710)37:1<114::AID-JBM14>3.0.CO;2-G.

Brink, M. (1997). The influence of alkali and alkaline earths on the working range for bioactive glasses, Journal of Biomedical Materials Research. doi: 10.1002/(SICI)1097-4636(199707)36:1<109::AID-JBM13>3.0.CO;2-D.

Brown, R. *et al.* (2009). *Conversion of Borate Glass to Hydroxyapatite and its Effect on Proliferation of MC3T3-E1 Cells*, Journal of biomedical materials research. Part A. doi: 10.1002/jbm.a.31679.

Brown, R. F. *et al.* (2009). Effect of borate glass composition on its conversion to hydroxyapatite and on the proliferation of MC3T3-E1 cells, Journal of Biomedical Materials Research - Part A, vol.88(2), pp. 392–400. doi: 10.1002/jbm.a.31679.

Brunello, G. *et al.* (2016). Powder-based 3D printing for bone tissue engineering, Biotechnology Advances. doi: 10.1016/j.biotechadv.2016.03.009.

Buckwalter, J. A. *et al.* (1995). Bone biology. Part I: Structure, blood supply, cells, matrix, and mineralization, Journal of Bone and Joint Surgery - Series A. doi: 10.2106/00004623-199508000-00019.

Butscher, A. *et al.* (2011). Structural and material approaches to bone tissue engineering in powder-based three-dimensional printing, Acta Biomaterialia. doi: 10.1016/j.actbio.2010.09.039.

Cambra-Moo, O. *et al.* (2014). An approach to the histomorphological and histochemical variations of the humerus cortical bone through human ontogeny, Journal of Anatomy. doi: 10.1111/joa.12172.

Carlisle, E. M. (1970). Silicon: a possible factor in bone calcification, Science (New York, N.Y.), vol.167(3916), pp. 279–80. doi: 10.1126/science.167.3916.279.

Carlisle, E. M. (1981). Silicon: a requirement in bone formation independent of vitamin D1, Calcified tissue international, vol.33(1), pp. 27–34. Available at: http://www.ncbi.nlm.nih.gov/pubmed/6257332 (Accessed: 12 July 2019).

Cavo, M. and Scaglione, S. (2016). Scaffold microstructure effects on functional and mechanical performance: Integration of theoretical and experimental approaches for bone tissue engineering applications, Materials Science and Engineering C. doi: 10.1016/j.msec.2016.07.041.

Chen, Q. Z., Thompson, I. D. and Boccaccini, A. R. (2006). 45S5 Bioglass-derived glass-ceramic scaffolds for bone tissue engineering, Biomaterials, vol.27(11), pp. 2414–25. doi: 10.1016/j.biomaterials.2005.11.025.

Chen, Z. *et al.* (2016). Osteoimmunomodulation for the development of advanced bone biomaterials, Materials Today. doi: 10.1016/j.mattod.2015.11.004.

Chia, H. N. and Wu, B. M. (2015). Recent advances in 3D printing of biomaterials, Journal of biological engineering, vol.9, p. 4. doi: 10.1186/s13036-015-0001-4.

Cohn, D., Sosnik, A. and Garty, S. (2005). Smart hydrogels for in situ generated implants, Biomacromolecules. doi: 10.1021/bm0495250.

Daga, D. *et al.* (2018). Tentpole technique for bone regeneration in vertically deficient alveolar ridges: A prospective study, Journal of Oral Biology and Craniofacial Research. doi: 10.1016/j.jobcr.2017.11.002.

Dallas, S. L., Prideaux, M. and Bonewald, L. F. (2013). The osteocyte: an endocrine cell ... and more, Endocrine reviews, vol.34(5), pp. 658–90. doi: 10.1210/er.2012-1026.

Daly, A. C. *et al.* (2018). 3D printed microchannel networks to direct vascularisation during endochondral bone repair, Biomaterials. doi:10.1016/j.biomaterials.2018.01.057.

Datta, H. K. *et al.* (2008). The cell biology of bone metabolism, Journal of clinical pathology, vol.61(5), pp. 577–87. doi: 10.1136/jcp.2007.048868.

Derby, B. (2012). Printing and prototyping of tissues and scaffolds, Science. doi: 10.1126/science.1226340.

Diba, M. *et al.* (2012). Magnesium-Containing Bioactive Glasses for Biomedical Applications, International Journal of Applied Glass Science. doi: 10.1111/j.2041-1294.2012.00095.x.

Dimitriou, R. *et al.* (2011). Bone regeneration: Current concepts and future directions, BMC Medicine. doi: 10.1186/1741-7015-9-66.

Doiphode, N. D. *et al.* (2011). Freeze extrusion fabrication of 13-93 bioactive glass scaffolds for bone repair, Journal of Materials Science: Materials in Medicine. doi: 10.1007/s10856-011-4236-4.

Downey, P. A. and Siegel, M. I. (2006). Bone Biology and the Clinical Implications for Osteoporosis, Physical Therapy, vol.86(1), pp. 77–91. doi: 10.1093/ptj/86.1.77.

Du, X., Fu, S. and Zhu, Y. (2018). 3D printing of ceramic-based scaffolds for bone tissue engineering: An overview, Journal of Materials Chemistry B. Royal Society of Chemistry, vol.6(27), pp. 4397–4412. doi: 10.1039/c8tb00677f.

Dzondo-Gadet, M. *et al.* (2002). Action of Boron at the Molecular Level Effects on Transcription and Translation in an Acellular System, Biological Trace Element Research, vol.85(1), pp. 23–33. doi: 10.1385/BTER:85:1:23.

El-Rashidy, A. A. *et al.* (2017). Regenerating bone with bioactive glass scaffolds: A review of in vivo studies in bone defect models, Acta Biomaterialia. Acta Materialia Inc., vol.62, pp. 1–28. doi: 10.1016/j.actbio.2017.08.030.

Fagerlund, Susanne *et al.* (2012). Dissolution kinetics of a bioactive glass by continuous measurement, Journal of the American Ceramic Society, vol.95(10), pp. 3130–3137. doi: 10.1111/j.1551-2916.2012.05374.x.

Fagerlund, S. *et al.* (2012). Phase composition and in vitro bioactivity of porous implants made of bioactive glass S53P4, Acta Biomaterialia, vol.8(6), pp. 2331–2339. doi: 10.1016/j.actbio.2012.03.011.

Fagerlund, S., Hupa, L. and Hupa, M. (2013). Dissolution patterns of biocompatible glasses in 2-Amino-2-hydroxymethyl- propane-1,3-diol (Tris) buffer, Acta Biomaterialia. Acta Materialia Inc., vol.9(2), pp. 5400–5410. doi: 10.1016/j.actbio.2012.08.051.

Fernandez-Yague, M. A. *et al.* (2015). Biomimetic approaches in bone tissue engineering: Integrating biological and physicomechanical strategies, Advanced Drug Delivery Reviews. Elsevier B.V., vol.84, pp. 1–29. doi: 10.1016/j.addr.2014.09.005.

Filho, O. P., La Torre, G. P. and Hench, L. L. (1996). Effect of crystallization on apatite-layer formation of bioactive glass 45S5, Journal of Biomedical Materials Research, vol.30(4), pp. 509–514. doi: 10.1002/(SICI)1097-4636(199604)30:4<509::AID-JBM9>3.0.CO;2-T.

Florencio-Silva, R. *et al.* (2015). Biology of Bone Tissue: Structure, Function, and Factors That Influence Bone Cells, BioMed Research International, vol.2015. doi: 10.1155/2015/421746.

Franco, J. *et al.* (2010). Direct write assembly of calcium phosphate scaffolds using a water-based hydrogel, Acta Biomaterialia. doi: 10.1016/j.actbio.2009.06.031.

Fu, H. *et al.* (2009). In vitro evaluation of borate-based bioactive glass scaffolds prepared by a polymer foam replication method, Materials Science and Engineering C. Elsevier B.V., vol.29(7), pp. 2275–2281. doi: 10.1016/j.msec.2009.05.013.

Fu, Q. *et al.* (2008). Mechanical and in vitro performance of 13-93 bioactive glass scaffolds prepared by a polymer foam replication technique, Acta biomaterialia, vol.4(6), pp. 1854–64. doi: 10.1016/j.actbio.2008.04.019.

Fu, Qiang *et al.* (2010). Silicate, borosilicate, and borate bioactive glass scaffolds with controllable degradation rate for bone tissue engineering applications. I. Preparation and in vitro degradation, Journal of Biomedical Materials Research - Part A, vol.95(1), pp. 164–171. doi: 10.1002/jbm.a.32824.

Fu, Q *et al.* (2010). Silicate, borosilicate, and borate bioactive glass scaffolds with controllable degradation rate for bone tissue engineering applications. II. In vitro and in vivo biological evaluation, J Biomed Mater Res A. doi: 10.1002/jbm.a.32823.

Fu, Q. *et al.* (2011). Bioactive glass scaffolds for bone tissue engineering: State of the art and future perspectives, Materials Science and Engineering C. Elsevier B.V., vol.31(7), pp. 1245–1256. doi: 10.1016/j.msec.2011.04.022.

García-Gareta, E., Coathup, M. J. and Blunn, G. W. (2015). Osteoinduction of bone grafting materials for bone repair and regeneration, Bone. doi: 10.1016/j.bone.2015.07.007.

Gariboldi, M. I. and Best, S. M. (2015). Effect of Ceramic Scaffold Architectural Parameters on Biological Response, Frontiers in Bioengineering and Biotechnology. doi: 10.3389/fbioe.2015.00151.

Gentleman, E. *et al.* (2010). The effects of strontium-substituted bioactive glasses on osteoblasts and osteoclasts in vitro, Biomaterials. doi: 10.1016/j.biomaterials.2010.01.121.

Gerhardt, L.-C. and Boccaccini, A. R. (2010). Bioactive Glass and Glass-Ceramic Scaffolds for Bone Tissue Engineering, Materials, vol.3(7), pp. 3867–3910. doi: 10.3390/ma3073867.

Goldstein, S. A. (1987). The mechanical properties of trabecular bone: dependence on anatomic location and function., Journal of biomechanics.

Gong, B. *et al.* (2017). Strain-controlled fatigue behaviors of porous PLA-based scaffolds by 3D-printing technology, Journal of Biomaterials Science, Polymer Edition. doi: 10.1080/09205063.2017.1388993.

Gorustovich, A. A. *et al.* (2006). Biological performance of boron-modified bioactive glass particles implanted in rat tibia bone marrow, Biomedical materials (Bristol, England), vol.1(3), pp. 100–5. doi: 10.1088/1748-6041/1/3/002.

Gorustovich, A. A. *et al.* (2008). Histomorphometric study of alveolar bone healing in rats fed a boron-deficient diet, Anatomical record (Hoboken, N.J. : 2007), vol.291(4), pp. 441–7. doi: 10.1002/ar.20672.

Gough, J. E., Notingher, I. and Hench, L. L. (2004). Osteoblast attachment and mineralized nodule formation on rough and smooth 45S5 bioactive glass monoliths, Journal of biomedical materials research. Part A, vol.68(4), pp. 640–50. doi: 10.1002/jbm.a.20075.

Gregor, A. *et al.* (2017). Designing of PLA scaffolds for bone tissue replacement fabricated by ordinary commercial 3D printer, Journal of Biological Engineering. doi: 10.1186/s13036-017-0074-3.

Grémare, A. *et al.* (2018). Characterization of printed PLA scaffolds for bone tissue engineering, Journal of Biomedical Materials Research - Part A. doi: 10.1002/jbm.a.36289.

Griffith, M. L. and Halloran, J. W. (2005). Freeform Fabrication of Ceramics via Stereolithography, Journal of the American Ceramic Society. doi: 10.1111/j.1151-2916.1996.tb09022.x.

Grigoriadis, A. E. *et al.* (1985). Subclone heterogeneity in a clonally-derived osteoblast-like cell line, Bone, vol.6(4), pp. 249–56. Available at: http://www.ncbi.nlm.nih.gov/pubmed/2996573 (Accessed: 13 July 2019).

Gu, Y. *et al.* (2013). Bone regeneration in rat calvarial defects implanted with fibrous scaffolds composed of a mixture of silicate and borate bioactive glasses, Acta Biomaterialia. doi: 10.1016/j.actbio.2013.06.039.

Guvendiren, M. *et al.* (2016). Designing Biomaterials for 3D Printing, ACS Biomaterials Science and Engineering. doi: 10.1021/acsbiomaterials.6b00121.

Haro Durand, L. A. *et al.* (2015). Angiogenic effects of ionic dissolution products released from a boron-doped 45S5 bioactive glass, Journal of Materials Chemistry B. doi: 10.1039/c4tb01840k.

Haugh, M. G. *et al.* (2010). Crosslinking and Mechanical Properties Significantly Influence Cell Attachment, Proliferation, and Migration Within Collagen Glycosaminoglycan Scaffolds, Tissue Engineering Part A. doi: 10.1089/ten.tea.2010.0590.

Hench, L. L., Roki, N. and Fenn, M. B. (2014). Bioactive glasses: Importance of structure and properties in bone regeneration, Journal of Molecular Structure. doi: 10.1016/j.molstruc.2014.03.066.

Hesaraki, S. *et al.* (2010). Physico-chemical and in vitro biological evaluation of strontium/calcium silicophosphate glass, Journal of materials science. Materials in medicine, vol.21(2), pp. 695–705. doi: 10.1007/s10856-009-3920-0.

Hirao, M. *et al.* (2007). Oxygen tension is an important mediator of the transformation of osteoblasts to osteocytes, Journal of bone and mineral metabolism, vol.25(5), pp. 266–76. doi: 10.1007/s00774-007-0765-9.

Hoppe, A. *et al.* (2014). In vitro reactivity of Sr-containing bioactive glass (type 1393) nanoparticles, Journal of Non-Crystalline Solids. doi: 10.1016/j.jnoncrysol.2013.12.010.

Hoppe, A., Güldal, N. S. and Boccaccini, A. R. (2011). A review of the biological response to ionic dissolution products from bioactive glasses and glass-ceramics, Biomaterials. Elsevier Ltd, vol.32(11), pp. 2757–2774. doi: 10.1016/j.biomaterials.2011.01.004.

Huang, W., Day, D. E., *et al.* (2006). Kinetics and mechanisms of the conversion of silicate (45S5), borate, and borosilicate glasses to hydroxyapatite in dilute phosphate solutions, Journal of materials science. Materials in medicine, vol.17(7), pp. 583–96. doi: 10.1007/s10856-006-9220-z.

Huang, W., N. Rahaman, M., *et al.* (2006). *Mechanisms for Converting Bioactive Silicate, Borate, and Borosilicate Glasses to Hydroxyapatite in Dilute Phosphate Solution*, Physics and Chemistry of Glasses - European Journal of Glass Science and Technology Part B.

Hupa, L. *et al.* (2016). Dissolution behavior of the bioactive glass S53P4 when sodium is replaced by potassium, and calcium with magnesium or strontium, Journal of Non-Crystalline Solids. Elsevier B.V., vol.432, pp. 41–46. doi: 10.1016/j.jnoncrysol.2015.03.026.

Hutmacher, D. W. (2000). Scaffolds in tissue engineering bone and cartilage, Biomaterials, vol.21(24), pp. 2529–2543. doi: 10.1016/S0142-9612(00)00121-6.

Hutmacher, D. W. (2006). Regenerative medicine will impact, but not replace, the medical device industry, Expert review of medical devices, vol.3(4), pp. 409–12. doi: 10.1586/17434440.3.4.409.

Hwa, L. C. *et al.* (2017). Recent advances in 3D printing of porous ceramics: A review, Current Opinion in Solid State and Materials Science. doi: 10.1016/j.cossms.2017.08.002.

Ivankovic, H. *et al.* (2010). Hydroxyapatite formation from cuttlefish bones: Kinetics, Journal of Materials Science: Materials in Medicine. doi: 10.1007/s10856-010-4115-4.

Jones, A. C. *et al.* (2007). Assessment of bone ingrowth into porous biomaterials using MICRO-CT, Biomaterials, vol.28(15), pp. 2491–504. doi: 10.1016/j.biomaterials.2007.01.046.

Jones, J. R. (2013). Review of bioactive glass: From Hench to hybrids, Acta Biomaterialia. Acta Materialia Inc., vol.9(1), pp. 4457–4486. doi: 10.1016/j.actbio.2012.08.023.

Julien, M. *et al.* (2009). Phosphate-dependent regulation of MGP in osteoblasts: role of ERK1/2 and Fra-1, Journal of bone and mineral research : the official journal of the American Society for Bone and Mineral Research, vol.24(11), pp. 1856–68. doi: 10.1359/jbmr.090508.

Jung, S. B. *et al.* (2013). Potential toxicity of bioactive borate glasses in-vitro and in-vivo, pp. 65–74.

Karageorgiou, V. and Kaplan, D. (2005). Porosity of 3D biomaterial scaffolds and osteogenesis, Biomaterials. doi: 10.1016/j.biomaterials.2005.02.002.

Kargozar, S., Baino, F., *et al.* (2018). Bioactive Glasses: Sprouting Angiogenesis in Tissue Engineering, Trends in Biotechnology. Elsevier Ltd, vol.36(4), pp. 430–444. doi: 10.1016/j.tibtech.2017.12.003.

Kargozar, S., Mozafari, M., *et al.* (2018). Osteogenic potential of stem cells-seeded bioactive nanocomposite scaffolds: A comparative study between human mesenchymal stem cells derived from bone, umbilical cord Wharton's jelly, and adipose tissue, Journal of Biomedical Materials Research - Part B Applied Biomaterials. doi: 10.1002/jbm.b.33814.

Kasperk, C. *et al.* (1995). Human bone cell phenotypes differ depending on their skeletal site of origin, The Journal of clinical endocrinology and metabolism, vol.80(8), pp. 2511–7. doi: 10.1210/jcem.80.8.7629252.

Katsamenis, O. L. *et al.* (2013). Load-bearing in cortical bone microstructure: Selective stiffening and heterogeneous strain distribution at the lamellar level, Journal of the mechanical behavior of biomedical materials, vol.17, pp. 152–65. doi: 10.1016/j.jmbbm.2012.08.016.

Katsimbri, P. (2017). The biology of normal bone remodelling, European Journal of Cancer Care. doi: 10.1111/ecc.12740.

Koester, K. J., Ager, J. W. and Ritchie, R. O. (2008). The true toughness of human cortical bone measured with realistically short cracks, Nature Materials. doi: 10.1038/nmat2221.

Kohli, N. *et al.* (2018). Bone remodelling in vitro: Where are we headed?: -A review on the current understanding of physiological bone remodelling and inflammation and the strategies for testing biomaterials in vitro, Bone. Elsevier Inc., vol.110, pp. 38–46. doi: 10.1016/j.bone.2018.01.015.

Kolan, K. C. R. *et al.* (2012). Effect of material, process parameters, and simulated body fluids on mechanical properties of 13-93 bioactive glass porous constructs made by selective laser sintering, Journal of the mechanical behavior of biomedical materials, vol.13, pp. 14–24. doi: 10.1016/j.jmbbm.2012.04.001.

Kumar, A. *et al.* (2016). Biocompatibility and mechanical behaviour of three-dimensional scaffolds for biomedical devices: Process-structure-property paradigm, International Materials Reviews. doi: 10.1080/09506608.2015.1128310.

Kureshi, A. *et al.* (2010). Alignment hierarchies: engineering architecture from the nanometre to the micrometre scale, Journal of the Royal Society, Interface, vol.7 Suppl 6, pp. S707-16. doi: 10.1098/rsif.2010.0346.focus.

Lee, J. and Cho, D.-W. (2015). 3D Printing Technology Over a Drug Delivery for Tissue Engineering, Current Pharmaceutical Design. doi: 10.2174/1381612821666150115125324.

Lee, J. W. (2015). 3D Nanoprinting Technologies for Tissue Engineering Applications, Journal of Nanomaterials, vol.2015, pp. 1–14. doi: 10.1155/2015/213521.

Lee, K. W. *et al.* (2007). Poly(propylene fumarate) bone tissue engineering scaffold fabrication using stereolithography: Effects of resin formulations and laser parameters, Biomacromolecules. doi: 10.1021/bm060834v.

Leis, H. J. *et al.* (1997). Phenotypic heterogeneity of osteoblast-like MC3T3-E1 cells: changes of bradykinin-induced prostaglandin E2 production during osteoblast maturation, Journal of bone and mineral research : the official journal of the American Society for Bone and Mineral Research, vol.12(4), pp. 541–51. doi: 10.1359/jbmr.1997.12.4.541.

Lenaerts, V. *et al.* (1987). Temperature-dependent rheological behavior of Pluronic F-127 aqueous solutions, International Journal of Pharmaceutics. doi: 10.1016/0378-5173(87)90206-7.

Lewandrowski, K. U. *et al.* (2000). Bioresorbable bone graft substitutes of different osteoconductivities: a histologic evaluation of osteointegration of poly(propylene glycol-co-fumaric acid)-based cement implants in rats, Biomaterials, vol.21(8), pp. 757–64. Available at: http://www.ncbi.nlm.nih.gov/pubmed/10721744 (Accessed: 9 July 2019).

Li, Y. *et al.* (2015). Bone defect animal models for testing efficacy of bone substitute biomaterials, Journal of Orthopaedic Translation. doi: 10.1016/j.jot.2015.05.002.

Liu, X. *et al.* (2013). Enhanced bone regeneration in rat calvarial defects implanted with surface-modified and BMP-loaded bioactive glass (13-93) scaffolds, Acta Biomaterialia. doi: 10.1016/j.actbio.2013.03.039.

Loh, Q. L. and Choong, C. (2013). Three-Dimensional Scaffolds for Tissue Engineering Applications: Role of Porosity and Pore Size, Tissue Engineering Part B: Reviews. doi: 10.1089/ten.teb.2012.0437.

Ma, H. *et al.* (2018). 3D-printed bioceramic scaffolds: From bone tissue engineering to tumor therapy, Acta Biomaterialia. Acta Materialia Inc., vol.79, pp. 37–59. doi: 10.1016/j.actbio.2018.08.026.

Maeno, S. *et al.* (2005). The effect of calcium ion concentration on osteoblast viability, proliferation and differentiation in monolayer and 3D culture, Biomaterials, vol.26(23), pp. 4847–55. doi: 10.1016/j.biomaterials.2005.01.006.

Malaval, L. *et al.* (2009). Absence of bone sialoprotein (BSP) impairs cortical defect repair in mouse long bone, Bone, vol.45(5), pp. 853–61. doi: 10.1016/j.bone.2009.06.005.

Malladi, P. *et al.* (2006). Effect of reduced oxygen tension on chondrogenesis and osteogenesis in adipose-derived mesenchymal cells, American journal of physiology. Cell physiology, vol.290(4), pp. C1139-46. doi: 10.1152/ajpcell.00415.2005.

Marie, P. J. *et al.* (2001). Mechanisms of action and therapeutic potential of strontium in bone, Calcified tissue international, vol.69(3), pp. 121–9. Available at: http://www.ncbi.nlm.nih.gov/pubmed/11683526 (Accessed: 12 July 2019).

Marie, P. J. (2010). The calcium-sensing receptor in bone cells: a potential therapeutic target in osteoporosis., Bone, vol.46(3), pp. 571–6. doi: 10.1016/j.bone.2009.07.082.

Martin, R. B. *et al.* (2015). *Skeletal Tissue Mechanics*, New York, NY: Springer New York. doi: 10.1007/978-1-4939-3002-9.

Martínez, M. E. *et al.* (1999). Influence of skeletal site of origin and donor age on osteoblastic cell growth and differentiation, Calcified tissue international, vol.64(4), pp. 280–6. Available at: http://www.ncbi.nlm.nih.gov/pubmed/10089218 (Accessed: 13 July 2019).

Massera, J. *et al.* (2015). The influence of SrO and CaO in silicate and phosphate bioactive glasses on human gingival fibroblasts, Journal of Materials Science: Materials in Medicine. doi: 10.1007/s10856-015-5528-x.

Massera, J. and Hupa, L. (2014). Influence of SrO substitution for CaO on the properties of bioactive glass S53P4, Journal of materials science. Materials in medicine, vol.25(3), pp. 657–68. doi: 10.1007/s10856-013-5120-1.

Massera, J., Hupa, L. and Hupa, M. (2012). Influence of the partial substitution of CaO with MgO on the thermal properties and in vitro reactivity of the bioactive glass S53P4, Journal of Non-Crystalline Solids. doi: 10.1016/j.jnoncrysol.2012.06.032.

Matsumoto, M. *et al.* (2016). Bone Tissue Healing Dynamics: From Damage to Reconstruction, Journal of Molecular Signaling Updates, vol.1, pp. 33–40.

Matsuo, K. and Irie, N. (2008). Osteoclast-osteoblast communication, Archives of biochemistry and biophysics, vol.473(2), pp. 201–9. doi: 10.1016/j.abb.2008.03.027.

Mello, A. S. da S. *et al.* (2016). Some aspects of bone remodeling around dental implants, Revista Clínica de Periodoncia, Implantología y Rehabilitación Oral. doi: 10.1016/j.piro.2015.12.001.

Mitrossilis, D. *et al.* (2009). Single-cell response to stiffness exhibits muscle-like behavior, Proceedings of the National Academy of Sciences. doi: 10.1073/pnas.0903994106.

Modglin, V. C. *et al.* (2013). Cytotoxicity assessment of modified bioactive glasses with MLO-A5 osteogenic cells in vitro, Journal of Materials Science: Materials in Medicine. doi: 10.1007/s10856-013-4875-8.

Mohamad Yunos, D., Bretcanu, O. and Boccaccini, A. R. (2008). Polymer-bioceramic composites for tissue engineering scaffolds, in Journal of Materials Science. doi: 10.1007/s10853-008-2552-y.

Monfoulet, L. *et al.* (2010). Bone sialoprotein, but not osteopontin, deficiency impairs the mineralization of regenerating bone during cortical defect healing, Bone, vol.46(2), pp. 447–52. doi: 10.1016/j.bone.2009.09.007.

Nelson, C. M. *et al.* (2005). Emergent patterns of growth controlled by multicellular form and mechanics, Proceedings of the National Academy of Sciences. doi: 10.1073/pnas.0502575102.

Ning, J. *et al.* (2007). Synthesis and in vitro bioactivity of a borate-based bioglass, Materials Letters. doi: 10.1016/j.matlet.2007.04.089.

Nommeots-Nomm, A., Lee, P. D. and Jones, J. R. (2018). Direct ink writing of highly bioactive glasses, Journal of the European Ceramic Society. Elsevier Ltd, vol.38(3), pp. 837–844. doi: 10.1016/j.jeurceramsoc.2017.08.006.

Nommeots-Nomm, A. and Massera, J. (2017). Glass and Glass-Ceramic Scaffolds: Manufacturing Methods and the Impact of Crystallization on In-Vitro Dissolution, in Scaffolds in Tissue Engineering - Materials, Technologies and Clinical Applications. doi: 10.5772/intechopen.70242.

Nuss, K. M. R. and Rechenberg, B. von (2008). Biocompatibility Issues with Modern Implants in Bone - A Review for Clinical Orthopedics, The Open Orthopaedics Journal. doi: 10.2174/1874325000802010066.

Ojansivu, M. *et al.* (2018). The effect of S53P4-based borosilicate glasses and glass dissolution products on the osteogenic commitment of human adipose stem cells, PLoS ONE. Public Library of Science, vol.13(8). doi: 10.1371/journal.pone.0202740.

Panda, N. N., Pramanik, K. and Sukla, L. B. (2014). Extraction and characterization of biocompatible hydroxyapatite from fresh water fish scales for tissue engineering scaffold, Bioprocess and biosystems engineering, vol.37(3), pp. 433–40. doi: 10.1007/s00449-013-1009-0.

Park, M. *et al.* (2004). NaBC1 is a ubiquitous electrogenic Na^+-coupled borate transporter essential for cellular boron homeostasis and cell growth and proliferation, Molecular Cell. doi: 10.1016/j.molcel.2004.09.030.

Pearce, A. I. *et al.* (2007). Animal models for implant biomaterial research in bone: A review, European Cells and Materials, pp. 1–10. doi: 10.22203/eCM.v013a01.

Pham, D. T. and Gault, R. S. (1998). A comparison of rapid prototyping technologies, International Journal of Machine Tools and Manufacture. doi: 10.1016/S0890-6955(97)00137-5.

Pohjola, J. (2017). *Borosilicate Scaffold Processing for Bone Tissue*. Tampere University of Technology.

Polo-Corrales, L., Latorre-Esteves, M. and Ramirez-Vick, J. E. (2014). Scaffold Design for Bone Regeneration, Journal of Nanoscience and Nanotechnology, vol.14(1), pp. 15–56. doi: 10.1166/jnn.2014.9127.

Porter, J. R., Ruckh, T. T. and Popat, K. C. (2009). Bone tissue engineering: A review in bone biomimetics and drug delivery strategies, Biotechnology Progress. doi: 10.1002/btpr.246.

Rahaman, M. N. *et al.* (2011). Bioactive glass in tissue engineering, Acta Biomaterialia. Acta Materialia Inc., vol.7(6), pp. 2355–2373. doi: 10.1016/j.actbio.2011.03.016.

Ratner, B. D. *et al.* (2004). *Biomaterials science: an introduction to materials in medicine*. Elsevier.

Reffitt, D. M. *et al.* (2003). Orthosilicic acid stimulates collagen type 1 synthesis and osteoblastic differentiation in human osteoblast-like cells in vitro, Bone, vol.32(2), pp. 127–35. Available at: http://www.ncbi.nlm.nih.gov/pubmed/12633784 (Accessed: 12 July 2019).

Reilly, D. T., Burstein, A. H. and Frankel, V. H. (1974). The elastic modulus for bone, Journal of biomechanics, vol.7(3), pp. 271–5. Available at: http://www.ncbi.nlm.nih.gov/pubmed/4846264 (Accessed: 11 July 2019).

Rho, J. Y., Hobatho, M. C., & Ashman, R. B. (1995). Relations of mechanical properties to density and CT numbers in human bone, Medical Engineering and Physics, 17(5), 347–355. http://doi.org/10.1016/1350-4533(95)97314-FRelations of mechanical properties , Medical Engineering and Physics. doi: 10.1016/1350-4533(95)97314-F.

Richards, R. G. R. *et al.* (2016). In search of an osteoblast cell model for in vitro research, European Cells and Materials, vol.24, pp. 1–17. doi: 10.22203/ecm.v024a01.

Robling, A. G., Castillo, A. B. and Turner, C. H. (2006). BIOMECHANICAL AND MOLECULAR REGULATION OF BONE REMODELING, Annual Review of Biomedical Engineering. doi: 10.1146/annurev.bioeng.8.061505.095721.

Roohani-Esfahani, S. I., Newman, P. and Zreiqat, H. (2016). Design and Fabrication of 3D printed Scaffolds with a Mechanical Strength Comparable to Cortical Bone to Repair Large Bone Defects, Scientific Reports. doi: 10.1038/srep19468.

Roy, T. D. *et al.* (2003). Performance of degradable composite bone repair products made via three-dimensional fabrication techniques, Journal of biomedical materials research. Part A. doi: 10.1002/jbm.a.10582.

Rude, R. K. *et al.* (2003). Magnesium deficiency: effect on bone and mineral metabolism in the mouse, Calcified tissue international, vol.72(1), pp. 32–41. doi: 10.1007/s00223-001-1091-1.

Rude, R. K. *et al.* (2004). Bone loss induced by dietary magnesium reduction to 10% of the nutrient requirement in rats is associated with increased release of substance P and tumor necrosis factor-alpha, The Journal of nutrition. doi: 10.1093/jn/134.1.79.

Rude, R. K. *et al.* (2005). Dietary magnesium reduction to 25% of nutrient requirement disrupts bone and mineral metabolism in the rat, Bone, vol.37(2), pp. 211–9. doi: 10.1016/j.bone.2005.04.005.

Rumpler, M. *et al.* (2008). The effect of geometry on three-dimensional tissue growth, Journal of the Royal Society Interface. doi: 10.1098/rsif.2008.0064.

Schindeler, A. *et al.* (2008). Bone remodeling during fracture repair: The cellular picture, Seminars in Cell and Developmental Biology. doi: 10.1016/j.semcdb.2008.07.004.

Schneider, A. *et al.* (2006). Polyelectrolyte multilayers with a tunable Young's modulus: influence of film stiffness on cell adhesion, Langmuir : the ACS journal of surfaces and colloids, vol.22(3), pp. 1193–200. doi: 10.1021/la0521802.

Seeman, E. (2009). Bone modeling and remodeling, Critical reviews in eukaryotic gene expression, vol.19(3), pp. 219–33. Available at: http://www.ncbi.nlm.nih.gov/pubmed/19883366 (Accessed: 14 July 2019).

Sheikh, Z. *et al.* (2015). Macrophages, foreign body giant cells and their response to implantable biomaterials, Materials. doi: 10.3390/ma8095269.

Sims, N. A. and Martin, T. J. (2014). Coupling the activities of bone formation and resorption: a multitude of signals within the basic multicellular unit, BoneKEy Reports. doi: 10.1038/bonekey.2013.215.

Soung, D. Y. *et al.* (2007). Runx3/AML2/Cbfa3 regulates early and late chondrocyte differentiation, Journal of bone and mineral research : the official journal of the American Society for Bone and Mineral Research, vol.22(8), pp. 1260–70. doi: 10.1359/jbmr.070502.

Souza, M. T. *et al.* (2013). Effect of magnesium ion incorporation on the thermal stability, dissolution behavior and bioactivity in Bioglass-derived glasses, Journal of Non-Crystalline Solids. doi: 10.1016/j.jnoncrysol.2013.10.001.

Sudo, H. *et al.* (1983). In vitro differentiation and calcification in a new clonal osteogenic cell line derived from newborn mouse calvaria, Journal of Cell Biology, vol.96(1), pp. 191–198. doi: 10.1083/jcb.96.1.191.

Sun, Z. L., Wataha, J. C. and Hanks, C. T. (1997). Effects of metal ions on osteoblast-like cell metabolism and differentiation, Journal of biomedical materials research, vol.34(1), pp. 29–37. Available at: http://www.ncbi.nlm.nih.gov/pubmed/8978650 (Accessed: 12 July 2019).

Suzuki, K. R. *et al.* (2011). Long-term histopathologic evaluation of bioactive glass and human-derived graft materials in macaca fascicularis mandibular ridge reconstruction, Implant Dentistry. doi: 10.1097/ID.0b013e3182263665.

Tainio, J. (2016). *IMPACT OF MAGNESIUM AND STRONTIUM ON DISSOLUTION*. Tampere University of Technology.

Tarafder, S. *et al.* (2015). SrO- and MgO-doped microwave sintered 3D printed tricalcium phosphate scaffolds: Mechanical properties and in vivo osteogenesis in a rabbit model, Journal of Biomedical Materials Research - Part B Applied Biomaterials. doi: 10.1002/jbm.b.33239.

Thavornyutikarn, B. *et al.* (2014). Bone tissue engineering scaffolding: computer-aided scaffolding techniques, Progress in Biomaterials. doi: 10.1007/s40204-014-0026-7.

Treiser, M. *et al.* (2013). Degradable and Resorbable Biomaterials, in Biomaterials Science: An Introduction to Materials: Third Edition. doi: 10.1016/B978-0-08-087780-8.00021-8.

Uysal, T. *et al.* (2009). Stimulation of bone formation by dietary boron in an orthopedically expanded suture in rabbits, The Angle orthodontist, vol.79(5), pp. 984–90. doi: 10.2319/112708-604.1.

Valerio, P. *et al.* (2009). Effects of extracellular calcium concentration on the glutamate release by bioactive glass (BG60S) preincubated osteoblasts, Biomedical materials (Bristol, England), vol.4(4), p. 045011. doi: 10.1088/1748-6041/4/4/045011.

Venkatesan, J. and Kim, S. K. (2010). Chitosan composites for bone tissue engineering - An overview, Marine Drugs. doi: 10.3390/md8082252.

Verberckmoes, S. C., De Broe, M. E. and D'Haese, P. C. (2003). Dose-dependent effects of strontium on osteoblast function and mineralization, Kidney international, vol.64(2), pp. 534–43. doi: 10.1046/j.1523-1755.2003.00123.x.

Wang, D. *et al.* (1999). Isolation and Characterization of MC3T3-E1 Vivo Differentiation / Mineralization Potential, Journal of Bone and Mineral Research. doi: 10.1359/jbmr.1999.14.6.893.

Wang, H. *et al.* (2014). Evaluation of borate bioactive glass scaffolds as a controlled delivery system for copper ions in stimulating osteogenesis and angiogenesis in bone healing, Journal of Materials Chemistry B. doi: 10.1039/c4tb01355g.

Wang, X. *et al.* (2016). Topological design and additive manufacturing of porous metals for bone scaffolds and orthopaedic implants: A review, Biomaterials. doi: 10.1016/j.biomaterials.2016.01.012.

Watabe, H. *et al.* (2011). Mechanotransduction activates $\alpha_5\beta_1$ integrin and PI3K/Akt signaling pathways in mandibular osteoblasts, Experimental cell research, vol.317(18), pp. 2642–9. doi: 10.1016/j.yexcr.2011.07.015.

Williams, D. F. (2008). On the mechanisms of biocompatibility, Biomaterials. doi: 10.1016/j.biomaterials.2008.04.023.

Williams, J. M. *et al.* (2005). Bone tissue engineering using polycaprolactone scaffolds fabricated via selective laser sintering, Biomaterials. doi: 10.1007/0-387-34403-9_99.

Witte, F. *et al.* (2005). In vivo corrosion of four magnesium alloys and the associated bone response, Biomaterials, vol.26(17), pp. 3557–63. doi: 10.1016/j.biomaterials.2004.09.049.

Woodruff, M. A. *et al.* (2012). Bone tissue engineering: From bench to bedside, Materials Today. doi: 10.1016/S1369-7021(12)70194-3.

Wu, Y. Y. *et al.* (2010). Evaluation of different culture techniques of osteoblasts on 3D scaffolds, Central European Journal of Biology. doi: 10.2478/s11535-010-0027-z.

Yamasaki, Y. *et al.* (2002). Synthesis of functionally graded MgCO3 apatite accelerating osteoblast adhesion, Journal of biomedical materials research, vol.62(1), pp. 99–105. doi: 10.1002/jbm.10220.

Yao, A. *et al.* (2007). In vitro bioactive characteristics of borate-based glasses with controllable degradation behavior, Journal of the American Ceramic Society. doi: 10.1111/j.1551-2916.2006.01358.x.

Zein, I. *et al.* (2002). Fused deposition modeling of novel scaffold architectures for tissue engineering applications, Biomaterials. doi: 10.1016/S0142-9612(01)00232-0.

Zhang, L. *et al.* (2017). Systematic evaluation of the osteogenic capacity of low-melting bioactive glass-reinforced 45S5 Bioglass porous scaffolds in rabbit femoral defects, Biomedical Materials (Bristol). doi: 10.1088/1748-605X/aa6b5c.

Zhang, L. *et al.* (2019). Three-dimensional (3D) printed scaffold and material selection for bone repair, Acta Biomaterialia. Acta Materialia Inc, vol.84, pp. 16–33. doi: 10.1016/j.actbio.2018.11.039.

Zhang, W. *et al.* (2017). 3D-printed scaffolds with synergistic effect of hollow-pipe structure and bioactive ions for vascularized bone regeneration, Biomaterials. doi: 10.1016/j.biomaterials.2017.05.005.

Zhu, H. *et al.* (2016). 3D plotting of highly uniform Sr 5 (PO 4) 2 SiO 4 bioceramic scaffolds for bone tissue engineering, Journal of Materials Chemistry B. doi: 10.1039/c6tb01692h.

Zreiqat, H. *et al.* (2002). Mechanisms of magnesium-stimulated adhesion of osteoblastic cells to commonly used orthopaedic implants, Journal of biomedical materials research, vol.62(2), pp. 175–84. doi: 10.1002/jbm.10270.

APPENDIX A: SBF REAGENTS AND IONIC CONCENTRATIONS

SBF was produced by dissolving the reagents presented in Table A.1 to distilled water in numerical order. Quantities are for 1 L of SBF. The pH of the solution was adjusted to 7.40 ± 0.2 at the temperature of 37.0 ± 0.2 °C by titration with 1 M HCl.

Table A 1. *Reagents for SBF production.*

Order	Reagent	Mass (g)
1	NaCl	7.996
2	NaHCO3	0.350
3	KCL	0.224
4	K2HPO4.3H2O	0.228
5	MgCL2.&H2O	0.305
6	1M HCL	40 ml
7	CaCL2.2H2O	0.368
8	Na2SO4	0.071
9	2-Amino-2-(hydroxymethyl)-1,3-propane-diol	6.057